

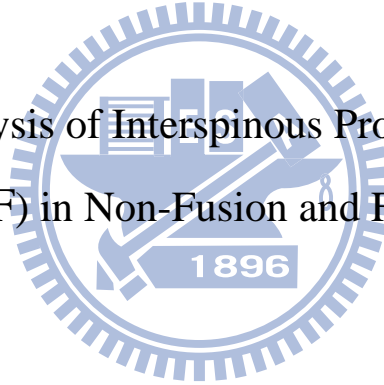
國立交通大學

機械工程學系

博士論文

脊突間裝置(Coflex and Coflex-F)在非融合與融合手術
的生物力學分析

Biomechanical Analysis of Interspinous Process Device (Coflex and
Coflex-F) in Non-Fusion and Fusion Surgery



研究生：羅正展

指導教授：洪景華 教授

中華民國一百年一月

脊突間裝置(Coflex and Coflex-F)在非融合與融合手術
的生物力學分析

Biomechanical Analysis of Interspinous Process Device (Coflex and
Coflex-F) in Non-Fusion and Fusion Surgery

研究生： 羅正展

Student: Cheng-Chan Lo

指導教授： 洪景華

Advisor: Chinghua Hung



A Thesis

Submitted to Department of Mechanical Engineering

College of Engineering

National Chiao Tung University

in Partial Fulfillment of the Requirements

for the Degree of

Doctor of Philosophy

in

Mechanical Engineering

January 2011

Hsinchu, Taiwan, Republic of China

中華民國一百年一月

脊突間裝置(Coflex and Coflex-F)在非融合與融合手術的 生物力學分析

研究生：羅正展

指導教授：洪景華 教授

國立交通大學機械工程學系

摘 要

在脊椎病變中，椎間盤初期退化常造成神經壓迫，形成腰椎狹窄症(Stenosis)。為改善神經壓迫而施予減壓手術，傳統的減壓手術會造成其他後續病發症，因此近年發展屬於非融合手術(Non-Fusion)的脊突間裝置 Coflex 希望能減少此類問題。椎間盤退化程度嚴重時會造成椎體不穩定，因此需要使用融合手術(Fusion)，新型的脊突間裝置 Coflex-F 可以改善傳統椎弓螺釘在手術過程的風險。

本研究利用有限元素軟體建構出五節的腰椎模型。第一階段，將脊突間裝置 Coflex 與 Coflex-F 分別放置腰椎第三與第四椎節之間，探討在非融合手術時的影響。第二階段，則將 TLIF 和 ALIF 椎間融合術搭配 Coflex-F 於腰椎第三與第四椎節之間，探討融合手術的效果。第三階段，則將 TLIF 椎間融合術搭配 Coflex-F 於腰椎第三與第四椎節之間，探討是否可以使用在微創的融合手術。以上研究的邊界條件則都施加 400N 的跟隨負荷(Follower load)，並使用混合控制方式(Hybrid test method)針對腰椎生理學動作進行分析比較。

第一階段結果發現，Coflex 在手術端可以穩定後彎(角度減少 70%)、側彎(角度減少 8%)與扭轉(角度減少 4.3%)，並且保留了前彎的活動(角度增加 8%)；對於鄰近端，後彎時有明顯的影響(角度增加 20~24%)。然而 Coflex-F 在手術端可以穩定所有動作，特別是前彎動作(角度減少 52%)；在鄰近端，前彎(角度增加 17~18%)與後彎(角度增加 20~24%)有明顯的影響。第二階段結果發現，ALIF 融合術搭配 Coflex-F 的穩定效果較好。第三階段結果發現，TLIF 融合術搭配 Coflex-F 無法提供較好的穩定效果。

關鍵字：融合、非融合、脊突間裝置、椎間融合術、混合控制、有限元素分析

Biomechanical Analysis of Interspinous Process Device (Coflex and Coflex-F) in Non-Fusion and Fusion Surgery

Student: Cheng-Chan Lo

Advisor: Prof. Chinghua Hung

Department of Mechanical Engineering

National Chiao Tung University

ABSTRACT

In current society, degenerative disc disease is a very common situation. It can cause nerve root compression, lumbar spinal stenosis, and lumbar instability. In order to relief patients' symptom, decompression and spinal fusion surgery were common practices by surgeons. In recent years, the concept of interspinous process Coflex device of non-fusion surgery is emerging to improve the complication of decompression surgery. The Coflex-F device is a minimally invasive lumbar fusion device that provides significant segmental stability with all the advantages of an interspinous implant. It can alternative to traditions pedicle screw fixation as an adjunct to spinal fusion.

This study was divided into three researches with purposes to investigate the biomechanical behavior between the Coflex and Coflex-F devices using finite element model of the L1-L5 lumbar spine. The first research was to investigate the biomechanical differences between the Coflex and Coflex-F implanted into the L3-L4 segment in non-fusion surgery. The second was to investigate the biomechanical characteristics of TLIF and ALIF spinal fusion combined with Coflex-F and with pedicle screw fixation implanted into the L3-L4 segment in fusion surgery. The third was to investigate the biomechanical characteristics of TLIF combined with Coflex-F and with unilateral pedicle screw fixation and translaminar

facet screw fixation implanted into the L3-L4 segment in minimally invasive lumbar fusion. A 400 N follower load and a 10 N-m moment were applied to the intact model to mimic physiological motions. The other implanted models to be compared with the intact model were also subjected to 400 N follower load and moments that produced overall motions equal to those of the above intact model (i.e. the hybrid test method).

The result of the first research showed that, the Coflex implantation can provide stability in extension (ROM decreased 70%), lateral bending (ROM decreased 8%), and axial rotation (ROM decreased 4.3 %) at the surgical segment, and retain flexible in flexion (ROM increased 8%). It had no influence at adjacent segments except during extension (ROM increased 20~24%). The Coflex device can restraint extension motion, and provide more space for foramen and spinal canal. Therefore, The Coflex device may improve or relieve the stenosis. In addition, the Coflex-F implantation can provide stability in all motions, especially in flexion (ROM decreased 52%). It had influence at adjacent segments during flexion (ROM increased 17~18%) and extension (ROM increased 20~24%). Therefore, the Coflex-F device can be used to treat stenosis combined with mild degenerative disc disease.

The result of the second research showed that, the ALIF combined with Coflex-F can provide more stability. The result of the third research showed that, the TLIF combined with Coflex-F cannot provide sufficient stability.

Keywords: Fusion, Non-Fusion, Interspinous Process Device, Interbody Fusion Surgery, Hybrid Test Method, Finite Element Analysis

誌謝

首先要衷心地感謝指導教授洪景華老師，願意耗費許多時間教導學生，使學生遭遇研究瓶頸時，不僅能迎刃而解，且能適時給予信心與鼓勵，引導學生培養獨立研究的態度與創新構想的思維，讓學生盡情的發揮。

特別感謝國泰醫院骨科蔡凱宙醫師，不但在研究上提供了專業智識與寶貴建議，也時常的照顧和提醒我，有如親兄弟的大哥。

感謝趙振綱教授、廖建忠博士、陳振昇教授、楊秉祥教授、蔡凱宙醫師在百忙之中挪出時間參加學生口試給於意見，讓學生的論文更加完整。

回首研究所期間，特別感謝實驗室榮崇學長、宇中學長、雅雯學姊、政成學長，在遇到困難時，適時剖析建議與協助；感謝研究室夥伴煌基、麒禎、銘傑、嘉偉、培峰、彥彬、宗駿、理強、黃詠、志嘉、運賢、世璿、俊羿、志傑、聖平、時恆、麒翔、建榮、忠諭、明輝、立釗、宗鎔、筱偉、正一、振傑、雅喬、書麟、馨云、中南、彥佑、致豪、品帆、呂翔、宜均在學業及生活中的指導與關懷，還有最佳化與齒輪實驗室的學長們，以及各位機械研究所的同學們，在研究生涯中的陪伴，所建立的深厚友誼與每一句歡笑將成為美好的回憶。期間，也受到交大機械所許多師長、助教的教導與提攜，同樣致上最誠摯的謝意。

感謝碩士班教導我的師長劉永生教授、以及大學時期的師長黃社振教授、嚴家銘教授、王威立教授、何智廷教授、林瑞璋教授長久以來在實質與精神上不斷的給我支持與鼓勵。

最後，僅以此論文獻給我最敬愛的雙親與家人，感恩他們多年來不辭辛勞的養育、栽培與無怨無悔的付出。

作者：羅正展 謹誌

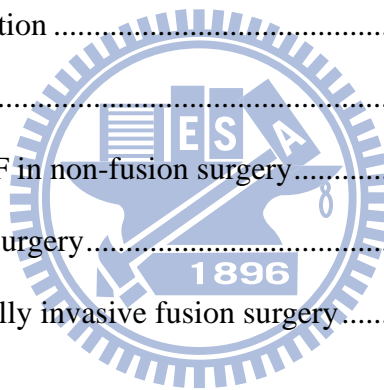
中華民國一百年一月

Table of Contents

摘要(Abstract in Chinese).....	i
Abstract.....	ii
誌謝(Acknowledgements in Chinese).....	iv
Table of Contents.....	v
List of Tables	viii
List of Figures.....	ix
Chapter 1: Introduction.....	1
1.1. Overview	1
1.2. Motivation and objectives	1
1.3. Outline	4
Chapter 2: Background.....	6
2.1. Spine anatomy and biomechanics	6
2.1.1. Vertebral.....	8
2.1.2. Intervertebral disc.....	9
2.1.3. Facet joint	10
2.1.4. Spinal ligaments	11
2.1.5. Neural foramen.....	12
2.1.6. Spinal cord and nerve roots	12
2.2. Spinal pathology and treatments	14
2.2.1. Lumbar spinal stenosis	14
2.2.2. Conservative therapy	18
2.2.3. Decompression	18
2.2.4. Non-fusion surgery	19
2.2.5. Fusion surgery	24

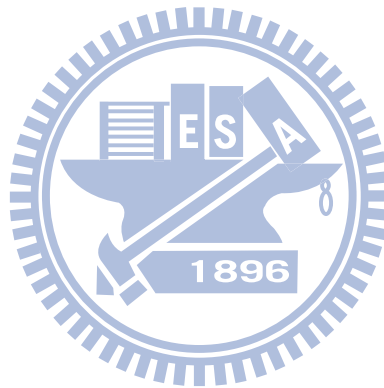
Chapter 3: Materials and methods	30
3.1 Coflex and Coflex-F in non-fusion surgery	30
3.1.1 FE model of intact lumbar spine (Intact model)	30
3.1.2 FE model of Coflex implanted into the L3-L4 segment (Coflex model).....	38
3.1.3 FE model of Coflex-F implanted into the L3-L4 segment (Coflex-F model)	38
3.1.4 FE model of bilateral pedicle screw fixation into the L3-L4 segment (Pedicle screw fixation model)	39
3.1.5 Boundary and loading conditions	40
(1) Follower load.....	40
(2) Validation of intact lumbar spine model with follower load	41
(3) Hybrid test method	42
3.2 Coflex-F in fusion surgery.....	46
3.2.1 FE model of TLIF combined with Coflex-F (Coflex-F + TLIF model)	46
3.2.2 FE model of ALIF combined with Coflex-F (Coflex-F + ALIF model).....	47
3.2.3 FE model of TLIF combined with bilateral pedicle screw fixation (Pedicle screw + TLIF model).....	48
3.2.4 FE model of ALIF combined with bilateral pedicle screw fixation (Pedicle screw + ALIF model).....	48
3.2.5 Boundary and loading conditions	50
3.3 Coflex-F in minimally invasive fusion surgery	52
3.3.1 FE model of TLIF combined with Coflex-F (Coflex-F model).....	52
3.3.2 FE model of TLIF combined with unilateral pedicle screw fixation with translaminar facet screw fixation (UPSF+TFSF model)	52
3.3.3 FE model of TLIF combined with bilateral pedicle screw fixation (BPSF model).....	53

Chapter 4: Results.....	56
4.1 Coflex and Coflex-F in non-fusion surgery.....	56
4.1.1 Range of motion (ROM).....	56
4.1.2 Maximal von-Mises stress at the disc annulus.....	59
4.1.3 Von-Mises stress distribution at the disc annulus	63
4.2 Coflex-F in fusion surgery.....	69
4.2.1 Range of motion.....	69
4.2.2 Von-Mises stress distribution on the cage-bone interface.....	71
4.2.3 Von-Mises stress distribution for the Coflex-F and the pedicle screw.....	74
4.3 Coflex-F in minimally invasive fusion surgery	75
4.3.1 Range of motion	75
Chapter 5: Discussion.....	79
5.1 Coflex and Coflex-F in non-fusion surgery.....	79
5.2 Coflex-F in fusion surgery.....	81
5.3 Coflex-F in minimally invasive fusion surgery.....	83
5.4 limitation.....	84
Chapter 6: Conclusion and future work.....	86
6.1 Conclusion.....	86
6.2 Future work	86
References	89
Vita.....	98



List of Tables

Table 3.1:	Material properties used in the FE model	35
Table 3.2:	Intervertebral range of motion and applied moment among the intact, defect, and implantation models under the hybrid test method	45
Table 3.3:	Intervertebral range of motion and applied moment among various surgical models under the hybrid test method	51
Table 3.4:	Intervertebral range of motion and applied moment among various surgical models under the hybrid test method	55



List of Figures

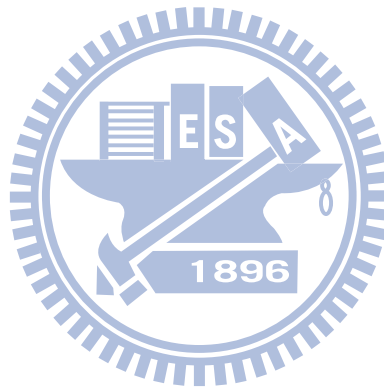
Figure 2.1:	Vertebral column: Anterior, left lateral and posterior views of the major regions of the spine	7
Figure 2.2:	The motion segment in the lumbar spine, which composed of two vertebrae and surrounding soft tissue.....	8
Figure 2.3:	The Shape of a human vertebra: (A) Superior view of the typical lumbar vertebra. (B) The trabecular structure of a lumbar vertebral body in sagittal section.....	9
Figure 2.4:	In the intervertebral disc, the annulus fibrosus, made up of laminar layers of criss-crossed collagen fibers, surrounds the nucleus pulposus	10
Figure 2.5:	Orientation of lumbar facet to the transverse plane (left) and the frontal plane (right).....	11
Figure 2.6:	The major ligaments of the spine	12
Figure 2.7:	Spinal Cord and Nerve Roots.....	13
Figure 2.8:	The radiograph shows the spinal instability	15
Figure 2.9:	Mono-segmental lumbar spinal stenosis at L4-L5 segment.....	16
Figure 2.10:	Multi-segmental lumbar spinal stenosis at L3-L5 segment	16
Figure 2.11:	Pathoanatomical illustration of lumbar spine stenosis	17
Figure 2.12:	Pedicle screw instrumentation.....	19
Figure 2.13:	X-STOP	22
Figure 2.14:	Wallis.....	22
Figure 2.15:	DIAM	22
Figure 2.16:	Coflex and Coflex-F.....	22
Figure 2.17:	This radiograph demonstrates a solid bony union between L3 and L4.....	24
Figure 2.18:	Common surgical techniques for insertion of a spinal cage. The black arrow	

indicates the ALIF approach, the red arrow indicates the PLIF approach, and the blue arrow indicates the TLIF approach.....	25
Figure 2.19: Various lumbar interbody fusion cages: (A) SynCage-Open (Synthes Spine, Inc., Mathys Medical Ltd., Bettlach, Switzerland); (B) O.I.C. (Stryker Spine, Mahwah, New Jersey, USA); (C) AVS-TL (Stryker Spine, Mahwah, New Jersey, USA).....	27
Figure 2.20: Interbody fusion combined with posterior pedicle screw fixation.....	27
Figure 2.21: Coflex-F device	28
Figure 2.22: unilateral pedicle screw fixation and translaminar facet screw fixation	29
Figure 3.1: Each spinal component was selected from computed tomography scan DICOM file to create material-related contours	32
Figure 3.2: Modeling process of the L3 vertebra: (A) surface geometries of vertebra were reconstructed through sequential processed computed tomography scan DICOM file; (B) surface geometry was exported to the DXF file; (C) FE model of the L3 vertebra	33
Figure 3.3: Finite element model of the L1 to L5 segments is shown: (A) intact model; (B) transverse views of facet joint curvature and gap	34
Figure 3.4: Convergence test of the intact model: (A) three mesh densities were selected; (B) result of motion changes under flexion; (C) result of motion changes under extension; (D) result of motion changes under axial rotation; (E) result of motion changes under lateral bending	37
Figure 3.5: Finite element models of the L1-L5 lumbar spine: (A) defect model implanted with Coflex at L3-L4 segment (Coflex model); (B) defect model implanted with Coflex-F at L3-L4 segment (Coflex-F model); (C) defect model implanted with Bilateral Pedicle Screw Fixation.....	40
Figure 3.6: (A) Illustration of traditional vertical preloads; (B) Illustration of follower	

load; (C) Intact lumbar spine model with follower load	41
Figure 3.7: Range of motion (ROM) calculated for the L1-L5 segments of intact lumbar spine is compared to previous <i>in vitro</i> experiments. (Left) intact lumbar spine without follower load data; (Right) intact lumbar spine with follower load data.....	42
Figure 3.8: Illustration of the Hybrid test method. (A) Whole spine specimen with various transducers and markers to monitor biomechanical parameters of interest. (B) Appropriate unconstrained pure moment is applied to the intact specimen to produce physiological motions. Resulting main total range of motion ($tRoM_{Intact}$) is recorded. (C) Unconstrained pure moment is applied to the spinal construct produce main total range of motion $tRoM_{Construct}$ equal to $tRoM_{Intact}$	44
Figure 3.9: Finite element models: (A) Coflex-F device combined with the TLIF model; (B) Coflex-F device combined with the ALIF model; (C) Pedicle screw fixation combined with the TLIF model; (D) Pedicle screw fixation combined with the ALIF model; (E) AVS-TL cage in the middle portion of the vertebral model; (F) SynCage-Open cage in the middle portion of the vertebral model; (G) Coflex-F device model.	49
Figure 4.1: Range of motion normalized to intact model in extension.....	57
Figure 4.2: Range of motion normalized to intact model in flexion.....	58
Figure 4.3: Range of motion normalized to intact model in lateral bending	58
Figure 4.4: Range of motion normalized to intact model in axial rotation.....	59
Figure 4.5: Disc annulus stress normalized to intact model in extension.....	61
Figure 4.6: Disc annulus stress normalized to intact model in flexion.....	61
Figure 4.7: Disc annulus stress normalized to intact model in lateral bending	62
Figure 4.8: Disc annulus stress normalized to intact model in axial rotation.....	62

Figure 4.9: von-Mises stress distribution of disc annulus in extension for various surgical models: (Top) L2-L3 adjacent segment; (Middle) L3-L4 surgical segment; (Bottom) L4-L5 adjacent segment.	63
Figure 4.10: von-Mises stress distribution of disc annulus in flexion for various surgical models: (Top) L2-L3 adjacent segment; (Middle) L3-L4 surgical segment; (Bottom) L4-L5 adjacent segment	65
Figure 4.11: von-Mises stress distribution of disc annulus in right lateral bending for various surgical models: (Top) L2-L3 adjacent segment; (Middle) L3-L4 surgical segment; (Bottom) L4-L5 adjacent segment.	66
Figure 4.12: von-Mises stress distribution of disc annulus in right axial rotation for various surgical models: (Top) L2-L3 adjacent segment; (Middle) L3-L4 surgical segment; (Bottom) L4-L5 adjacent segment.....	67
Figure 4.13: Range of motion normalized to intact model in flexion.....	70
Figure 4.14: Range of motion normalized to intact model in extension.....	70
Figure 4.15: Range of motion normalized to intact model in left lateral bending.....	70
Figure 4.16: Range of motion normalized to intact model in right lateral bending	70
Figure 4.17: Range of motion normalized to intact model in left axial rotation	71
Figure 4.18: Range of motion normalized to intact model in right axial rotation.....	71
Figure 4.19: The von-Mises stress distribution on the cage-bone interfaces of the superior surface of the L4 vertebra under left lateral bending and right lateral bending. .	72
Figure 4.20: The von-Mises stress distribution on the cage-bone interfaces of the superior surface of the L4 vertebra under left axial rotation and right axial rotation.	73
Figure 4.21: The von-Mises stress distribution on the cage-bone interfaces of the superior surface of the L4 vertebra under flexion and extension.	73
Figure 4.22: The von-Mises stress distribution in the Coflex-F device and the pedicle screw fixation under flexion, extension, right lateral bending, and right axial	

rotation.	74
Figure 4.23: The maximum von-Mises stress of the Coflex-F device and pedicle screw under flexion, extension, right lateral bending, and right axial rotation	75
Figure 4.24: Range of motion normalized to intact model in flexion.....	76
Figure 4.25: Range of motion normalized to intact model in extension.....	76
Figure 4.26: Range of motion normalized to intact model in right lateral bending	77
Figure 4.27: Range of motion normalized to intact model in left lateral bending.....	77
Figure 4.28: Range of motion normalized to intact model in right axial rotation	77
Figure 4.29: Range of motion normalized to intact model in left axial rotation	78



Chapter 1 Introduction

1.1 Overview

Degeneration of the intervertebral disc, called degenerative disc disease (DDD) of the spine, is a condition that can be painful and can greatly affect the quality of patient's life. Spinal diseases from DDD become more and more serious and dangerous for human population. Affecting up to 85 % of population at some point in their lifetime, the problem of low back pain reached epidemic proportions in the United States [1]. It has become one of the leading reasons why patients seek treatment, and it has been estimated to cost the national economy over \$50 billion per year [2][3]. These diseases cost large medical resources, and add huge encumbrances for our society.

1.2 Motivation and objectives

Recently, the concept of using non-fusion surgery via dynamic stabilization device to treat DDD has become popular. A dynamic stabilization device has been defined as: a flexible system that can preserve the spinal movement and improve load transmission of spinal motion segments through the non-fusion technique. In other words, such a system would restrict motion in the direction or plane that produces pain or painful motion [4]. The concept of dynamic stabilization device has changed from traditional stable fusion to mobile non-fusion that attempts to lessen the deterioration of the adjacent element. There have been a number of dynamic stabilization devices trialed in lumbar spinal disease, many with differing biomechanical principles. Some examples include anterior artificial disc, dynamic pedicle screw system, and interspinous process device.

Currently, there exist a number of interspinous process devices that have been tested for treating lumbar spinal stenosis from slightly degenerative disc disease with different biomechanical designs such as Coflex, Wallis, Diam, and X-Stop. The Coflex (Paradigm

Spine, Wurmlingen, Germany) is one of non-fusion spinal implants that was developed to restore normal physiological motion and to overcome the disadvantage of decompression surgery procedure. The Coflex was originally developed as an interspinous U-shaped device and is placed between two adjacent spinous processes. After implantation, the lateral wings are crimped toward the spinous processes to improve fixation. The U-shaped structure is designed to allow the lumbar spine to have controlled movement in forward and backward bending. To improve stability in all motions, a modified version called the Coflex-F has also been developed, which adds a rivet to the Coflex.

The Coflex devices are primarily used for lumbar spinal stenosis (LSS) without degenerative spondylolisthesis, angular instability, and retrolisthesis. Only a few reports of *in vitro* flexibility tests of the Coflex device are available in the literature. Among them, results regarding the biomechanical effects of the Coflex device at the surgical segment are inconsistent [56][57][59], especially the stability in lateral bending and axial rotation. The short-term clinical reports indicated that Coflex could provide physiological motion-sparing tend to the healthy spinal disc and reduce adjacent segment effect in flexion-extension [5]. However, the long-term outcome of these patients and other motion are still not clear. In addition, these existing studies are mostly concerning a short-segment analysis focused on the surgical segment. The effect of Coflex and Coflex-F device on adjacent segments is still not clear.

In order to understand the results of initial post-surgery and long-term complication of segment disease, and effect of implantation on adjacent segments, a number of biomechanical researches have intervened in evaluating various spinal implants, whether to use of *in vitro* experimental test or finite element (FE) analysis. However, in Taiwan, human cadaveric lumbar spine specimen is difficult to obtain for the experimental study.

Therefore, the first subject was to investigate the biomechanical behavior between the Coflex and Coflex-F devices at surgical and adjacent segments by using FE analyses on a

five-segment spinal model.

In addition, spinal fusion is a commonly performed surgical procedure to treat serious degenerative disc disease. In order to provide a stable environment for fusion, the use of pedicle screw fixation is usually necessary. Recently, the Coflex-F, which has been claimed to provide stabilization of the posterior spine elements similar to pedicle screw fixation, was adopted to interbody fusion in minimally invasive surgery.

Therefore, the second subject was to investigate the biomechanical behavior of the Coflex-F device and pedicle screw fixation, in combination with anterior lumbar interbody fusion (ALIF) or transforaminal lumbar interbody fusion (TLIF).

All types of interbody fusion approaches are recommended for combination with traditional bilateral pedicle screw fixation to increase stabilization and fusion rates. In the evolving surgical trend of minimally invasive spinal surgery, recent authors have employed TLIF and unilateral pedicle screw fixation. Besides, some surgeons purport that the unilateral pedicle screw fixation may be as effective as bilateral fixation. However, Goel [107] had compared that unilateral and bilateral pedicle screw fixation by *in vitro* biomechanics, *in vivo* biomechanics, and finite element method. His results showed that unilateral pedicle screw fixation was less stability than bilateral fixation. Therefore, supplementing the unilateral pedicle screw fixation using a percutaneous facet screw has been suggested as a means of stabilizing a TLIF construct employing unilateral pedicle screws. However, the Translaminar facet screw fixation requires long passage through the lamina for the crossing screws before they can traverse the facet joint, and necessitating a large surgical field. Recently, the Coflex-F has been adopted to combine interbody fusion in minimally invasive surgery; however, the effectiveness of this procedure is still unclear.

The third subject was to investigate the biomechanical characteristics of TLIF combined with Coflex-F and supplemented with one unilateral pedicle screw fixation and one translaminar facet screw fixation implanted into the L3-L4 segment in minimally invasive

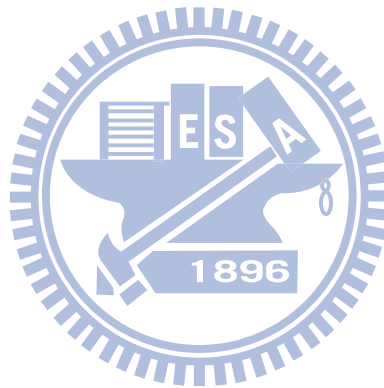
lumbar fusion.

1.3 Outline

This dissertation is divided into six chapters:

- (1) Introduction: this chapter introduces the overview, objectives, and outline of this dissertation.
- (2) Background: this chapter reviews the spine anatomy and biomechanics, spinal pathology and treatments, decompression, fusion surgery and non-fusion surgery.
- (3) Materials and Methods:
 1. The first subject includes FE modeling of the five-segment intact lumbar spine, defect lumbar spine, Coflex implantation, Coflex-F implantation, and Pedicle Screw Fixation models.
 2. The second subject includes TLIF and ALIF combined with Coflex-F or with pedicle screw fixation models.
 3. The third subject includes TLIF combined with Coflex-F or with unilateral pedicle screw fixation and translaminar facet screw fixation models.
- (4) Results:
 1. The first subject includes data of intact lumbar spine, defect lumbar spine, both implant models under the Coflex or Coflex-F, and pedicle screw fixation.
 2. The second subject includes data of intact lumbar spine, TLIF and ALIF combined with Coflex-F model, TLIF and ALIF combined with pedicle screw fixation model.
 3. The third subject includes data of intact lumbar spine, TLIF combined with Coflex-F model, TLIF combined with unilateral pedicle screw fixation and translaminar facet screw fixation models
- (5) Discussion:
 1. The first subject finds effect of Coflex and Coflex-F.

2. The second subject finds effect of TLIF and ALIF combined with Coflex-F.
 3. The third subject finds effect of TLIF combined with Coflex-F.
 4. Model limitations.
- (6) Conclusion and Future Work: several topics can be extended from this research is introduced in this chapter.



Chapter 2 Background

The following sections contain a review of the anatomy of the spine, its biomechanics, spine pathology and treatments, fusion and non-fusion techniques, clinical outcomes after interspinous process device, and the characteristics of *in vitro* tests versus FE simulations.

2.1. Spine anatomy and biomechanics

The spine consists of a curved stack of 33 vertebra divided structurally into five regions (Figure 2.1). Proceeding from superior to inferior, there are seven cervical vertebrae (C1-C7), twelve thoracic vertebrae (T1-T12), five lumbar vertebrae (L1-L5), five fused sacrum vertebrae (S1-S5), and four small fused coccygeal vertebrae. The vertebrae from each region have similar parts, but the shapes of vertebrae vary considerably from region to region in the spine. There may be one extra vertebra or one less, particularly in the lumbar region.

Because of structural differences and the ribs, varying amounts of movement are permitted between adjacent vertebrae in the cervical, thoracic, and lumbar portions of the spine. Within these regions, two adjacent vertebrae and the soft tissues between them are known as a motion segment. The motion segment is considered to be the functional unit of the spine (Figure 2.2).

Each motion segment contains three joints. The vertebral bodies separated by the intervertebral disc form a symphysis type of amphiarthrosis. The right and left facet joints between the superior and inferior articular processes are diarthroses of the gliding type that are lined with articular cartilage.

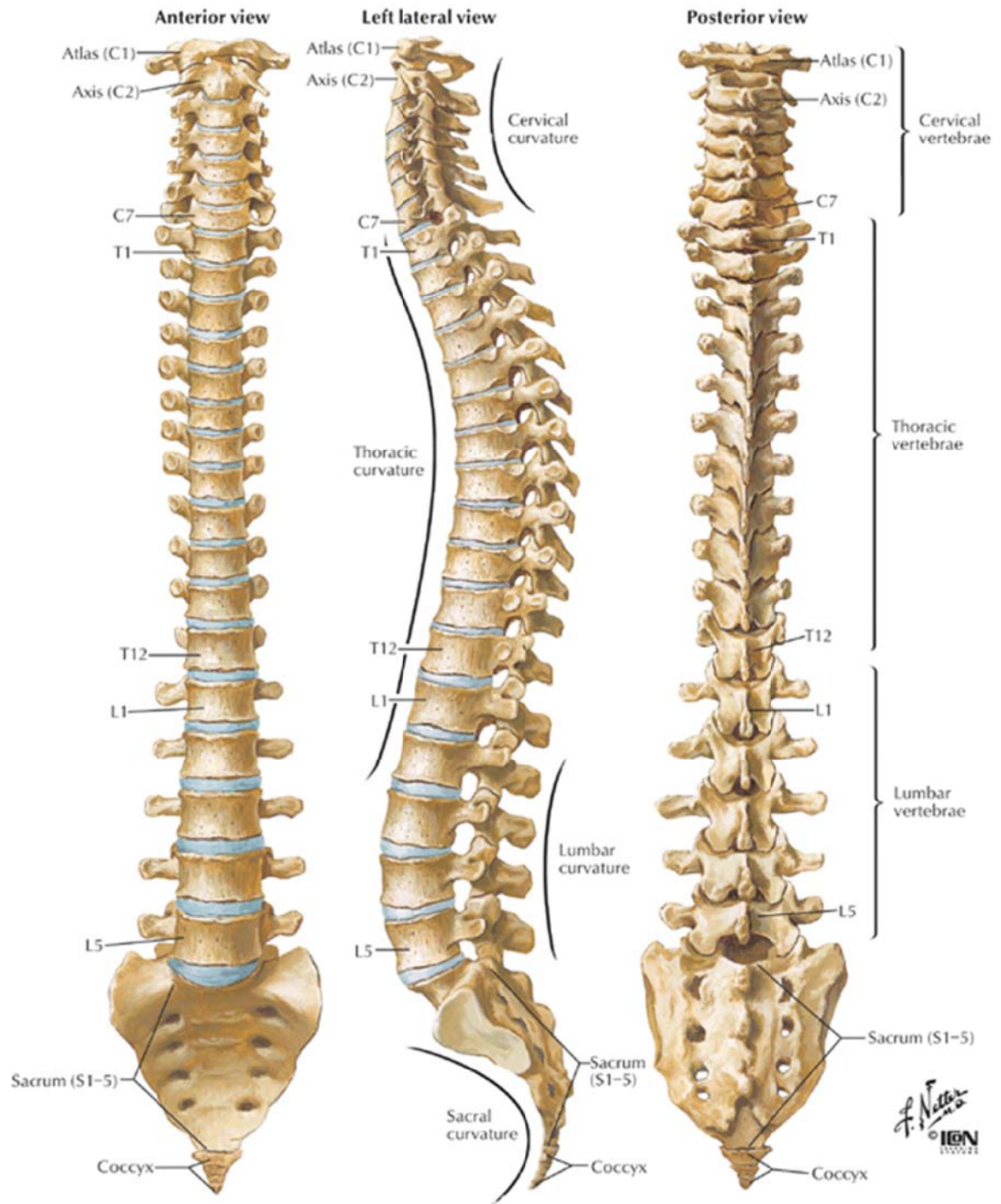


Figure 2.1: Vertebral column: Anterior, left lateral and posterior views of the major regions of the spine [6].

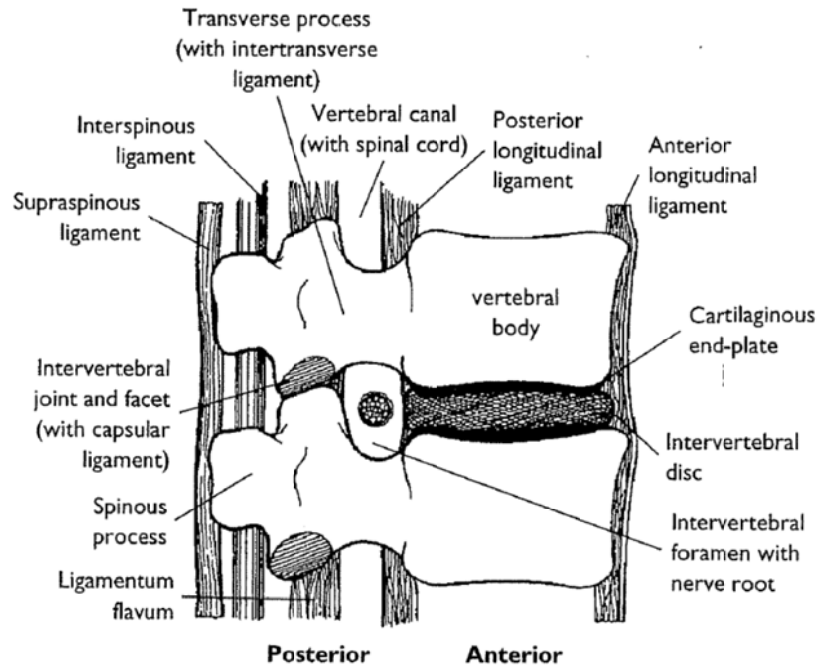


Figure 2.2: The motion segment in the lumbar spine, which composed of two vertebrae and surrounding soft tissue [7].

2.1.1.1. Vertebral

A typical vertebra consists of a body, a hollow ring, and several bony processes, such as the pedicle, lamina, spinous process, and transverse process, as shown in Figure 2.3(a). Each vertebral body consists of an outer shell of cortical bone and an inner core of cancellous bone. The vertical and horizontal structure of bone in the cancellous core is called trabecular bone (Figure 2.3 b). Most of the compressive force acting down the long axis of the spine is resisted by the cancellous bone because of its dense network of trabecular bone [8]. In general, the vertebral size is progressively increased from the cervical region to the lumbar region.

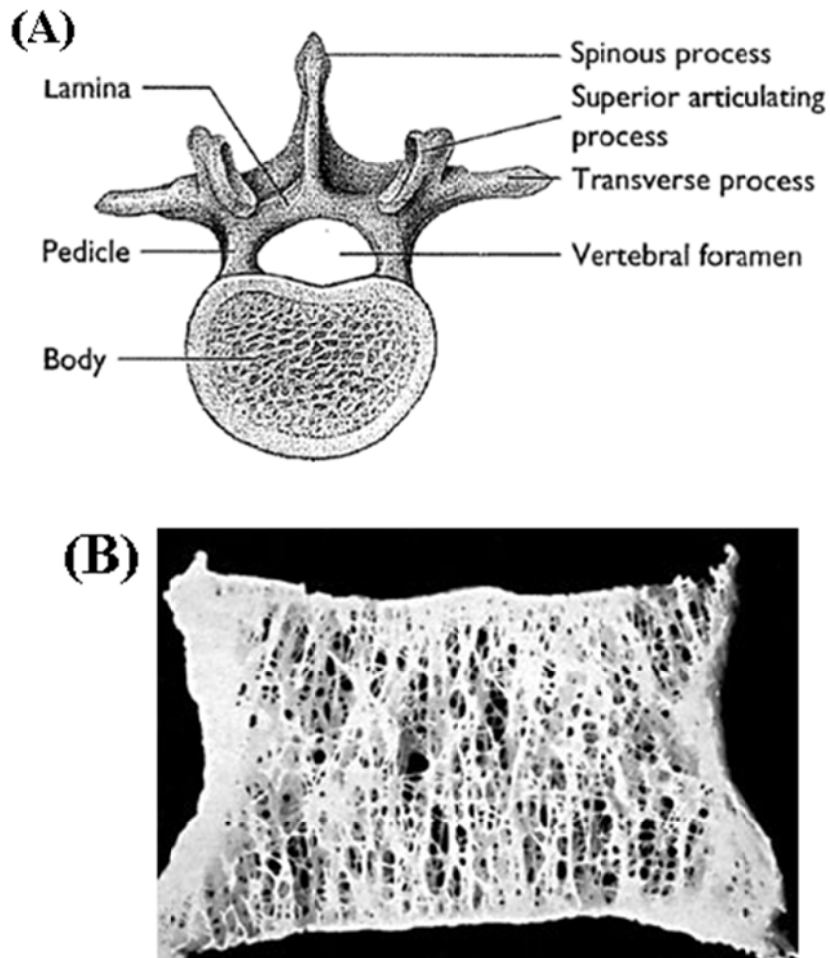


Figure 2.3: The Shape of a human vertebra: (A) Superior view of the typical lumbar vertebra [7]. (B) The trabecular structure of a lumbar vertebral body in sagittal section [9].

2.1.2. Intervertebral disc

The intervertebral disc is composed of two parts: the nucleus pulposus and annulus fibrosus (Figure 2.4). The nucleus pulposus located in the central of each disc which is only slightly compressible and with 80 % to 88 % water content [10]. In general, the lumbar nucleus fills 30 % to 50 % of the total disc area in cross-section [11]. The annulus fibrosus consists of approximately 15-25 concentric lamellae in the circumferential around the nucleus which contain collagen fibers [12]. The collagen fibers are oriented approximately 30° angle to the horizontal plane and crisscross to each other in the adjacent lamella. The superior and

inferior cartilaginous endplates cover disc and connect with adjacent vertebrae bodies.

The primary function of the disc is transfer compressive forces evenly from one vertebral body to the next, while allowing for small-amplitude twisting and sliding movements [13]. The tensile properties of the annulus are stiffer in anterior than the posterolateral regions, with the outer region being stiffer than the inner regions [14]. The outer lamellae resist excessive bending and twisting of adjacent vertebrae, while the innermost lamellae are deformable and normally behave like a fluid. The endplate not only helps to equalize loading of the vertebral body but also prevents rapid fluid loss from the nucleus [15].

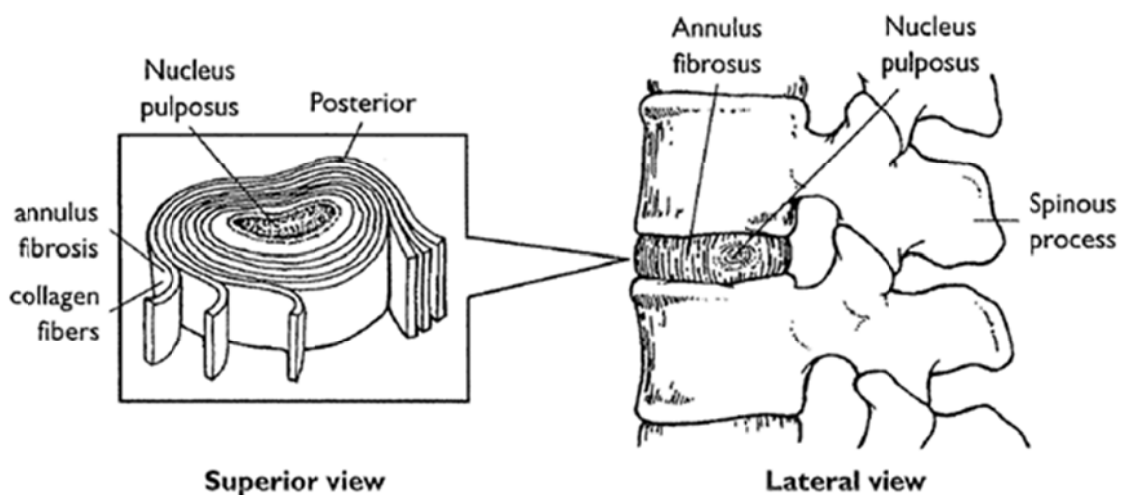


Figure 2.4: In the intervertebral disc, the annulus fibrosus, made up of laminar layers of criss-crossed collagen fibers, surrounds the nucleus pulposus [7].

2.1.3. Facet joint

The size and angulation of the vertebral processes vary throughout the spinal column (Figure 2.5). This changes the orientation of the facet joints, which limit ROM in the different spinal regions. In addition to channeling the movement of the motion segment, the facet joints assist in load bearing. The facet joints and discs provide about 80 % of the spine's ability to resist rotational torsion and shear, with half of this contribution from the facet joints [16] [17].

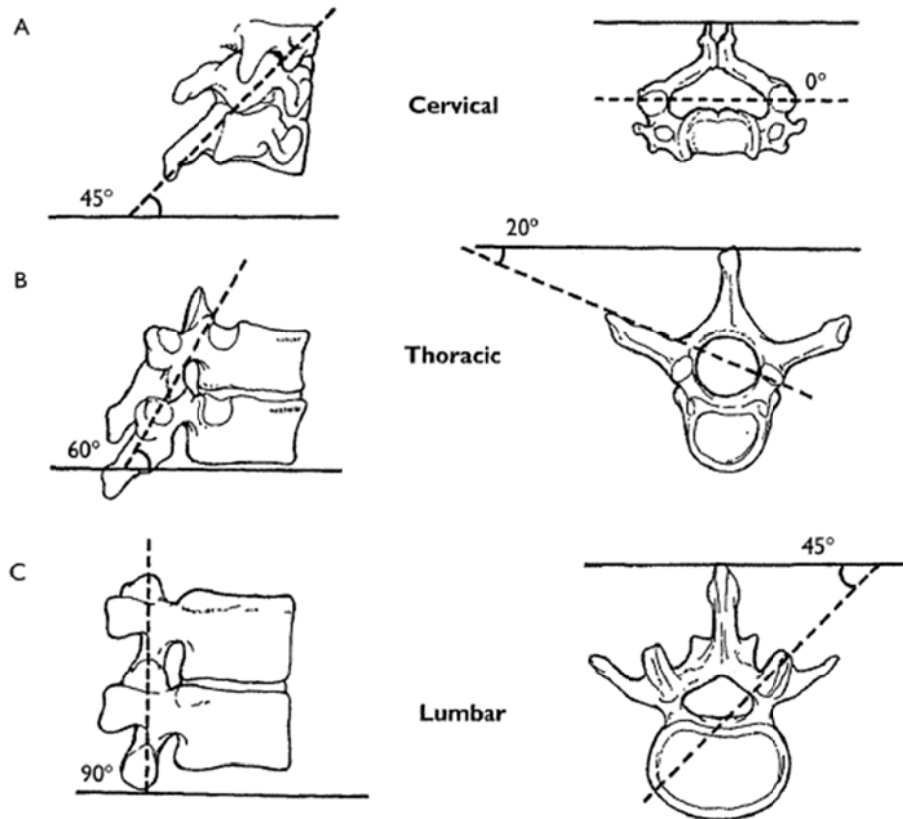


Figure 2.5: Orientation of lumbar facet to the transverse plane (left) and the frontal plane (right) [7].

2.1.4. Spinal ligaments

There are a series of ligaments that are important to the stability of the vertebral column. Important to the lumbar spine are seven types of ligaments (Figure 2.6): Anterior longitudinal ligament (ALL) and posterior longitudinal ligament (PLL) are associated with each joint between the vertebrae. The anterior longitudinal ligament runs along the front and outer surfaces of the vertebral bodies. The posterior longitudinal ligament runs within the vertebral canal along the back surface of the vertebral bodies. The ligamentum flavum (LF) is located on the back surface of the canal where the spinal cord or cauda equina runs. The interspinous ligament (ISL) runs from the base of one spinous process (the projections at the back of each vertebra) to another. Intertransverse ligament (ITL) and supraspinous ligaments (SSL) run along the tips of the spinous processes. Joint-related structures called facet capsular ligament

(CL) also play an important role in stabilization and movement.

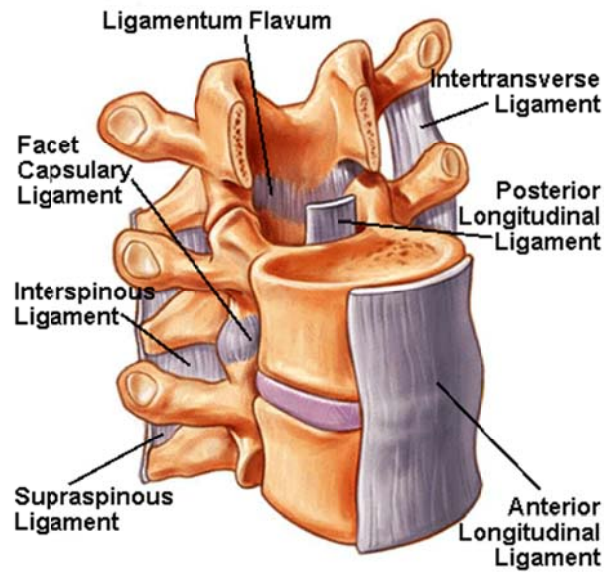


Figure 2.6: The major ligaments of the spine [18].

2.1.5. Neural foramen

The segmental spinal nerve roots exit through the intervertebral foramen (Figure 2.2). The intervertebral foramen is bounded by the pedicles superiorly and inferiorly, and ventrally and dorsally by two major intervertebral articulations. It is bounded ventrally by the dorsum of the intervertebral disc and the lateral expansion of the posterior longitudinal ligament. Foraminal disc herniations can impinge on the exiting nerve root, causing radiculopathy. The joint capsule of the articular facets and the ligament flavum make up the dorsal boundary of the intervertebral foramen. The remaining space is composed of loose areolar tissue and fat.

2.1.6. Spinal cord and nerve roots

The spinal cord is a column of millions of nerve fibers that run through spinal canal (Figure 2.7). It extends from the brain to the area between the end of first lumbar vertebra and top of second lumbar vertebra. At the second lumbar vertebra, the spinal cord divides into several different groups of fibers that form the nerves that will go to the lower half of the body.

For a small distance, the nerves actually travel through the spinal canal before exiting out the neural foramen. This collection of nerves is called the cauda equina while it is still inside the spinal canal.

A protective membrane called the dura mater covers the spinal cord. The dura mater forms a watertight sack around the spinal cord and the spinal nerves. Inside this sack, the spinal cord is surrounded by spinal fluid.

The nerve fibers in spinal cord branch off to form pairs of nerve roots that travel through the small openings (foramina) between vertebrae and vertebrae. The nerves in each area of the spinal cord connect to specific parts of body. This is why damage to the spinal cord can cause paralysis in certain areas and not others; it depends on which spinal nerves are affected. The nerves of the cervical spine go to the upper chest and arms. The nerves in the thoracic spine go to chest and abdomen. The nerves of the lumbar spine then reach to legs, bowel, and bladder. These nerves coordinate and control all the body's organs and parts, and body muscles.

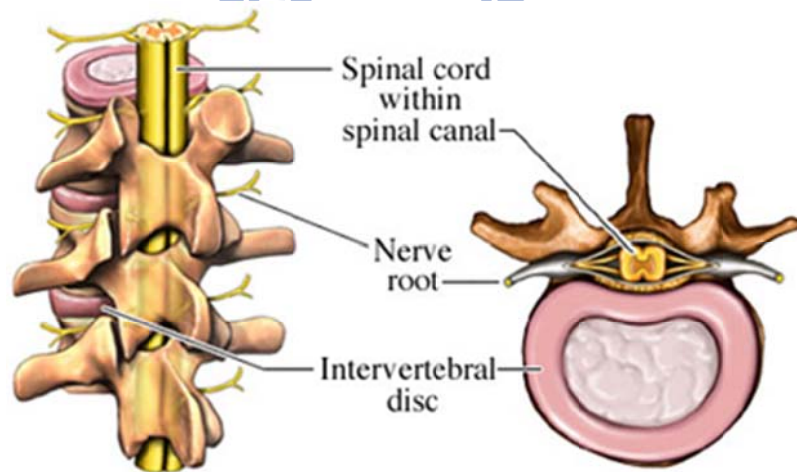


Figure 2.7: Spinal Cord and Nerve Roots [19].

2.2. Spinal pathology and treatments

The functions of spine are to provide the longitudinal weight support, limit excessive movement, and protect posterior spinal cord. However, the spinal instability may induce due to several pathological changes, such as degenerative disc disease, spinal deformity, tumor, infection, trauma, congenital anomaly, inflammatory, etc (Figure 2.8). Thus spinal nerve roots or spinal cord may be compressed and leading low back pain (Figure 2.9). The first choice of treatment for low back pain is conservative therapy, such as physical therapy or medication. When conservative treatments fail, spine surgeons may perform either fusion or non-fusion surgery, with the aim of reducing pain and decreasing disability [20].

2.2.1. Lumbar spinal stenosis

The most common cause of lumbar spinal stenosis (LSS) is initial stage of degeneration intervertebral disc. LSS defined as narrowing of the spinal canal or intervertebral foramina, is a common cause of pain, numbness, and weakness. Early descriptions of neurogenic claudication secondary to lumbar stenosis have been attributed to Verbiest [22]. This syndrome is displayed by radicular pain, which is exacerbated by standing, walking, and other positions that place the lumbar spine in extension. A flexed posture improves or relieves the symptoms. In severe cases, sensory loss or motor deficits are evident. Although several theories have been postulated to explain the occurrence of these symptoms, the precise mechanism remains unclear [23]. It is obvious that the pathological progression begins with degeneration of disc, which finally leads to loss of disc height. Resultant instability may worsen the spondylosis by inducing facet joint hypertrophy [24]. Furthermore, hypertrophy of the ligamentum flavum, particularly during extension, contribute to the reduction in size of the thecal sac limiting the space available for the cauda equine [4].

LSS can be mono-segmental or multi-segmental (Figure 2.10), and unilateral or bilateral. Anatomically, the stenosis can be classified as central, lateral or foraminal [21]. Depending on

the degree of degeneration, central, lateral and foraminal stenosis can occur alone or in combination. The L4-L5 spinal discs are most frequently affected by LSS, followed by L3-L4, L5-S1, and S1-S2 [25]. Degeneration of disc often causes a protrusion, which leads to ventral narrowing of the spinal canal (Figure 2.11). As a consequence of disc degeneration, the height of intervertebral space is reduced, which causes the intervertebral foramina to narrow (foraminal stenosis), exerting strain on the facet joints. Such an increase in load can lead to facet joint arthrosis, hypertrophy of the joint capsules and the development of expanding joint cysts (lateral stenosis), which in combination propagate spinal instability [25][26]. The reduced height of the segment leads the ligamentum flavum to form creases, which exert pressure on the spinal dura from the dorsal side (central stenosis). Concomitant instability due to loosened tendons (ligamentum flavum) further propagates preexisting hypertrophic changes in the soft tissue and osteophytes, creating the characteristic trefoil-shaped narrowing of the central canal [25]-[33].



Figure 2.8: The radiograph shows the spinal instability [21].



Figure 2.9: Mono-segmental lumbar spinal stenosis at L4-L5 segment [25].



Figure 2.10: Multi-segmental lumbar spinal stenosis at L3-L5 segment [25].

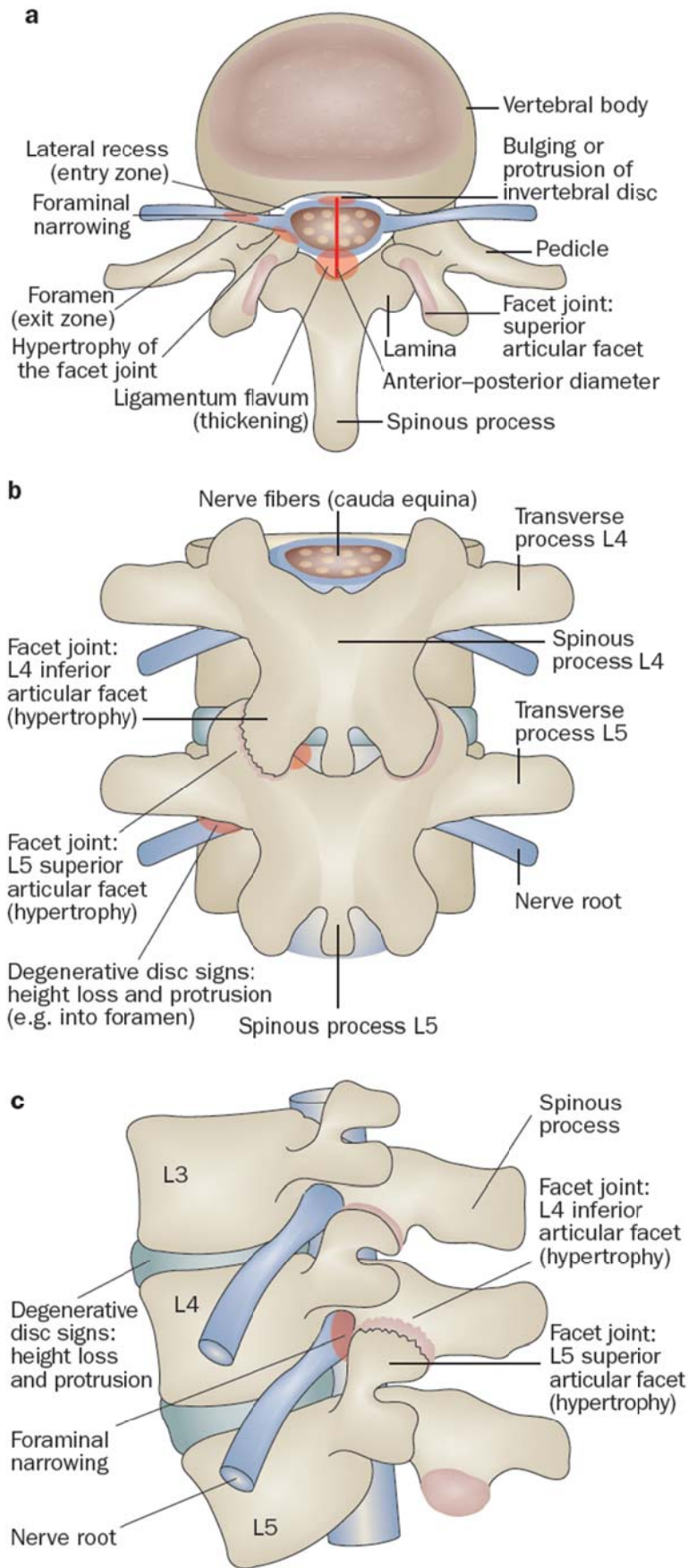


Figure 2.11: Pathoanatomical illustration of lumbar spine stenosis [25].

2.2.2. Conservative therapy

The conservative treatment of LSS comprises a wide variety of methods, such as ergotherapy, physical therapy, behavioral therapy, girdles, acupuncture, manual therapy and pharmacological intervention. Few studies have been conducted to demonstrate the effectiveness of conservative therapy in treating LSS, although those that reported had success rates of up to 70 % [25][34]-[36]. However, none of the available studies provide sufficient data to support the effectiveness, or any one of the wide range of conservative treatments [37]. In the absence of evidence-based clinical guidelines, multidisciplinary approach should be given preference over a significant therapy [38][39].

2.2.3. Decompression surgery

In patients in whom severe symptoms persist and functional impairment develops, surgery is the recommended option. Decompression surgery used in LSS aim to decompress the neural elements, without occur instability of the segment. Such decompression surgery usually leads to relief of pain in the legs and low back pain [41]. Decompressive surgical procedures include laminectomy and hemilaminectomy, hemilaminotomy, fenestration, and foraminotomy [40]. The complication rates for decompression surgery range from 14 % to 35 % or more [42]-[45]. Typical complications of decompression surgery include inadequate decompression with significant residual stenosis, instability of segment, renewed nerve compression, and reossification. All of these complications result in renewed nerve compression [44]-[47].

Decompression surgery may cause as mentioned above if weight bearing structures are compromised. Therefore, instrumented is necessary when preexisting or surgically induced instability is present. Pedicle screw instrumentation is a popular method of strong fixation to achieve stabilization rate (Figure 2.12). For stabilization of one spinal functional unit, four pedicle screws are usually used.

However, the use of pedicle screws is technically demanding and associated with certain risks. Complications were divided into three categories: 1. Infections: deep infections. 2. Neurological complications: postoperative neurapraxias or permanent neurological disorders. 3. Implant failures: malposition, breakage or loss of correction [49].

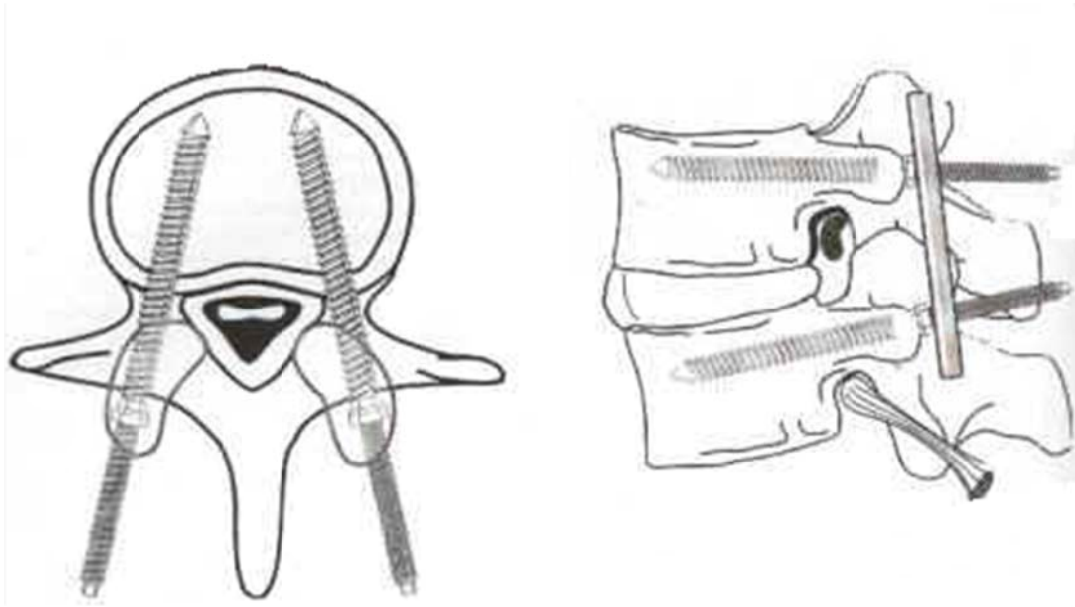


Figure 2.12: Pedicle screw instrumentation [50].

2.2.4. Non-fusion surgery

Two such technological strategies have emerged for managing lumbar stenosis in a dynamic manner, such as interspinous process device [51] and dynamic pedicle screw system. Interspinous process device are inserted between the spinous processes of the lumbar spine, and generally speaking, attempt to reduce neural compression by preventing lumbar extension, distracting across the intervertebral disc, or promoting lumbar flexion. Dynamic pedicle screw systems utilize a non-rigid means of connecting otherwise standard pedicle screws that nevertheless allow for distraction across the intervertebral disc or regulate the amount of intervertebral flexion through band technology.

The basic rationale of interspinous process device for inserting an implant between the lumbar spinous processes as a treatment for stenosis is that the symptoms of neurogenic

claudication are often relieved with the lumbar spine in the flexed position, and worsened in extension. Conceptually, a device that induced some flexion of the motion segment would increase the caliber of the spinal canal and the intervertebral foramen. Furthermore, if such a device merely prevented extension, it could minimize the narrowing of the spinal canal and foramen observed with extension. Additionally, an interspinous process device might also provide for some degree of distraction which could unload both the facet joints and intervertebral discs, potentially reducing back pain. Finally, on a practical note, the ability to access the interspinous area with a small incision and minimal paraspinal muscle stripping implies that the implantation of such a device could be performed in much less traumatic way than current decompression techniques. The interspinous process device can be called the non-fusion surgery is to restore normal physiological motions, or to allow restrained motions within a certain range, through various mobile non-fusion devices that aim to avoid or alleviate adjacent segment disease.

Four such interspinous process devices have been designed and are currently available: the Coflex (Paradigm Spine, Wurmlingen, Germany), the Wallis (Abbott spine, Bordeaux, France), the Diam (Medtronic, Tolochenaz, Switzerland), and X-Stop (Medtronic, Tolochenaz, Switzerland). As a general note, at the time of this writing, the four devices described here are in various stages of clinical development.

(1) X-STOP

The X-STOP consists of a titanium oval spacer with two lateral wings to prevent lateral migration (Figure 2.13). It is inserted into the interspinous space without disruption of the interspinous ligament. A biomechanical study demonstrated that the force required to insert the device in the appropriate position is 4.5 times less than the force required to break off the spinous process with the device placed too caudally or cranially, suggesting that the device insertion is relatively safe. The body of biomechanical and clinical literature for the X-STOP far exceeds that of the other devices and as such it is described in the most detail here. It has

been formally evaluated in patients with computed tomography or MRI confirmed lumbar stenosis who complained of leg, buttock, or groin pain relieved by flexion, with or without back pain. In one article, it is speculated that the implant may confer some benefit to patients with pressure-related discogenic back pain, under the hypothesis that the implant provides some distraction and thus decreases pressure within the intervertebral disc.

(2) Wallis

The Wallis system consists of an interspinous blocker made from PEEK (Polyetheretherketone) with two woven Dacron ligaments which wrap around the caudal and cranial spinous processes (Figure 2.14). The interspinous ligament is removed and the Dacron ligaments are inserted around the caudal and cranial spinous processes. At the end of the procedure, the interspinous ligament is repaired. The designer of this device advocates the following indications for its implantation: recurrent disc herniation after primary discectomy, primary discectomy for voluminous herniated disc, discectomy for herniation of a transitional disc segment, disc degeneration adjacent to a previous fusion, and isolated Modic I lesion leading to chronic low back pain.

(3) DIAM

The DIAM for intervertebral assisted motion, is an interspinous implant that consists of a silicone core surrounded by a polyester outer mesh which is secured to the cephalad and caudal spinous processes by two polyester tethers (Figure 2.15). These tethers are inserted through the interspinous processes using attached steel needles and then are secured to the device by means of two titanium crimps.

(4) Coflex and Coflex-F

The Coflex device is made of titanium. It was originally developed as an interspinous U-shaped and is placed between two adjacent spinous processes (Figure 2.16) [52][53][54]. After implantation, the lateral wings are crimped towards the spinous processes to improve fixation. The U-shaped structure is designed to allow the lumbar spine to have controlled

movement in forward and backward bending. To improve stability in all motions, a modified version called the Coflex-F (Coflex rivet) has also been developed, which adds a rivet to the Coflex [56].



Figure 2.13: X-STOP [55]



Figure 2.14: Wallis [55]



Figure 2.15: DIAM [55]

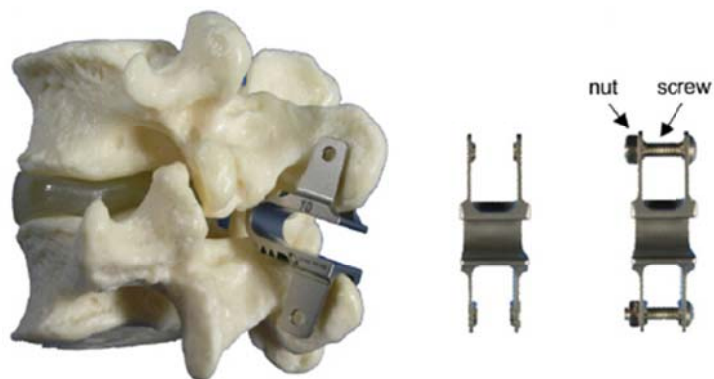


Figure 2.16: Coflex and Coflex-F [56].

Recently, many studies have evaluated the biomechanical behaviors of the Coflex and Coflex-F devices. Tsai [57] used cadaveric lumbar L4 and L5 segments with implanted Coflex device to examine their biomechanical behavior, and the results showed that the implanted Coflex device can provide stability for the lumbar spine in flexion-extension and axial rotation, except in lateral bending. Kong [58] reported 1-year follow-up outcomes after Coflex device implantation and traditional fusion for degenerative spinal stenosis. The results indicated that both the Coflex device and traditional fusion reduced the range of motion (ROM) at the surgical segment, but fewer effects were found at the adjacent segments with the Coflex device as compared with the increasing ROM with traditional fusion. Kettler [56] compared the Coflex and Coflex-F devices using biomechanical experiments and found that both implants had strong stability in extension. However, the Coflex implant could not compensate the instability in flexion, lateral bending, and axial rotation as well as the Coflex-F did. Wilke [59] examined the biomechanical effects of different interspinous process devices for flexibility. The Coflex device had the best stabilizing effect in extension but poor stability in flexion. In lateral bending and axial rotation, the Coflex device had neither a stabilizing nor a destabilizing effect. Inconsistent results regarding the biomechanical effects of the Coflex device have been shown in previous studies. In addition, these studies are mostly a short-segment analysis focused on the surgical segment. The effect of the Coflex device and the Coflex-F device on adjacent segments is still not clear.

Therefore, the first subject was to investigate the biomechanical differences between the Coflex device and the Coflex-F at surgical and adjacent segments by using finite element (FE) analyses on a five-segment spinal model. In addition, the study also compared these two interspinous process implantations with pedicle screw fixation.

2.2.5. Fusion surgery

Fusion surgery is needed in cases of severe degeneration disc, instability (rotational or vertical mobility of the vertebral body >3 mm), spondylolisthesis (>5 mm forward movement of a lumbar vertebra relative to one below) or scoliosis (lateral curvature of the spine) $>20^\circ$, because instability can make nerve root compression. Success rates for decompression surgery in cases of LSS range from 40-90 % in the literature and depend on a wide variety of factors such as type of decompression, duration of follow-up, age of patients and co-morbidities [60]-[67].

Spinal fusion is defined as a bony union between two vertebrae spaces following surgical manipulation [68], and aims to completely eliminate movement by the motion segment (Figure 2.17). It is an effective technique for treating degenerative spinal instability, and the final goal of the procedure is to restore disc height, enlarge the stenotic foramen, and support the anterior spinal column. In general, bone grafts are placed into the interface between vertebral bodies to maintain disc height and to accelerate bone growth into neighboring vertebrae. These bone grafts may be autografts, allografts or synthetic materials which can be adopted from fibulae, illia, the iliac crest, or ribs.



Figure 2.17: This radiograph demonstrates a solid bony union between L3 and L4 [69].

The most common surgical techniques for the insertion of a spinal cage can be classified as the anterior lumbar interbody fusion (ALIF) approach, posterior lumbar interbody fusion (PLIF) approach, and transforaminal lumbar interbody fusion (TLIF) approach. In general, the ALIF approach includes the removal of the ALL, the anterior portions of the disc annulus, and the nucleus before implanting an interbody fusion cage (Figure 2.18; black arrow) [70]. For the PLIF approach, a partial laminectomy, discectomy and nucleotomy are performed, which includes the removal of the ISL, SSL, LF, posterior portions of the disc annulus, and the total nucleus. In addition, a certain portion of the facet joint can be removed to give the nerve roots more space (Figure 2.18; red arrow) [71]. Recently, the TLIF approach has been proposed and modified from the PLIF method to provide a minimally invasive surgical technique. After the spine is approached, an inferior hemi-laminectomy and a unilateral facetectomy are performed (Figure 2.18; blue arrow) [72].

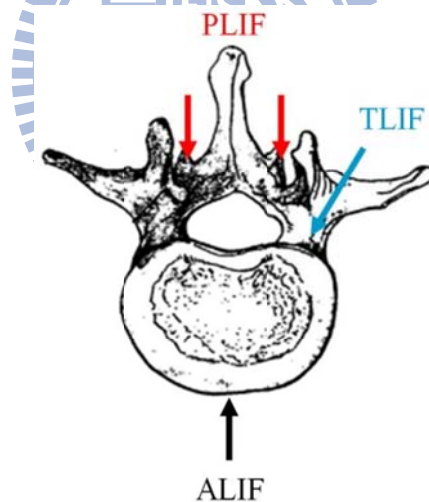


Figure 2.18: Common surgical techniques for insertion of a spinal cage. The black arrow indicates the ALIF approach, the red arrow indicates the PLIF approach, and the blue arrow indicates the TLIF approach.

The spinal interbody fusion cage can replace the degenerative disc and distension the intervertebral body, thus restoring physiological disc height. In general, there are several features of this device (Figure 2.19). First, the spinal fusion cage is made of a variety of

biocompatible materials, including stainless steel, titanium alloy, carbon fiber-reinforced polymer (CFRP), and polyetheretherketone (PEEK) [73]. Due to the high mechanical strength of these materials, a spinal interbody fusion cage can provide better longitudinal support than a traditional bone graft, without causing collapse. Second, rough or specific designs can be found on the contact surfaces of spinal cages. In order to prevent cage slippage, rough contact surfaces, saw teeth, spikes or threads have been designed to increase stability between fusion devices and endplates. Third, these implants are usually designed to be hollow, with small pore or openings on the wall. These hollow cages can be filled with bone grafts to promote bone growth. Furthermore, only small amounts of cancellous bone are required, because there is no longer need for the cubic graft to be a spacer. The small pores and openings on the wall allow the growth of bone through the cage, resulting in bony fusion. Therefore, spinal fusion cages can avoid donor site morbidity and increase fusion rates.

Currently, many kinds of spinal cage designs are available on the market, which can be classified by the various surgical approaches used in their implantation. Large single lumbar cage designs are used for the ALIF procedure (Figure 2.19 A). Some paired cage designs are used strictly for PLIF procedures (Figure 2.19 B). In addition, some specific shapes of cages are designed for minimally invasive surgical techniques such as the TLIF procedure (Figure 2.19 C).

All types of interbody fusion approaches are recommended for combination with traditional posterior pedicle screw fixation to increase stabilization and fusion rates (Figure 2.20). A pedicle screw is a device composed of rods and screws contoured to restore lumbar lordosis and disc height, and can be used for unilateral or bilateral pedicle screw fixation.



Figure 2.19: Various lumbar interbody fusion cages: (A) SynCage-Open (Synthes Spine, Inc., Mathys Medical Ltd., Bettlach, Switzerland); (B) O.I.C. (Stryker Spine, Mahwah, New Jersey, USA); (C) AVS-TL (Stryker Spine, Mahwah, New Jersey, USA).

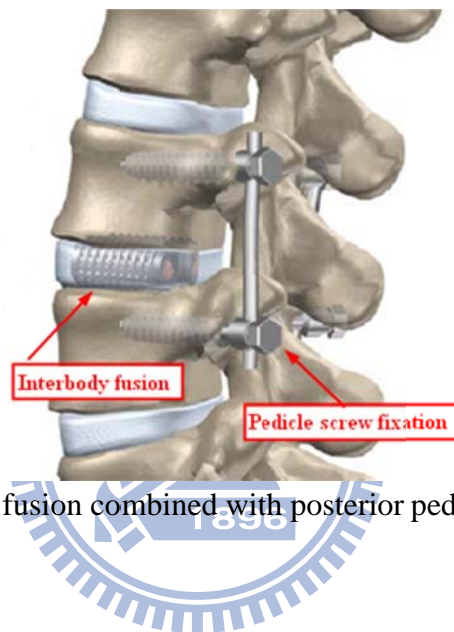


Figure 2.20: Interbody fusion combined with posterior pedicle screw fixation [74].

The fusion is very successful in the treatment of deformity as well as degenerative conditions of the lumbar spine. Fusion provides stabilization of the spine, protection of neural elements, maintenance of neural decompression. However, the use of pedicle screws is technically demanding and associated with certain risks. Typical complications of pedicle screws surgery include infections, neurological risk and implant failures [49].

Recently, the Coflex-F (Figure 2.21), which has been claimed to provide stabilization of the posterior spine elements similar to pedicle screw fixation, was adopted to interbody fusion in minimally invasive surgery. The Coflex-F spacer is an interspinous process device with rivets modified from the original Coflex device. The rivets joining the wings of the Coflex device and the spinous processes allow for rigid attachment to the posterior element. It retains

the advantages of interspinous process implants and minimally invasive surgery, such as sparing tissue, preserving pedicle anatomy, minimizing muscle trauma, blood loss, skin incisions, and operating time, thus speeding patient recovery.

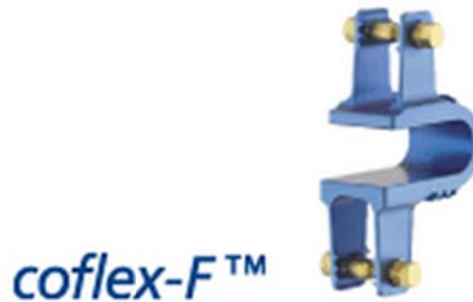


Figure 2.21: Coflex-F device [75].

Therefore, the second subject was to investigate the biomechanical behavior of the Coflex-F device and pedicle screw fixation, in combination with ALIF or TLIF in fusion surgery. In addition, Because of the PLIF surgical process needed to remove parts of the lamina bone and spinous process to get approach which may make the Coflex-F cannot implant in the interspinous process.

All types of fusion surgery approaches are recommended for combination with traditional pedicle screw fixation to increase stabilization and fusion rates. A pedicle screw can be used for unilateral or bilateral pedicle screw fixation. Unilateral pedicle screw fixation was used with the TLIF surgery to provide stability in minimally invasive surgery, but the asymmetric construct will result in spine segment destabilization and a decrease in spine stiffness. Therefore, supplementation of a translaminar facet screw is recommended to increase stability of TLIF combined with unilateral pedicle screw fixation (Figure 2.22) [76]. However, the Translaminar facet screw fixation requires long passage through the lamina for the crossing screws before they can traverse the facet joint, and necessitating a large surgical field [77][78][79].

The Coflex-F has been adopted to combine interbody fusion in minimally invasive surgery; however, the effectiveness of this procedure is still unclear.

The third subject was to investigate the biomechanical characteristics of TLIF combined with Coflex-F and supplemented with one unilateral pedicle screw fixation and one translaminar facet screw fixation implanted into the L3-L4 segment in minimally invasive lumbar fusion.

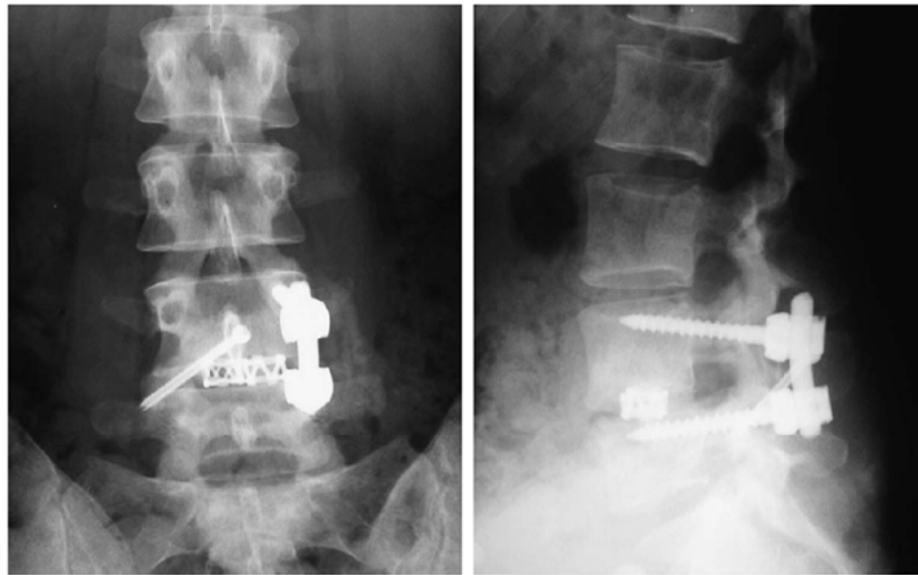


Figure 2.22: unilateral pedicle screw fixation and translaminar facet screw fixation [76].

Chapter 3 Materials and Methods

3.1 Coflex and Coflex-F in non-fusion surgery

The first subject of following sections includes FE modeling and simulation technique of this study. Five FE models of the lumbar spine were constructed for this study. The first model was the intact lumbar spine. The other four models were the defect lumbar spine, the defect lumbar spine combined with Coflex, defect lumbar spine combined with Coflex-F, and defect lumbar spine combined with pedicle screw fixation.

3.1.1 FE model of intact lumbar spine (Intact model)

To create a three-dimensional FE model, computed tomography scan DICOM files of the L1 to L5 lumbar spine of a middle-aged male were obtained at 1-mm intervals. The commercially available visualization software Amira 3.1.1 (Mercury Computer Systems, Inc., Berlin, Germany) was used to describe cross-section contours of each spinal component in accordance with gray scale value (Figure 3.1). Then, the three-dimensional surface geometries were constructed through sequential processed cross-section contours as shown in Figure 3.2 A. Each spinal component was exported as a Drawing eXchange Format (DXF) file and converted to the Initial Graphics Exchange Specification (IGES) file as shown in Figure 3.2 B. The FE analysis software ANSYS 9.0 (ANSYS Inc., Canonsburg, PA) was used to reconstruct the FE model by converting the IGES file to ANSYS Parametric Design Language (APDL) code in Figure 3.2 C. The INT model was an osseo-ligamentous lumbar spine, which included the vertebrae, intervertebral discs, endplates, posterior bony elements, and all seven ligaments (Figure 3.3 A).

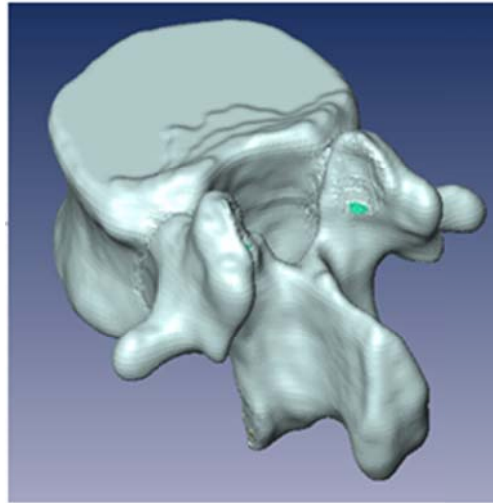
An eight-node solid element (SOLID185) was used for modeling the cortical bone, cancellous bone, posterior bony element, cartilage endplate, and annulus ground substance. The cortical bone and cancellous bone were assumed to be homogeneous and transversely

isotropic [81]. The posterior bony element and cartilage endplate were assumed to be homogeneous and isotropic [82]. The intervertebral disc consisted of annulus ground substance, nucleus pulposus and collagen fibers embedded in the ground substance. The nonlinear annulus ground substance was simulated by using a hyper-elastic Mooney-Rivlin formulation [83][84]. The collagen fibers simply connected between nodes on adjacent endplates to create an irregular criss-cross configuration. These irregular angles of collagen fibers were oriented within the range of the Marchand's [85] study. In the radial direction, twelve double cross-linked fiber layers were defined to decrease elastic strength proportionally from the outermost layer to the innermost. Therefore, the collagen fibers in different annulus layers were weighted (elastic modulus at the outermost layers 1-3: 1.0, layers 4-6: 0.9, layers 7-9: 0.75, and at the innermost layers 10-12: 0.65; cross sectional areas at the outermost layers 1-3: 1.0, layers 4-6: 0.78, layers 7-9: 0.62, and at the innermost layers 10-12: 0.47) based on previous studies [86][87]. The nucleus pulposus was modeled as an incompressible fluid with a bulk modulus of 1666.7 MPa by eight-node fluid elements (FLUID80) [81]. The 43 % of the cross-sectional area in the disc was defined as the nucleus, which was within the range of the study by Panagiotacopoulos (30-50 %) [88] Therefore, approximately 47 % to 49 % disc volume was assigned to nucleus pulposus. All seven ligaments and collagen fibers were simulated by two-node bilinear link elements (LINK10) with uniaxial tension resistance only, which were arranged in an anatomically correct direction [89]. The cross-sectional area of each ligament was obtained from previous studies [82][87][90][91], and material properties of the spine are listed in Table 3.1. The facet joint was treated as having sliding contact behavior using three-dimensional eight-node surface-to-surface contact elements (CONTA174), which may slide between three-dimensional target elements (TARGE170). The coefficient of friction was set at 0.1[92]. The initial gap between a pair of facet surfaces was kept within 0.5 mm as shown in Figure 3.3 (b) [81]. The stiffness of the spinal structure changes depending on the contact status, so

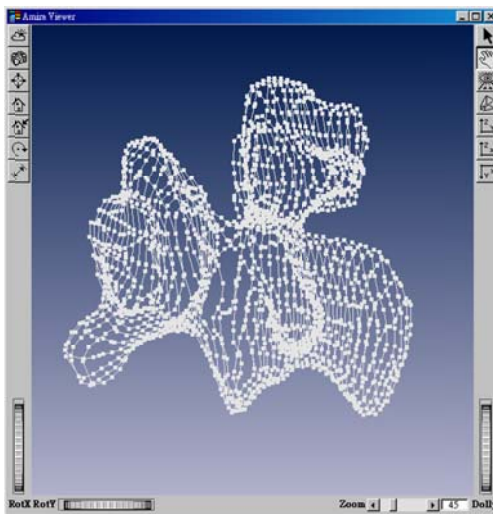
the standard contact option in ANSYS was adopted to account for the changing-states nonlinear problem in this study. In addition, the element's shape will change after applying bending moments, thus changing the individual element stiffness. Therefore, the large displacement analysis option in ANSYS was chosen to solve this geometric nonlinear problem. The INT model consisted of 84,584 elements and 94,162 nodes [93][94].



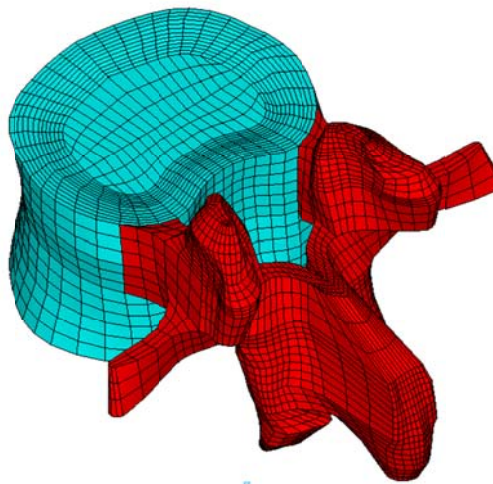
Figure 3.1: Each spinal component was selected from computed tomography scan DICOM file to create material-related contours.



(A)



(B)



(C)

Figure 3.2: Modeling process of the L3 vertebra: (A) surface geometries of vertebra were reconstructed through sequential processed computed tomography scan DICOM file; (B) surface geometry was exported to the DXF file; (C) FE model of the L3 vertebra.

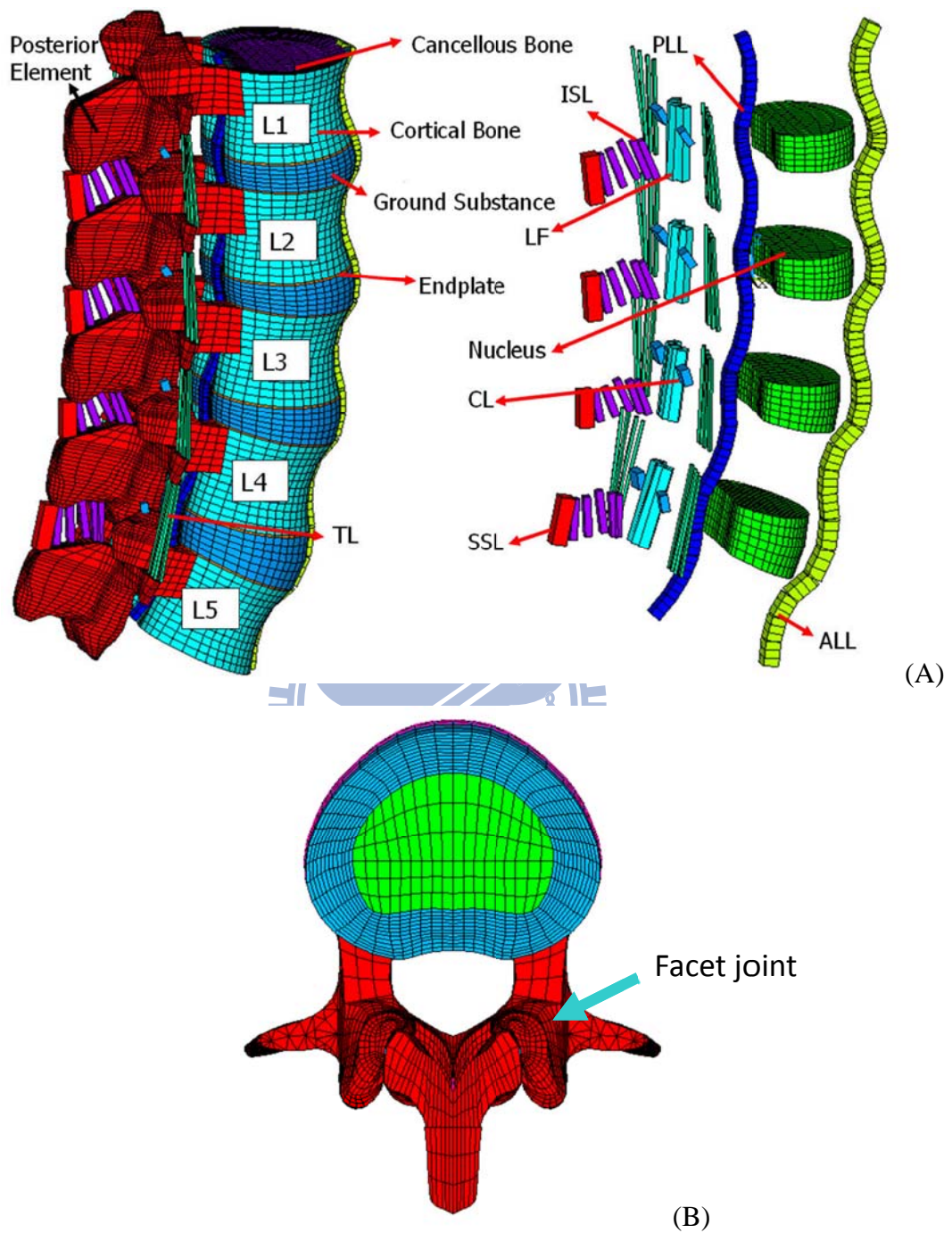


Figure 3.3: Finite element model of the L1 to L5 segments is shown: (A) intact model; (B) transverse views of facet joint curvature and gap.

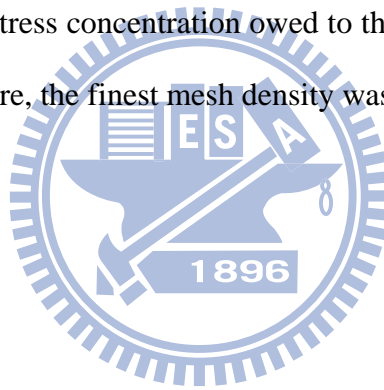
Table 3.1: Material properties used in the FE model

Material	Element type	Young's modulus (MPa)	Poisson's ratio	Area (mm ²)	References
Vertebral					
Cortical	8node-Solid 185	$E_x=11300$	$\nu_{xy}=0.484$	-	[81]
		$E_y=11300$	$\nu_{xz}=0.203$		
		$E_z=22000$	$\nu_{yz}=0.203$		
		$G_x=3800$			
		$G_y=5400$			
		$G_z=5400$			
Cancellous	8node-Solid 185	$E_x=140$	$\nu_{xy}=0.45$	-	[81]
		$E_y=140$	$\nu_{xz}=0.315$		
		$E_z=200$	$\nu_{yz}=0.315$		
		$G_x=48.3$			
		$G_y=48.3$			
		$G_z=48.3$			
Posterior bony element	8node-Solid 185	3500	0.25	-	[81]
Disc					
Nucleus pulposus	8node-Fluid 80	1666.7	-	-	[81]
Annulus Ground substance	8node-Solid 185	$C_{10}=0.42$	-	-	[83][84]
		$C_{01}=0.105$			
Annulus fibers	2node-Link 10				[86][87]
Outmost (1-3 layers)		550	-	0.76	
Second (4-6)		495	-	0.5928	
Third (7-9)		412.5	-	0.4712	
Innermost (10-12)		357.5	-	0.3572	
Cartilaginous endplates	8node-Solid 185	24	0.4	-	[81]
Ligaments*	2node-Link 10				[82][87][90]
ALL		7.8	-	24	[91]
PLL		10	-	14.4	
TL		10	-	3.6	
LF		15	-	40	
ISL		10	-	26	
SSL		8	-	23	
CL		7.5	-	30	

*ALL, anterior longitudinal ligament; PLL, posterior longitudinal ligament; TL, transverse ligament; LF, ligamentum flavum; ISL, interspinous ligament; SSL, supraspinous ligament; CL, capsular ligament.

In order to get reliable data, convergence test were conducted. Three mesh densities (coarse model: 4,750 elements / 4,960 nodes; normal model: 27,244 elements / 30,630 nodes; finest model: 112,174 elements / 94,162 nodes) were selected to test ROM in the intact model (Figure 3.4). The boundary and loading conditions of the test were that the inferior surface of L5 vertebra was fixed, and 10 N-m moment and a 150 N preload were applied to the superior surface of L1 vertebra.

Compared with normal model and finest model, the variation of ROM was within 1.03% in flexion (less than 0.2°), 4.39% in extension (less than 0.5°), 0.01% in axial rotation (less than 0.2°), and 0.001% in lateral bending (less than 0.1°). From the simulation results, the normal model only required fewer computational times to complete. However, several contact surfaces in facet joint have stress concentration owed to the lower smooth geometry for fewer elements and nodes. Therefore, the finest mesh density was selected in this study.



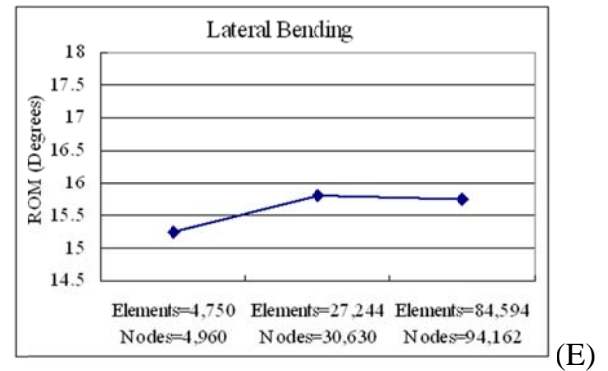
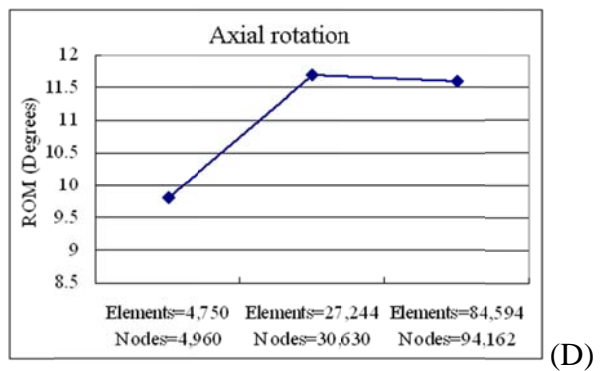
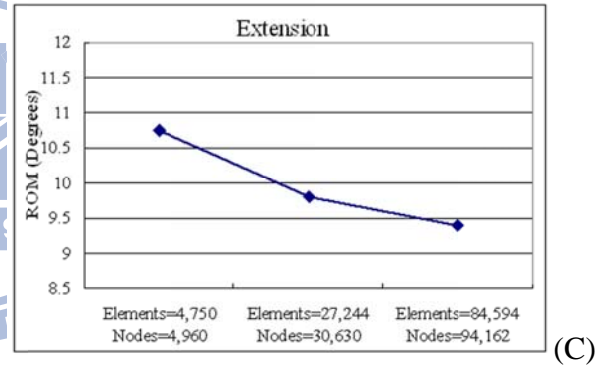
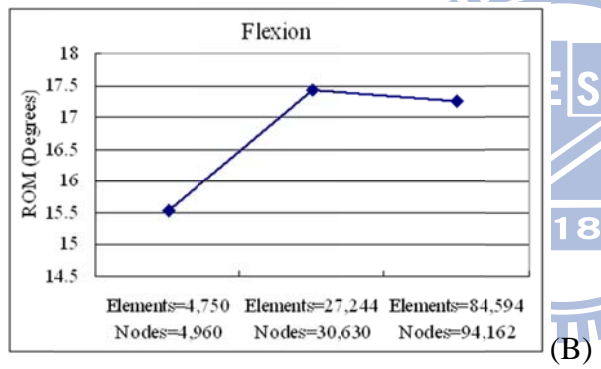
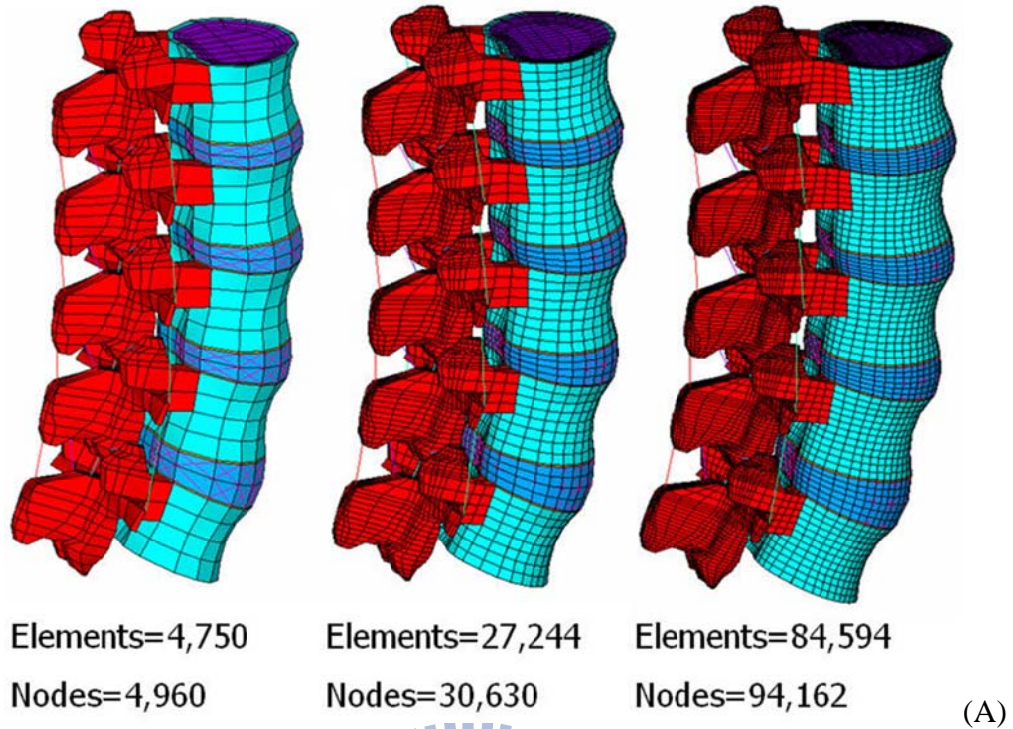


Figure 3.4: Convergence test of the intact model: (A) three mesh densities were selected; (B) result of motion changes under flexion; (C) result of motion changes under extension; (D) result of motion changes under axial rotation; (E) result of motion changes under lateral bending.

3.1.2 FE model of Coflex implanted into the L3-L4 segment (Coflex model)

This model was a defect model implanted with the Coflex device at the L3-L4 segment. The defect model was used to simulate decompression and instability by cutting the ligamentum flavum, the facet capsules, and 50 % of the inferior bony facet bilaterally at the L3-L4 segment [55][57]. The process is designed to remove a small portion of the bone to give the nerve root more space and prevents nerve compression. In addition, the supraspinous ligaments and interspinous ligaments had to be resected before insertion.

The Coflex device is available in five sizes from 8 mm through 16 mm in 2-mm increments. The most suitable size of Coflex device was chosen based on the patient's lumbar spine. In this study, a height of 14 mm was the best fit to our FE model. The geometry of the Coflex device was re-created by CAD software from the real product and then transferred into the ANSYS software to construct the Coflex FE model. To implant the Coflex device (Figure 3.5 A), part of the L3-L4 interspinous process was removed to provide sufficient space into which the Coflex could be placed between the interspinous processes. The surface between the spinous processes and the wings of the Coflex was modeled as a surface-to-surface contact. The effect of teeth on the wings of the Coflex device was simplified by assigning a higher coefficient of friction (0.8) to the wing contact area (Figure 3.5 A, yellow region), and the coefficient of friction for the rest of the contact regions was set to 0.1 (Figure 3.5 A, red region). The higher coefficient of friction (0.8) was used in the contact interface to prevent device slip motion [86]. The material used for the Coflex device was Ti-6Al-4V alloy. The Young's modulus and Poisson's ratio were respectively assigned to be 113 GPa and 0.3.

3.1.3 FE model of Coflex-F implanted into the L3-L4 segment (Coflex-F model)

This model was a defect model implanted with the Coflex-F device at the L3-L4 segment. The defect model was used to simulate instability by cutting the ligamentum flavum, the facet capsules, and 50 % of the inferior bony facet bilaterally at the L3-L4 segment [55][57]. In

addition, the supraspinous ligaments and interspinous ligaments had to be resected before insertion.

The Coflex-F differs from the original Coflex implant by adding two rivets joining the wings and spinous processes (Fig 3.5 B). The effect of the teeth on the wings of the Coflex-F was also simplified by assigning a higher coefficient of friction (0.8) to the wing contact area (Fig 3.5 B, yellow region), and the coefficient of friction for the rest of the contact regions was set to 0.1 (Figure 3.5 B, red region). The rivets were simplified as cylinders and were constrained to both holes on the wings of the Coflex and the spinous processes in all degrees of freedom (The degrees of freedom of rivet nodes are interpolated with the corresponding degrees of freedom of the nodes on the Coflex and spinous processes during the execution of ANSYS program). The material used for the Coflex-F was a Ti-6Al-4V alloy. The Young's modulus and Poisson's ratio were respectively assigned to be 113 GPa and 0.3.

3.1.4 FE model of bilateral pedicle screw fixation into the L3-L4 segment (Pedicle screw fixation Model)

This model was a defect model implanted with pedicle screw fixation at the L3-L4 segment. The difference between the pedicle screw fixation model and the above implantation models was that the pedicle screw fixation model preserved the supraspinous ligaments and interspinous ligaments (Figure 3.5 C). The pedicle screw fixation consisted of two rods (diameter, 4.5 mm) and four pedicle screws (diameter, 6 mm). The pedicle screws were inserted through the pedicles of the L3 and L4 vertebrae bilaterally. The pedicle screws were simplified as cylinders. The screw-bone interfaces were assigned to be fully constrained. The material used for the pedicle screws was Ti-6Al-4V. The Young's modulus and Poisson's ratio were assigned to be 113 GPa and 0.3, respectively.

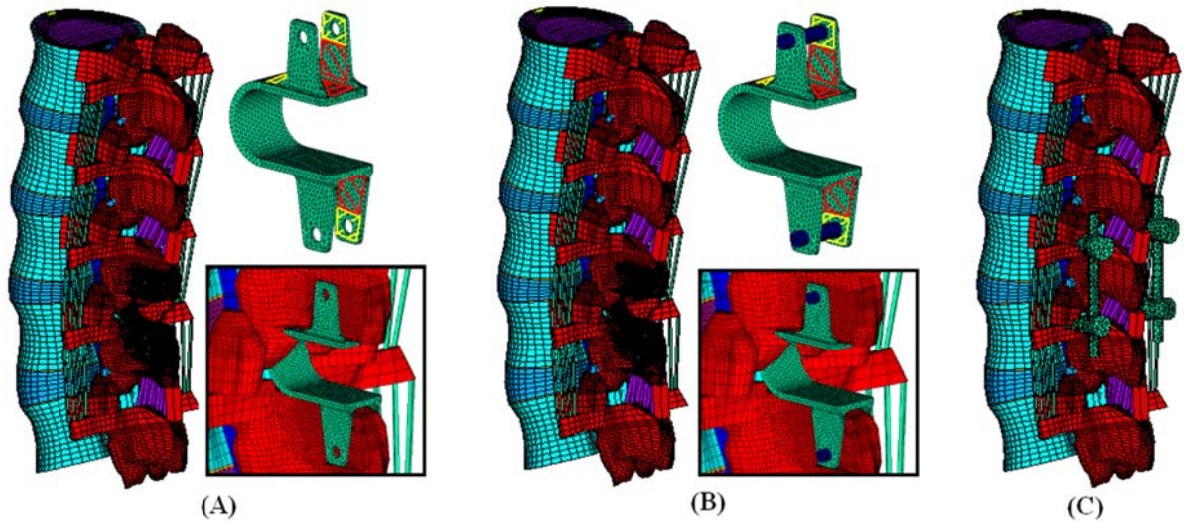


Figure 3.5: Finite element models of the L1-L5 lumbar spine: (A) defect model implanted with Coflex at L3-L4 segment (Coflex model); (B) defect model implanted with Coflex-F at L3-L4 segment (Coflex-F model); (C) defect model implanted with bilateral pedicle screw fixation (pedicle screw fixation model).

3.1.5 Boundary and loading conditions

(1) Follower load

For the preload method, traditional vertical preloads are unable to support the kinematics study of long lumbar spine specimens under higher physiological compressive loads because the spine without active musculature buckles under just 120 N of vertical preload (Figure 3.6 A) [95][98].

Patwardhan *et al.* [95] proposed a follower load to mimic the more realistic physiological compressive loads seen *in vivo* (Fig 3.6 B). This consists of a compressive load applied along a follower load path that approximates the tangent to the curve of the lumbar spine, thus subjecting the whole lumbar spine to nearly pure compression. Besides follower load, there are several methods have been presented for mimicking the role of muscles.

In this study, the follower load was adopted and simulated at each motion segment in the model through the use of two-node thermal link elements (Figure 3.6 C). The 400 N compressive follower load was applied to each motion segment through induced contraction

in these link elements by decreasing the temperature [99][100]. The link elements were attached near the centers of each vertebral body such that each element spanned the mid-plane of the discs. With these arrangements, a nearly ideal follower load was constructed, which remains tangent to the spine curve, and each spinal segment would be loaded in nearly pure compression without artifact motions.

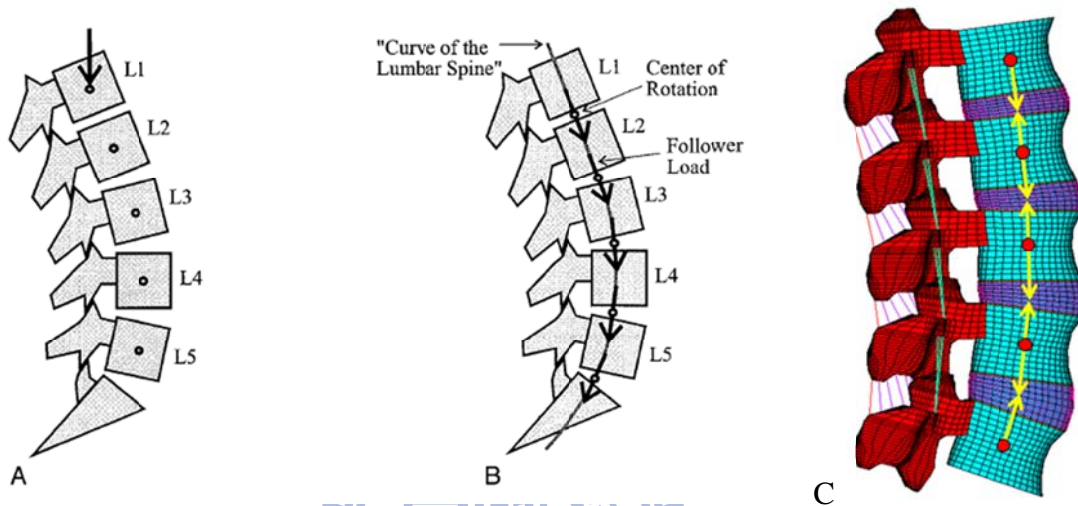


Figure 3.6: (A) Illustration of traditional vertical preloads [95]; (B) Illustration of follower load [95]; (C) Intact lumbar spine model with follower load.

(2) Validation of intact lumbar spine model with follower load

For the follower load model validation, the ROM of the intact model under different loading moments was compared to Rohlmann's [101] *in vitro* cadaveric study. Under 7.5 N-m moments without preload and with a 280 N follower load, the total ROM of five segments lumbar were within one standard deviation in flexion-extension, axial rotation, and lateral bending. The results are shown in Figure 3.7. The present model was verified for further simulations.

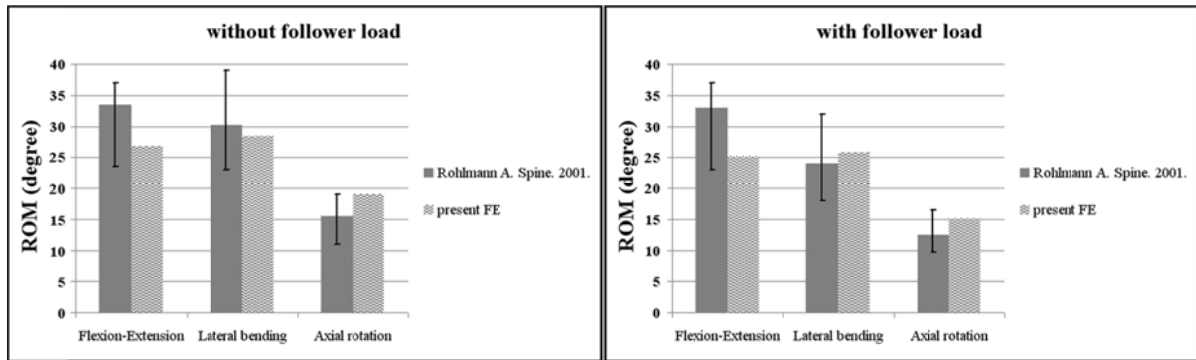


Figure 3.7: Range of motion (ROM) calculated for the L1-L5 segments of intact lumbar spine is compared to previous *in vitro* experiments. Intact lumbar spine without follower load (Left); intact lumbar spine with follower load (Right).

(3) Hybrid test method

The hybrid test method was first introduced by Panjabi in 2002 [102]. This approach applies different pure moments to each of the spinal constructs, and then the same overall ROMs are achieved for both intact and implant models. The detailed description about this method has been presented in 2007 (Figure 3.8) [103]. The four steps of the Hybrid test method are described in detail as below.

1. First, the specimen and its preparation. In order to reveal characteristic of motion re-distribution, whole mobile region should be tested. Therefore, the specimen of a T12-S1 long segment is recommended for *in vitro* test.
2. Second, intact spine test. The traditional load control method is used for testing intact lumbar spine, and the specimens should not cause of injury during the test. Then, the total ROM of intact lumbar spine is measured.
3. Third, spinal construct test. The spinal construct (specimen with a fusion and/or a non-fusion device) is subjected to increasing pure unstrained moment until the total ROM of the construct equals the ROM of the intact measured under the load control method (step 2).
4. Fourth, data analysis. In order to evaluate adjacent segment effects, the increase in ROM or other biomechanical parameters at a non-operated spinal segment should be measured.

Goel *et al.* [104] indicated that, in real life, people bend their spines within a similar, limited ROM regardless of whether their spine is healthy or has undergone spinal surgery. In

addition, the patient's main aim following surgery is to go back to normal daily life. Thus, the surgically treated spine should be able to go through the same ROM as in a normal person. Therefore, they suggested that the spinal construct should be tested under the same ROM and the hybrid test method should be more clinically relevant.

In this study, by applying bending moments from the hybrid test method, a 400 N follower load was first applied on the superior surface of the L1 vertebra, and then a moment of 30 N-m was applied incrementally by 1 Nm in 30 loading steps. Therefore, the resultant total ROMs of the implantation models (L1 to L5) under different moments would match the total ROMs of the intact lumbar model which was subjected to 10 N-m loadings according to the *in vitro* study of Yamamoto *et al.*[105]. The detailed total lumbar ROMs of the intact model under the hybrid test method are 16.37° in flexion, 10.75° in extension, 15.27° in right lateral bending, and 8.44° in right axial rotation. These ROMs are a baseline with which to match the total lumbar motion among the intact and implantation models under the hybrid test method (Table 3.2). The resulting deviation of ROMs among the three FE models were controlled to within 0.64° in flexion, 0.14° in extension, 0.63° in right lateral bending, and 0.22° in right axial rotation.

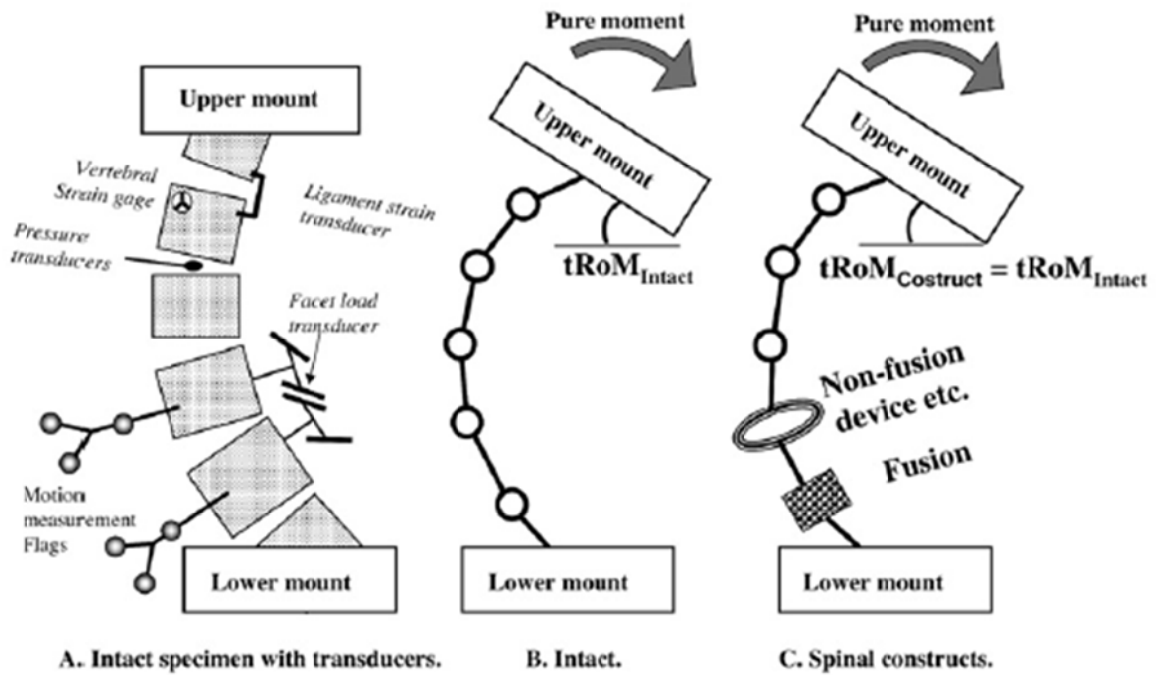
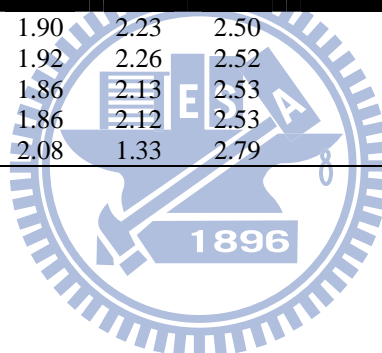


Figure 3.8: Illustration of the Hybrid test method. (A) Whole spine specimen with various transducers and markers to monitor biomechanical parameters of interest. (B) Appropriate unconstrained pure moment is applied to the intact specimen to produce physiological motions. Resulting main total range of motion ($TROM_{Intact}$) is recorded. (C) Unconstrained pure moment is applied to the spinal construct produce main total range of motion $TROM_{Construct}$ equal to $TROM_{Intact}$. [103]

Table 3.2 Intervertebral range of motion and applied moment among the intact, defect, and implantation models under the hybrid test method.

Model	ROM (degree)				Total lumbar ROM(degree) (L1-L5)	Moment(Nm)
	L1-L2	L2-L3	L3-L4	L4-L5		
Flexion						
Intact	3.66	3.78	3.82	5.11	16.37	10
Defect	3.62	3.75	4.32	5.05	16.74	10
Coflex	3.49	3.63	4.14	4.84	16.10	10
Coflex-F	4.33	4.47	1.87	6.01	16.68	12
Pedicle screw fixation	4.51	4.67	1.23	6.31	16.72	13
Extension						
Intact	2.70	2.47	2.30	3.27	10.74	10
Defect	2.37	2.05	3.75	2.61	10.78	8
Coflex	3.36	3.06	0.68	3.89	10.99	14
Coflex-F	3.36	3.08	0.54	3.92	10.90	14
Pedicle screw fixation	3.24	2.93	0.22	4.11	10.50	13
Lateral bending						
Intact	3.69	3.59	3.67	4.32	15.27	10
Defect	3.69	3.62	3.69	4.33	15.33	10
Coflex	3.72	3.65	3.39	4.34	15.10	10
Coflex-F	3.78	3.70	3.01	4.43	14.92	10
Pedicle screw fixation	4.41	4.17	1.74	5.23	15.55	13
Axial rotation						
Intact	1.81	1.90	2.23	2.50	8.44	10
Defect	1.83	1.92	2.26	2.52	8.53	10
Coflex	1.80	1.86	2.13	2.53	8.32	10
Coflex-F	1.80	1.86	2.12	2.53	8.31	10
Pedicle screw fixation	2.17	2.08	1.33	2.79	8.37	13



3.2 Coflex-F in fusion surgery

The second subject of following sections includes FE modeling and simulation technique of this study. The first model of second subject was the intact lumbar spine same first subject (3.1.1) model. The other five models were the TLIF or ALIF combined with Coflex-F and TLIF or ALIF combined with bilateral pedicle screw fixation.

3.2.1 FE model of TLIF combined with Coflex-F (Coflex-F + TLIF model)

The intact model was modified to a TLIF model by implanting an AVS-TL cage (30 mm width x 11 mm depth x 21 mm height; Polyetheretherketon (PEEK); Stryker Orthopaedics) (Figure 3.9 E) between the L3 and L4 vertebrae. To simulate the standard TLIF procedure, unilateral total facetectomy and partial discectomy were performed at the L3-L4 segment. The left facet joint, ligamentum flavum, and partial disc were removed, but the posterior elements, contralateral facet joint, supraspinous ligaments, and interspinous ligaments were preserved. The cage-bone interface was modeled by surface-to-surface contact elements to simulate the early postoperative stage after spinal implantation. These contact elements were able to transmit compression, but not tension. The coefficient of friction at the cage-bone interface was set at 0.8 to mimic the effect that the cage's small teeth have on contact surfaces. The higher coefficient of friction (0.8) was used in the contact interface to prevent device slip motion [86]. The Young's modulus and Poisson's ratio of AVS-TL cage were assigned to be 3.5 GPa and 0.3, respectively.

The TLIF model was again modified to implant the Coflex-F device between the L3 and L4 vertebrae to complete the Coflex-F combined with TLIF model, requiring the removal of supraspinous ligaments and interspinous ligaments (Figure 3.9 A). The Coflex-F is available in five sizes from 8-16 mm in 2 mm increments. In this study, the optimal height for the FE model was 14 mm. Part of the L3-L4 interspinous process was removed to provide sufficient space for implanting the Coflex-F between the interspinous processes. The surface between

the spinous processes and the wings of the Coflex-F was modeled as a surface-to-surface contact. The effect of the teeth on the wings of the Coflex-F was simplified by assigning a higher coefficient of friction (0.8) to the wing contact area (Figure 3.9 G, yellow region), and the coefficient of friction for the rest of the contact regions was set at 0.1 (Figure 3.9 G, red region). The rivets were modeled as cylinders (diameter = 2.8 mm) and were constrained to both holes on the wings of the Coflex-F and the spinous processes in all degrees of freedom (The degrees of freedom of rivet nodes are interpolated with the corresponding degrees of freedom of the nodes on the Coflex and spinous processes during the execution of ANSYS program). The Coflex-F was constructed using Ti-6Al-4V alloy. The Young's modulus and Poisson's ratio were assigned to be 113 GPa and 0.3, respectively.

3.2.2 FE model of ALIF combined with Coflex-F (Coflex-F + ALIF model)

The intact model was modified to an ALIF model by implanting a SynCage-Open cage (Figure 3.9 F) (30 mm width x 24 mm depth x 21 mm height; Titanium alloy; Synthes spine, Inc.) between the L3 and L4 vertebrae. To simulate the standard ALIF procedure, the L3-L4 segment of the intact model underwent partial discectomy and total nucleotomy by the anterior approach, which included removal of the anterior longitudinal ligament, anterior portions of the annulus, and the entire nucleus pulposus. All the other ligaments were preserved. The ALIF cage-bone has the same interface conditions as those of the TLIF cage-bone in section 2.2. The SynCage-Open cage was constructed out of Ti-6Al-7Nb alloy. The Young's modulus and Poisson's ratio were assigned to be 110 GPa and 0.28, respectively. In addition, the ALIF model was modified for implanting the Coflex-F between the L3 and L4 vertebrae to complete the Coflex-F combined with ALIF model. The ALIF model and the TLIF model implant the Coflex-F under the same conditions (Figure 3.9 B).

3.2.3 FE model of TLIF combined with bilateral pedicle screw fixation (Pedicle screw + TLIF model)

The previous TLIF model was combined with bilateral pedicle screws to form the pedicle screw fixation model (Figure 3.9 C). The difference between the pedicle screw fixation model and the Coflex-F model is that the pedicle screw fixation model preserves the supraspinous ligaments and interspinous ligaments. The pedicle screws were inserted bilaterally through the pedicles of the L3 and L4 vertebrae. The pedicle screw fixation in this study consisted of two rods (diameter = 4.5 mm) and four pedicle screws (diameter = 6 mm). The pedicle screws were modeled as cylinders. The screw-bone interfaces were designed to be fully constrained (The degrees of freedom of screw nodes are interpolated with the corresponding degrees of freedom of the nodes on the Coflex and spinous processes during the execution of ANSYS program). The pedicle screws were made of Ti-6Al-4V alloy. The Young's modulus and Poisson's ratio were assigned to be 113 GPa and 0.3, respectively.

3.2.4 FE model of ALIF combined with bilateral pedicle screw fixation (Pedicle screw + ALIF model)

The previous ALIF model was combined with bilateral pedicle screws (Figure 3.9 D). This model preserved the supraspinous ligaments and interspinous ligaments. Both this model and the previous TLIF model (combined with bilateral pedicle screws) used the same conditions and materials for pedicle screws.

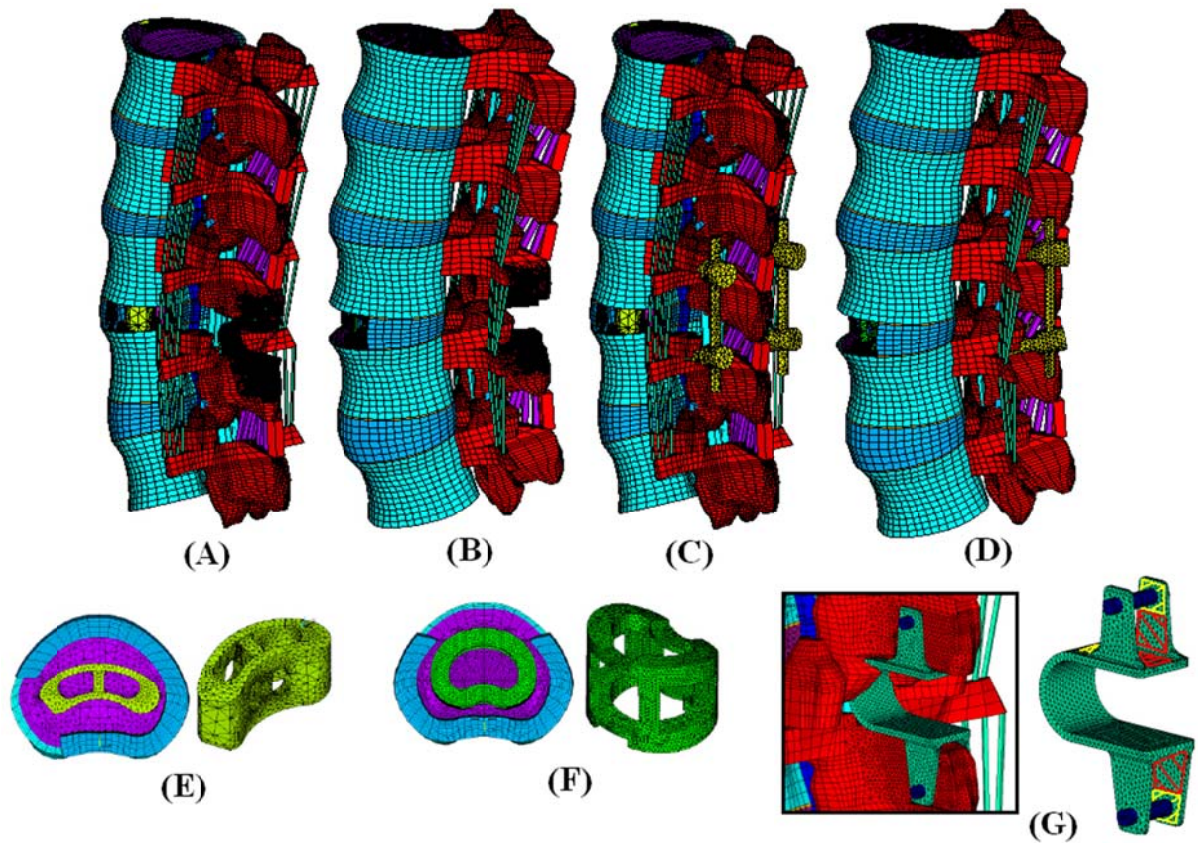


Figure 3.9: Finite element models: (A) Coflex-F device combined with the TLIF model; (B) Coflex-F device combined with the ALIF model; (C) Pedicle screw fixation combined with the TLIF model; (D) Pedicle screw fixation combined with the ALIF model; (E) AVS-TL cage in the middle portion of the vertebral model; (F) SynCage-Open cage in the middle portion of the vertebral model; (G) Coflex-F device model.

3.2.5 Boundary and loading conditions

In this second subject, the boundary and loading conditions are all same first subject (3.1.5). The 400 N compressive follower load was applied to each motion segment through induced contraction in these link elements by decreasing the temperature. The link elements were attached near the centers of each vertebral body such that each element spanned the mid-plane of the discs. These arrangements directed the construction of a nearly ideal follower load, which remains tangent to the spine curve, loading each spinal segment in nearly pure compression.

A 10 Nm moment was applied to the intact model to mimic physiological motion [105]. These motions subject the multilevel lumbar spine to a maximal possible load without causing spinal injury. The other implanted models under comparison were subjected to specific moments that produced overall motions that were equal to those of the intact model, using a hybrid test method. The detailed total lumbar ROMs of the intact model under the hybrid test method are 16.36° in flexion, 10.31° in extension, 15.25° in lateral bending to both sides, and 8.43° in axial rotation to both sides. These ROMs are a baseline to match the total lumbar motion among the intact and implantation models under the hybrid test method (Table 3.3). The resulting deviation of ROMs among the three FE models were controlled to within 0.33° in flexion, 0.56° in extension, 0.22° in right lateral bending, 0.24° in left lateral bending, 0.21° in right axial rotation, and 0.21° in left axial rotation.

Table 3.3 Intervertebral range of motion and applied moment among various surgical models under the hybrid test method.

Model	ROM (deg)				Total lumbar ROM(deg) (L1-L5)	Moment(Nm)
	L1-L2	L2-L3	L3-L4	L4-L5		
Flexion						
Intact	3.66	3.78	3.82	5.10	16.36	10
Coflex-F+TLIF	4.37	4.54	0.96	6.38	16.25	12
Coflex-F+ALIF	4.46	4.60	0.92	6.44	16.42	12
Pedicle screw + TLIF	4.40	4.59	0.62	6.48	16.09	12
Pedicle screw + ALIF	4.49	4.66	0.61	6.47	16.23	12
Extension						
Intact	2.27	2.47	2.30	3.27	10.31	10
Coflex-F+TLIF	3.26	3.17	0.43	4.01	10.87	11
Coflex-F+ALIF	3.33	3.01	0.55	3.96	10.85	12
Pedicle screw + TLIF	3.26	3.16	0.27	4.16	10.85	11
Pedicle screw + ALIF	3.32	2.98	0.22	4.09	10.61	12
Right lateral bending						
Intact	3.69	3.59	3.67	4.30	15.25	10
Coflex-F+TLIF	4.08	3.97	2.40	5.00	15.45	11
Coflex-F+ALIF	4.46	4.37	1.26	5.15	15.24	12
Pedicle screw + TLIF	4.47	4.32	1.17	5.50	15.46	12
Pedicle screw + ALIF	4.48	4.35	0.92	5.54	15.29	12
Left lateral bending						
Intact	3.69	3.59	3.67	4.30	15.25	10
Coflex-F+TLIF	4.11	4.03	1.95	5.07	15.16	11
Coflex-F+ALIF	4.46	4.37	1.26	5.15	15.24	12
Pedicle screw + TLIF	4.47	4.38	1.04	5.51	15.40	12
Pedicle screw + ALIF	4.48	4.35	0.92	5.54	15.29	12
Right axial rotation						
Intact	1.81	1.90	2.23	2.49	8.43	10
Coflex-F+TLIF	2.00	2.09	1.52	2.80	8.41	11
Coflex-F+ALIF	2.12	2.19	1.06	2.94	8.31	12
Pedicle screw + TLIF	2.29	2.22	0.81	2.99	8.31	13
Pedicle screw + ALIF	2.38	2.31	0.70	3.13	8.52	14
Left axial rotation						
Intact	1.81	1.90	2.23	2.49	8.43	10
Coflex-F+TLIF	2.01	2.09	1.44	2.81	8.35	11
Coflex-F+ALIF	2.12	2.19	1.06	2.94	8.31	12
Pedicle screw + TLIF	2.29	2.22	0.81	2.99	8.31	13
Pedicle screw + ALIF	2.38	2.31	0.70	3.13	8.52	14

3.3 Coflex-F in minimally invasive fusion surgery

The third subject of following sections includes FE modeling and simulation technique of this study. The first model of third subject was the intact lumbar spine same first subject (3.1.1) model. The other three models were the TLIF combined with Coflex-F, with unilateral pedicle screw fixation and translaminar facet screw fixation model, and with bilateral pedicle screw fixation.

3.3.1 FE model of TLIF combined with Coflex-F (Coflex-F model)

The intact model was modified to TLIF model and implant Coflex-F between L3 and L4 (Figure 10 A). The model of third subject was the Coflex-F same second subject (3.2.1) model. Both this model and the previous TLIF combined with Coflex-F model used the same conditions and materials.

3.3.2 FE model of TLIF combined with unilateral pedicle screw fixation with translaminar facet screw fixation (UPSF+TFSF model)

The previous TLIF model was combined with pedicle screws between L3 and L4. The pedicle screw fixation consisted of one rods (diameter = 4.5 mm) and two pedicle screws (diameter= 6 mm). The pedicle screws were inserted respectively through the pedicles of L3 and L4 vertebrae unilaterally. The UPSF model was combined with translaminar facet screw fixation (diameter= 4 mm) (Figure 10 B). The unilateral pedicle screw and translaminar facet screw were modeled as cylinders and screw-bone interfaces were designed to be fully constrained. The material used for the pedicle screws and fact screw were Ti-6Al-4V alloy. The Young's modulus and Poisson's ratio were assigned to be 113 GPa and 0.3.

3.3.3 FE model of TLIF combined with bilateral pedicle screw fixation (BPSF model)

The intact model was modified to TLIF combined with bilateral pedicle screw fixation between L3 and L4 (Figure 10 C). The model of third subject was the TLIF combined with bilateral pedicle screw fixation same second subject (3.2.3) model. Both this model and the previous TLIF combined with bilateral pedicle screw fixation model used the same conditions and materials.

3.3.4 Boundary and loading conditions

In this third subject, the boundary and loading conditions is all same 3.1.5 and 3.2.5 sections. A 400 N follower load and a 10 N-m moment were applied to the intact model to obtain physiological motions as comparison baseline. The implanted models were subjected to 400 N follower load and specific moments in accordance with the hybrid test method.

These ROMs are a baseline to match the total lumbar motion among the intact and implantation models under the hybrid test method (Table 3.4). The resulting deviation of ROMs among the three FE models were controlled to within 0.35° in flexion, 0.46° in extension, 0.29° in right lateral bending, 0.16° in left lateral bending, 0.11° in right axial rotation, and 0.11° in left axial rotation.

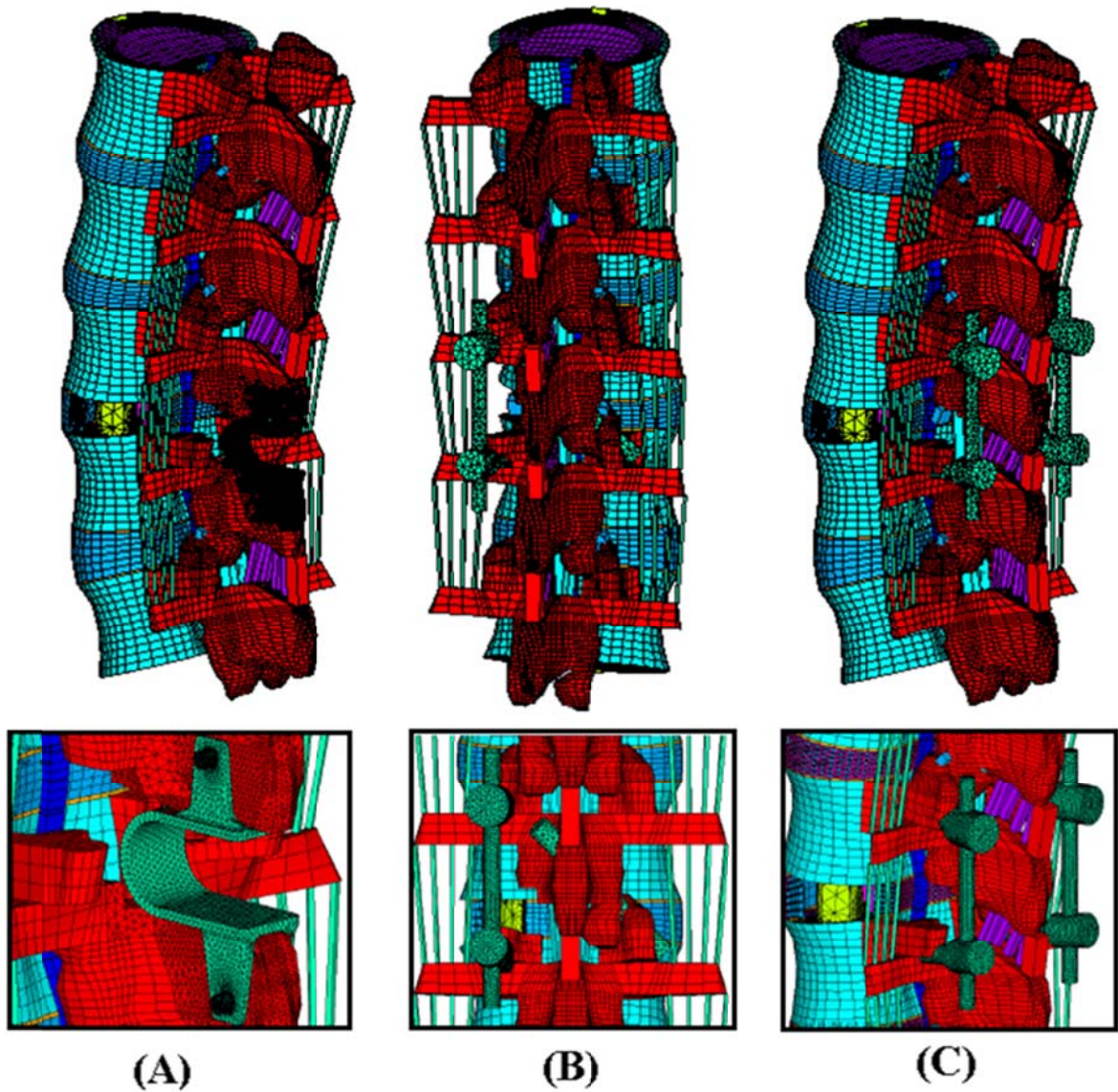


Figure 3.10: Finite element models: (A) TLIF combined with Coflex-F device; (B) TLIF model combined with unilateral pedicle screw fixation with translaminar facet screw fixation; (C) TLIF model combined with pedicle screw fixation.

Table 3.4 Intervertebral range of motion and applied moment among various surgical models under the hybrid test method.

Model	ROM (deg)				Total lumbar ROM(deg) (L1-L5)	Moment(Nm)
	L1-L2	L2-L3	L3-L4	L4-L5		
Flexion						
Intact	3.66	3.78	3.82	5.10	16.36	10
Coflex-F	4.37	4.54	0.96	6.38	16.25	12
UPSF + TFSF	4.38	4.56	0.61	6.43	16.01	12
BPSF	4.40	4.59	0.62	6.48	16.09	12
Extension						
Intact	2.27	2.47	2.30	3.27	10.31	10
Coflex-F	3.26	3.17	0.43	4.01	10.87	11
UPSF + TFSF	3.26	3.17	0.23	4.17	10.83	11
BPSF	3.26	3.16	0.27	4.16	10.86	11
Right lateral bending						
Intact	3.69	3.59	3.67	4.30	15.25	10
Coflex-F	4.08	3.97	2.40	5.00	15.45	11
UPSF + TFSF	4.46	4.35	1.23	5.48	15.54	12
BPSF	4.40	4.32	1.17	5.50	15.40	12
Left lateral bending						
Intact	3.69	3.59	3.67	4.30	15.25	10
Coflex-F	4.11	4.03	1.95	5.07	15.16	11
UPSF + TFSF	4.48	4.36	0.99	5.55	15.40	12
BPSF	4.47	4.38	1.04	5.51	15.41	12
Right axial rotation						
Intact	1.81	1.90	2.23	2.49	8.43	10
Coflex-F	2.00	2.09	1.52	2.80	8.41	11
UPSF + TFSF	2.28	2.24	0.77	3.01	8.32	13
BPSF	2.29	2.22	0.81	2.99	8.32	13
Left axial rotation						
Intact	1.81	1.90	2.23	2.49	8.43	10
Coflex-F	2.01	2.09	1.44	2.81	8.35	11
UPSF + TFSF	2.28	2.33	0.77	3.02	8.42	13
BPSF	2.29	2.22	0.81	2.99	8.32	13

Chapter 4 Results

4.1 Coflex and Coflex-F in non-fusion surgery

Biomechanical behaviors of the lumbar spine with the Coflex model, the Coflex-F model, and the pedicle screw fixation model were compared with those of the intact model. Data were normalized with respect to the intact model as percentage values under each loading condition.

4.1.1 Range of motion (ROM)

In extension, the ROM increased 64 % in the defect model at the surgical segment (Figure 4.1). After implantation, the ROM effectively decreased 70 % in the Coflex model, 76 % in the Coflex-F model, and 90 % in the pedicle screw fixation model as compared with the intact model. In addition, the ROM increased 24 % in the Coflex and Coflex-F models at the adjacent L1-L3 segments and increased 20 % at the adjacent L4-L5 segment. The ROM increased 19 % in the pedicle screw fixation model at the adjacent L1-L3 segments and increased 25 % at the adjacent L4-L5 segment.

In flexion, the ROM increased 13 % in the defect model and 8 % in the Coflex model at the surgical segment (Figure 4.2). In contrast to the above two models, the ROM decreased 52 % in the Coflex-F and 68 % in the pedicle screw fixation models at the surgical segment. On the other hand, the ROMs of the defect model and the Coflex model were similar to that of the intact model at both adjacent L1-L3 (deviation within 4 %) and L4-L5 segments (deviation within 4 %). However, the ROM increased 17 % to 18 % in the Coflex-F model and 23 % to 24 % in the pedicle screw fixation model at both adjacent L1-L3 and L4-L5 segments.

In lateral bending, the ROM decreased 8 % in the Coflex model, decreased 20 % in the Coflex-F model, and decreased 51 % in the pedicle screw fixation model at the surgical segment as compared with the intact model (Figure 4.3). The ROMs of the Coflex and Coflex-F models were similar to that of the intact model at both adjacent L1-L3 (1 % to 2 %)

and L4-L5 segments (1 % to 2 %). However, the ROM increased 16 % to 23 % in the pedicle screw fixation model at both adjacent L1-L3 and L4-L5 segments.

In axial rotation, the ROM decreased 4.3 % in the Coflex model, decreased 4.8 % in the Coflex-F model, and decreased 40 % in the pedicle screw fixation model at the surgical segment as compared with the intact model (Figure 4.4). The ROMs of the defect, Coflex, and Coflex-F models were similar to that of the intact model at both adjacent L1-L3 (deviation within 2 %) and L4-L5 segments (deviation within 2 %). However, in the pedicle screw fixation model, the ROM increased 20 % at the adjacent L1-L2 segment, increased 10 % at the adjacent L2-L3 segment, and increased 14 % at the adjacent L4-L5 segment.

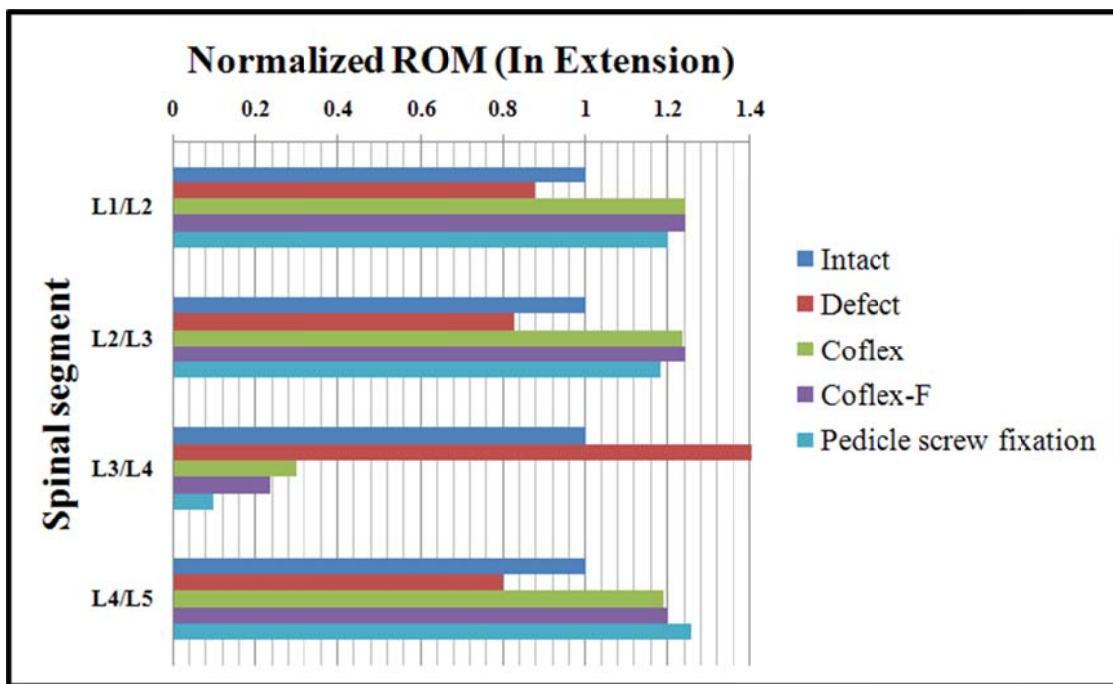


Figure 4.1: Range of motion normalized to intact model in extension.

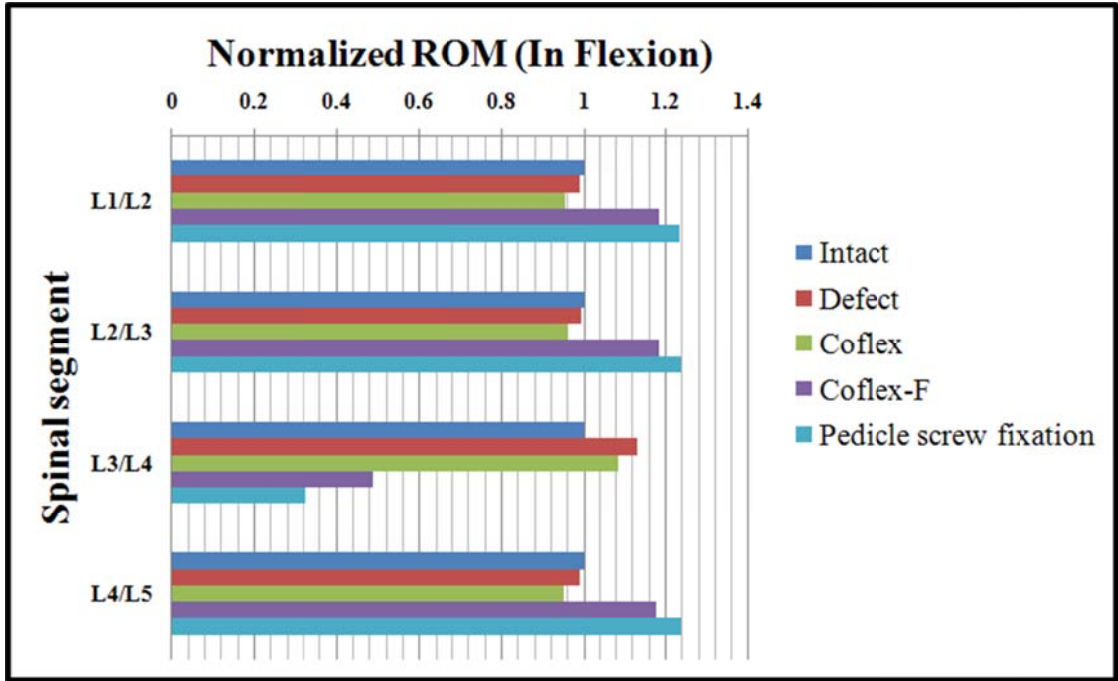


Figure 4.2: Range of motion normalized to intact model in flexion.

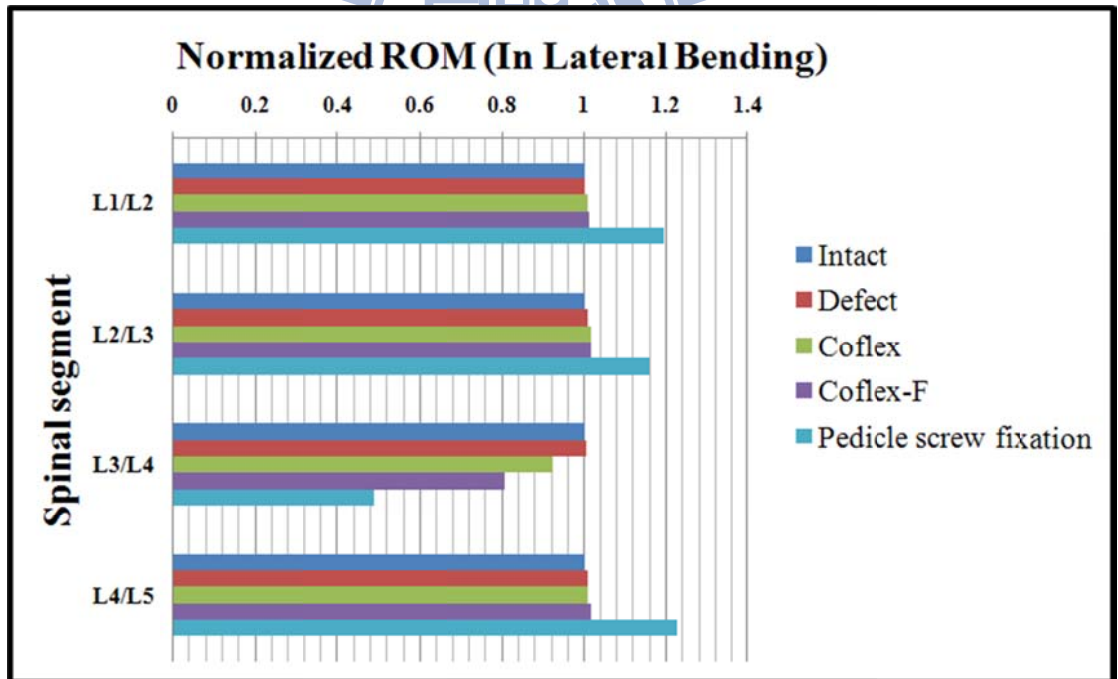


Figure 4.3: Range of motion normalized to intact model in lateral bending.

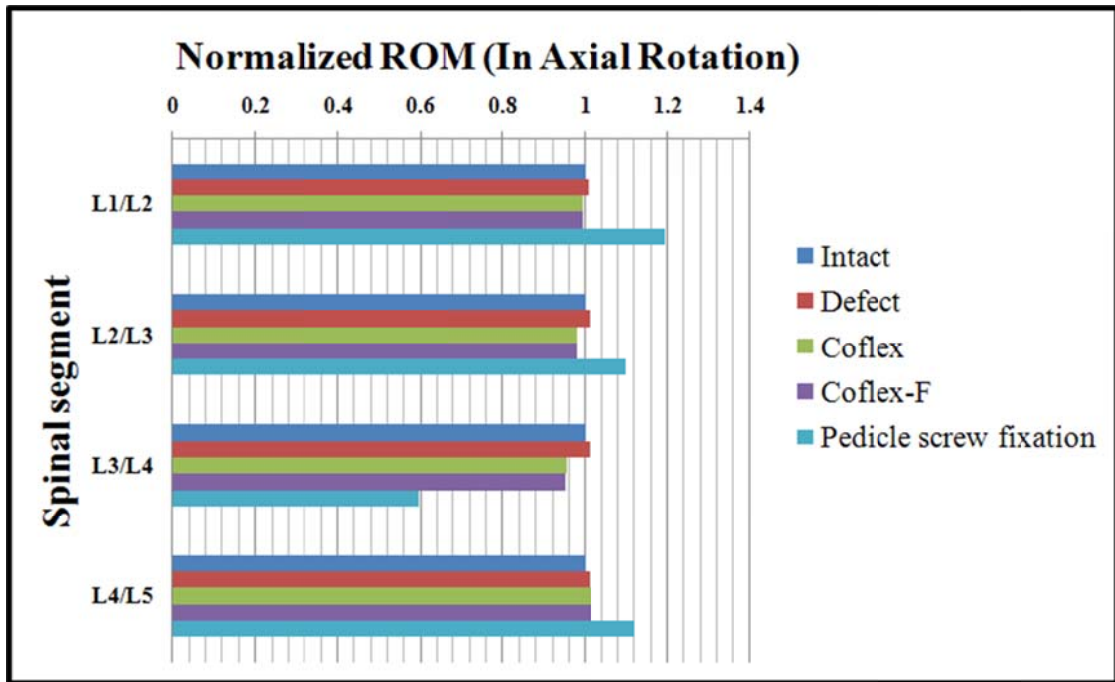


Figure 4.4: Range of motion normalized to intact model in axial rotation.

4.1.2 Maximal von-Mises stress at the disc annulus

In extension, the maximal disc annulus stress decreased 75 % in the Coflex model, 81 % in the Coflex-F model, and 79 % in the pedicle screw fixation model at the surgical segment as compared with the intact model (Figure 4.5). The maximal disc annulus stress of the Coflex and Coflex-F models was similar to that of the intact model at the adjacent L1-L2 segment (deviation within 2 %). The maximal disc annulus stress of the Coflex and Coflex-F models increased 10 % at the adjacent L2-L3 segment and decreased 4 % at the adjacent L4-L5 segment. The maximal disc annulus stress of the pedicle screw fixation model increased 7 % at the adjacent L1-L2 segment, increased 12 % at the adjacent L2-L3 segment, and increased 18 % at the adjacent L4-L5 segment.

In flexion, the maximal disc annulus stress increased 5 % in the Coflex model at the surgical segment as compared with the intact model (Figure 4.6). In contrast to the Coflex model, the maximal disc annulus stress decreased 15 % in the Coflex-F and 27 % in the pedicle screw fixation models. On the other hand, the maximal disc annulus stress of the

Coflex model was similar to that of the intact model at both adjacent L1-L3 and L4-L5 segments (deviation within 4 %). However, the Coflex-F and pedicle screw fixation models increased maximal disc annulus stress by 18 % to 22 % at both the adjacent L1-L3 and L4-L5 segments.

In lateral bending, the maximal disc annulus stress decreased 18 % in the Coflex model, 25 % in the Coflex-F model, and 41 % in the pedicle screw fixation model at the surgical segment as compared with the intact model (Figure 4.7). The maximal disc annulus stress of the Coflex and Coflex-F models decreased 6 % to 8 % at both adjacent L1-L3 and L4-L5 segments. However, the maximal disc annulus stress of the pedicle screw fixation model increased 15 % to 21 % at both adjacent L1-L3 and L4-L5 segments.

In axial rotation, the maximal disc annulus stress decreased 15 % to 16 % in all implanted models at the surgical segment as compared with the intact model (Figure 4.8). The maximal disc annulus stress increased 11 % in the Coflex and Coflex-F models, and 7 % in the pedicle screw fixation model at the adjacent L1-L2 surgical segment. The maximal disc annulus stress of all implanted models increased 15 % at the adjacent L2-L3 segment. The maximal disc annulus stress of the Coflex model and Coflex-F model were similar to that of the intact model at the adjacent L4-L5 segment (deviation within 2 %). The maximal disc annulus stress of the pedicle screw fixation model increased 19 % at the adjacent L4-L5 segment.

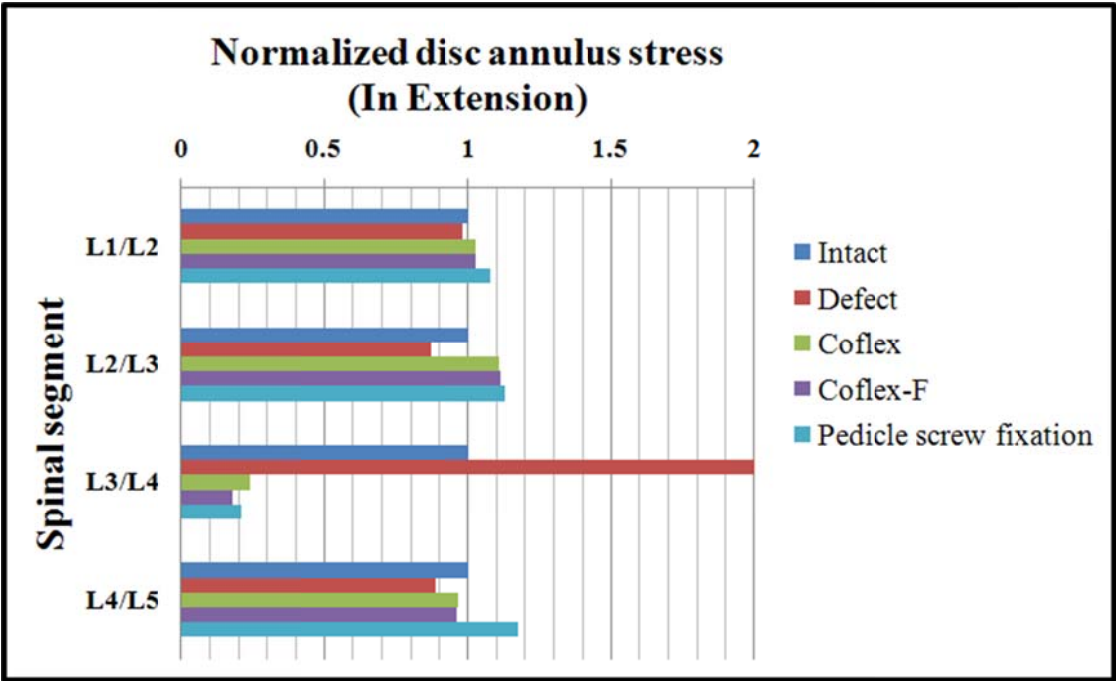


Figure 4.5: Disc annulus stress normalized to intact model in extension.

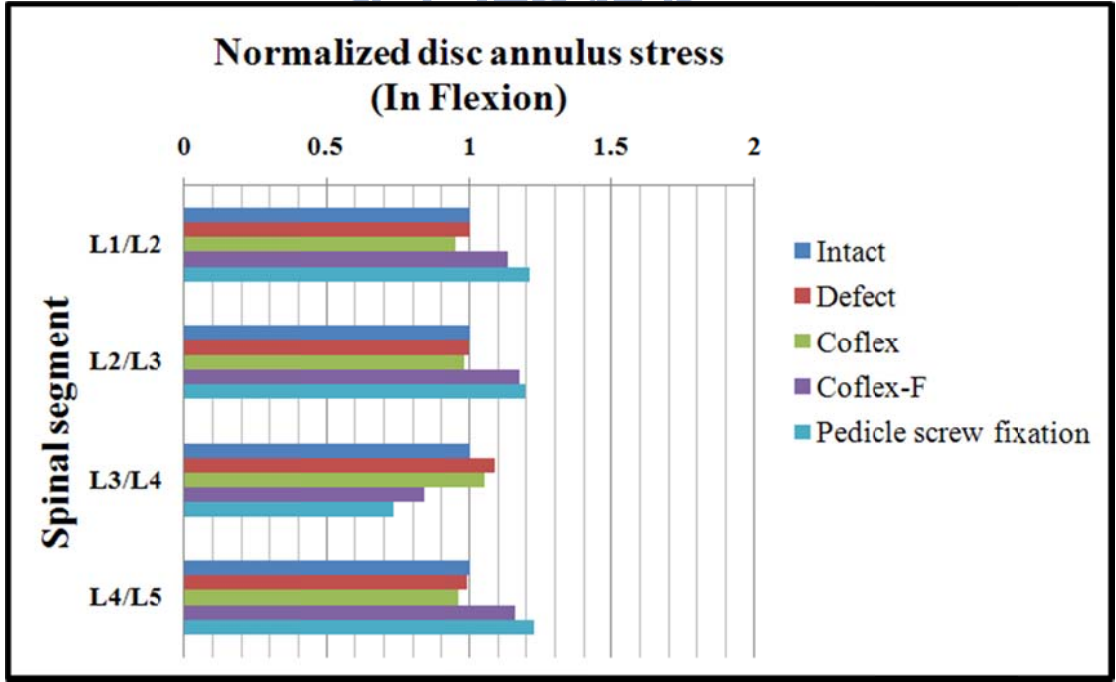


Figure 4.6: Disc annulus stress normalized to intact model in flexion.

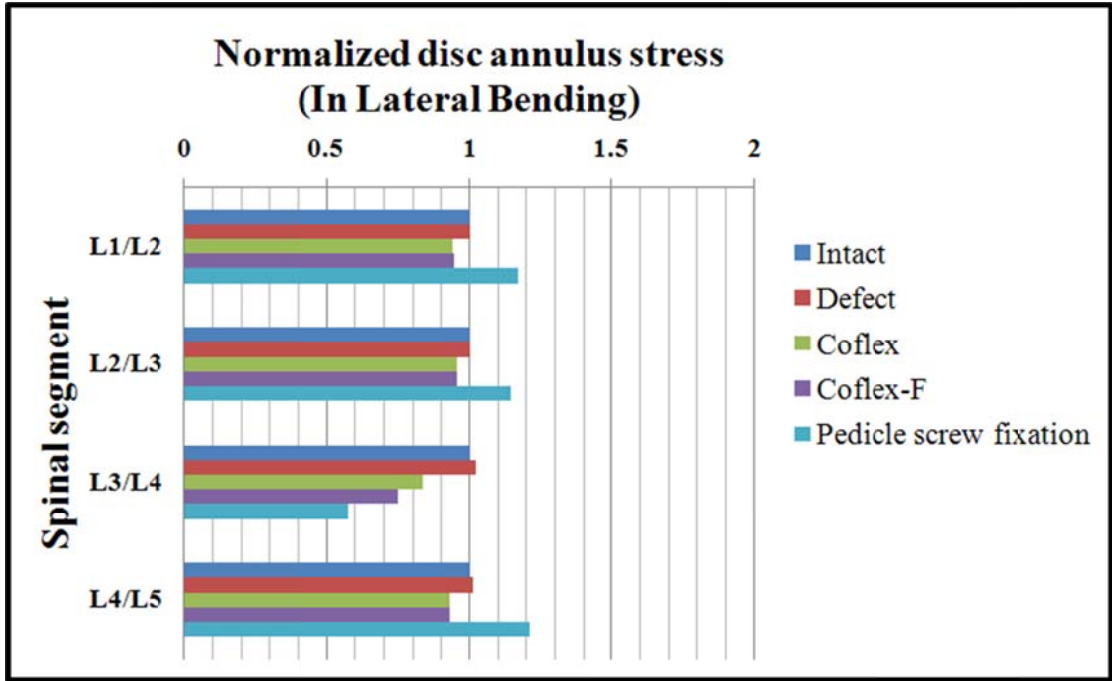


Figure 4.7: Disc annulus stress normalized to intact model in lateral bending.

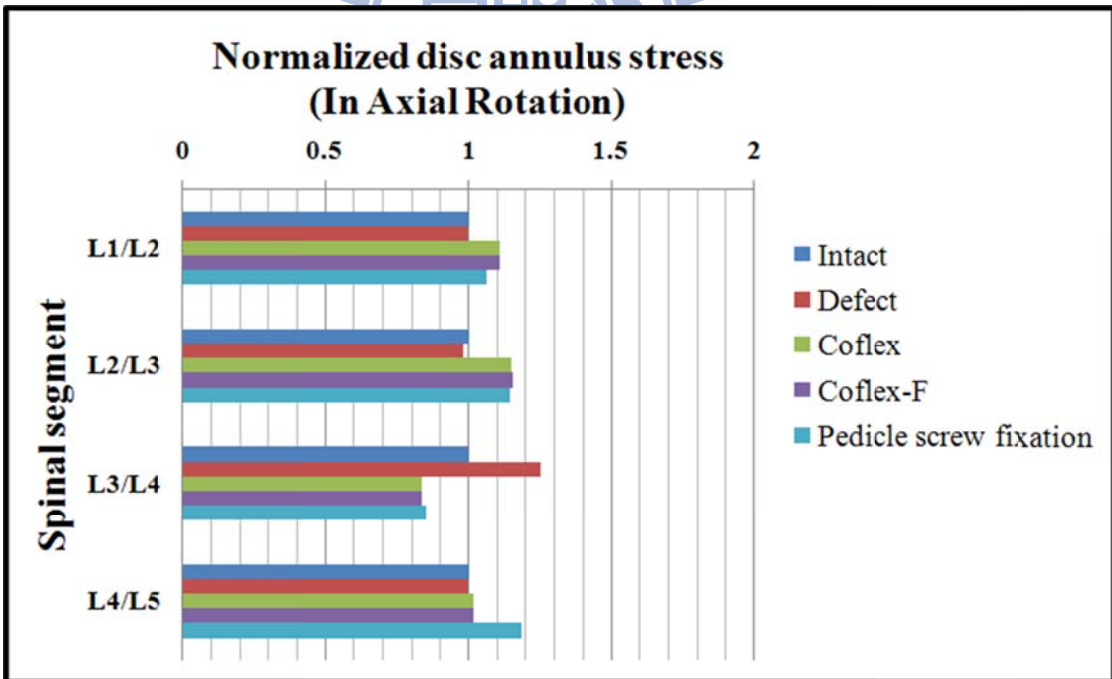


Figure 4.8: Disc annulus stress normalized to intact model in axial rotation.

4.1.3 Von-Mises stress distribution at disc annulus

The stress concentration and distribution pattern of the disc annulus at the surgical segment (L3-L4) changed obviously in these models. In extension, the stress of the defect model was concentrated at the posterior inferior regions of the annulus (Figure 4.9 middle). However, after implantation, the stress concentration of the disc annulus at the posterior disc diminished obviously. Furthermore, in flexion, the stress concentrated at the anterior of the annulus regions, close to the superior and inferior sides of the endplate, in both defect and Coflex models as compared with the intact model (Figure 4.10 middle). The Coflex-F and pedicle screw fixation models have the most even disc annulus stress distribution in flexion, even when compared with the intact model. In lateral bending and in axial rotation, the stress was concentrated at the right part of the annulus regions, close to the superior and inferior sides of the endplate in the defect model as compared with the intact model (Figures 4.11 middle, 4.12 middle). After implantation, the stress concentration of the disc annulus at the posterior disc also diminished.

The stress distribution pattern of the disc annulus at adjacent segment (L2-L3, L4-L5) was affected in these models. In extension, stress of disc annulus decrease in defect model; stress increase in implantation model, compared with the intact model (Figure 4.9 top and bottom). In flexion, stress distribution of disc annulus in both defect and Coflex models was close to the intact model (Figure 4.10 top and bottom). However, after implantation, stress concentrated at the anterior of the annulus regions, close to the superior and inferior sides of the endplate, in both Coflex-F and pedicle screw fixation models as compared with the intact model. In lateral bending and in axial rotation, stress distribution of disc annulus in both defect, Coflex, Coflex-F models was close to the intact model (Figures 4.11 top and bottom, 4.12 top and bottom). After pedicle screw fixation, the stress was concentrated at the right part of the annulus regions.

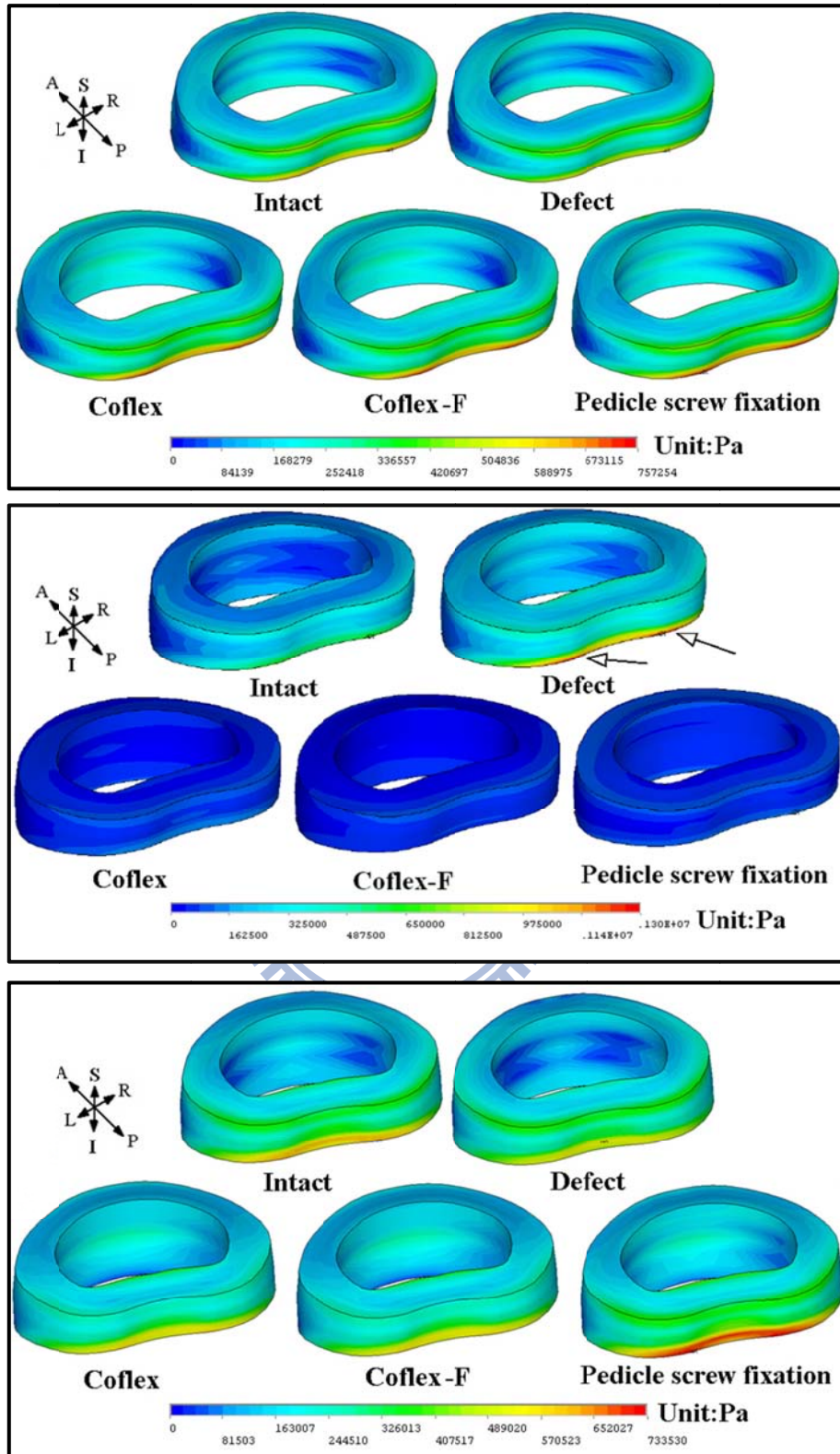


Figure 4.9: von-Mises stress distribution of disc annulus in extension for various surgical models: (Top) L2-L3 adjacent segment; (Middle) L3-L4 surgical segment; (Bottom) L4-L5 adjacent segment.

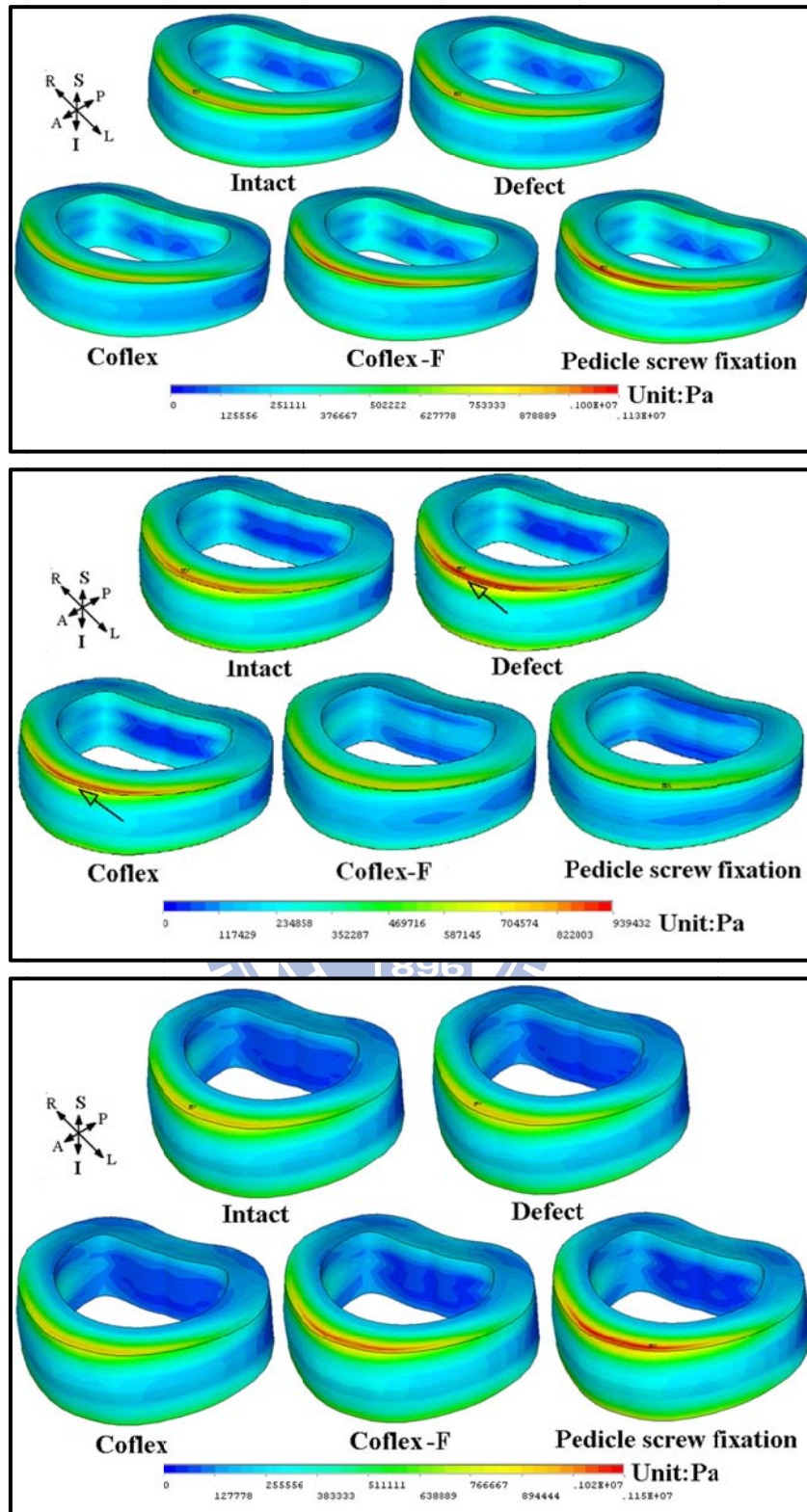


Figure 4.10: von-Mises stress distribution of disc annulus in flexion for various surgical models: (Top) L2-L3 adjacent segment; (Middle) L3-L4 surgical segment; (Bottom) L4-L5 adjacent segment.

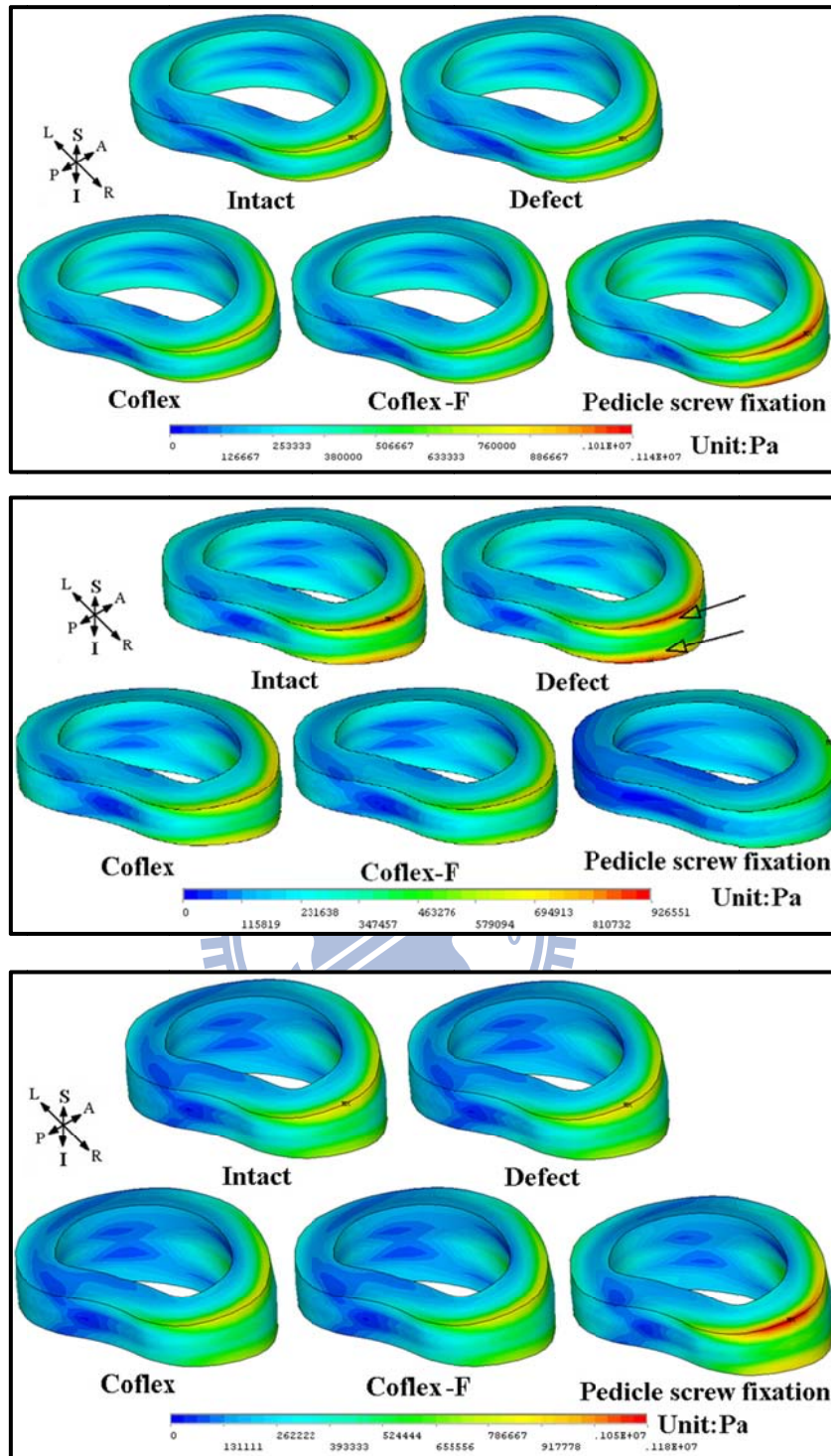


Figure 4.11: von-Mises stress distribution of disc annulus in right lateral bending for various surgical models: (Top) L2-L3 adjacent segment; (Middle) L3-L4 surgical segment; (Bottom) L4-L5 adjacent segment.

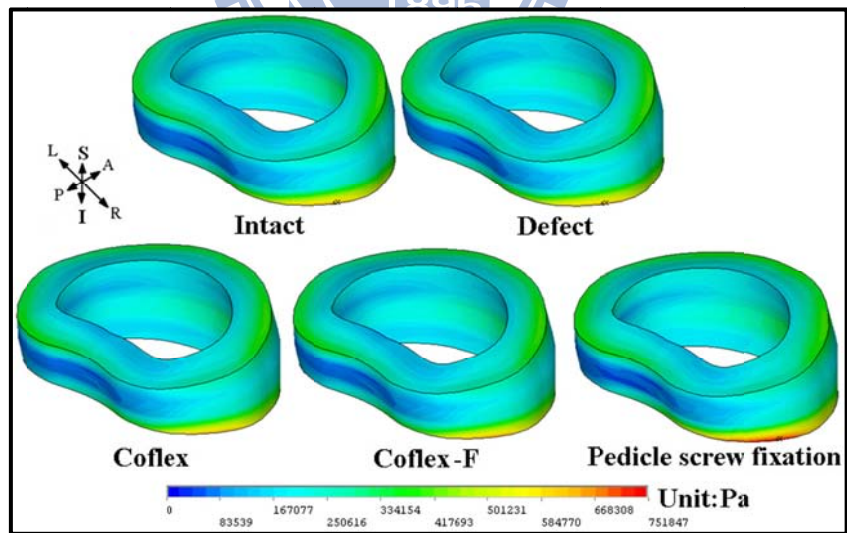
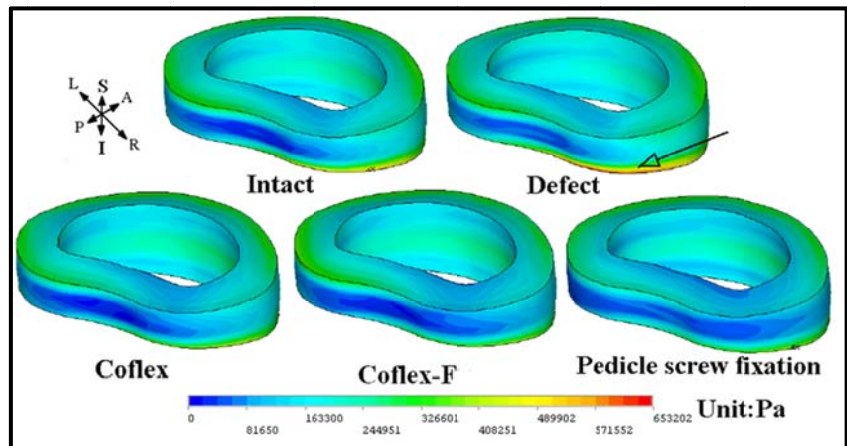
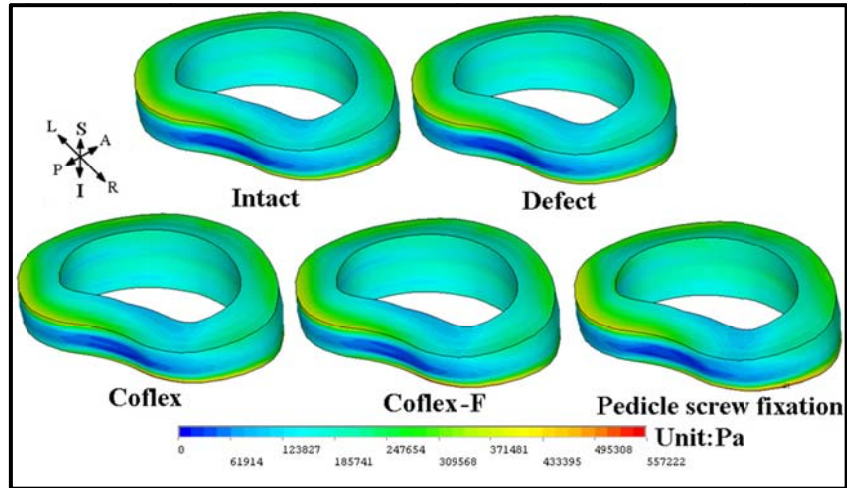
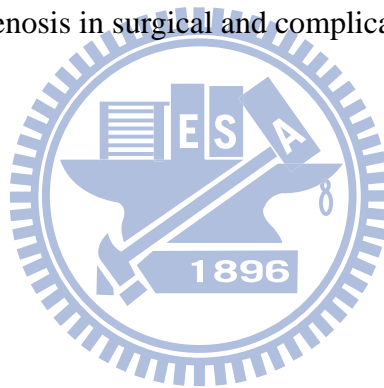


Figure 4.12: von-Mises stress distribution of disc annulus in right axial rotation for various surgical models: (Top) L2-L3 adjacent segment; (Middle) L3-L4 surgical segment; (Bottom) L4-L5 adjacent segment.

The pedicle screw fixation procedure frequently associated with postoperative long-term complication of adjacent segment disease, resulting in the cause of another surgery for extended pedicle screw fixation at the adjacent segments. The higher incidence of adjacent segment disease was reported when patient was treated with rigid instrumentation.

According to the above ROM and von-Mises stress distribution of disc results, the Coflex device can provide stability in extension, lateral bending, and axial rotation at the surgical segment and retain flexible in flexion. The Coflex device restraint extension motion, and provide more space of foramen and spinal canal. Besides, it had no influence than pedicle screw fixation at adjacent segments except during extension. Therefore, the use of Coflex device may decrease rate of adjacent segment disease. As a result, it may replace pedicle screw fixation to improve stenosis in surgical and complication in adjacent segments.



4.2 Coflex-F in fusion surgery

Biomechanical behaviors of the lumbar spine with the TLIF and ALIF combined with Coflex-F model and the TLIF and ALIF combined with pedicle screw fixation model were compared with those of the intact model. Data were normalized with respect to the intact model as percentage values under each loading condition.

4.2.1 Range of motion

For the Coflex-F combined with TLIF, range of motion at the surgical segment (L3-L4) decreased by 75 %, 81 %, 35 %, 47 %, 32 %, and 36 % in flexion, extension, right lateral bending, left lateral bending, right axial rotation, and left axial rotation, respectively, in comparison with the intact model (Figure 4.13 ~ Figure 4.18). For the Coflex-F combined with ALIF, ROM at the surgical segment decreased by 75 %, 77 %, 66 %, 66 %, 52 %, and 52 % in the six physiological motions, respectively.

For the pedicle screw fixation combined with TLIF, ROM at the surgical segment decreased by 83 %, 88 %, 68 %, 71 %, 64 %, and 64 % in six physiological motions, respectively. For the pedicle screw fixation combined with ALIF, ROM at the surgical segment decreased by 83 %, 90 %, 74 %, 74 %, 68 %, and 68 % in the six physiological motions, respectively.

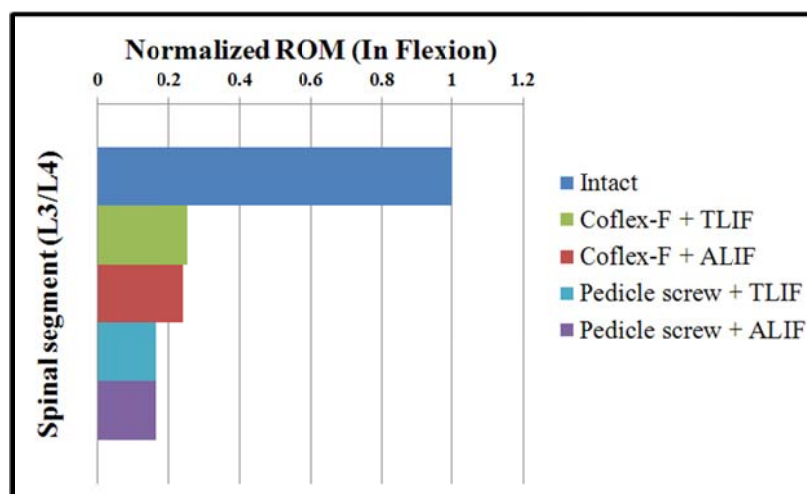


Figure 4.13: Range of motion normalized to intact model in flexion.

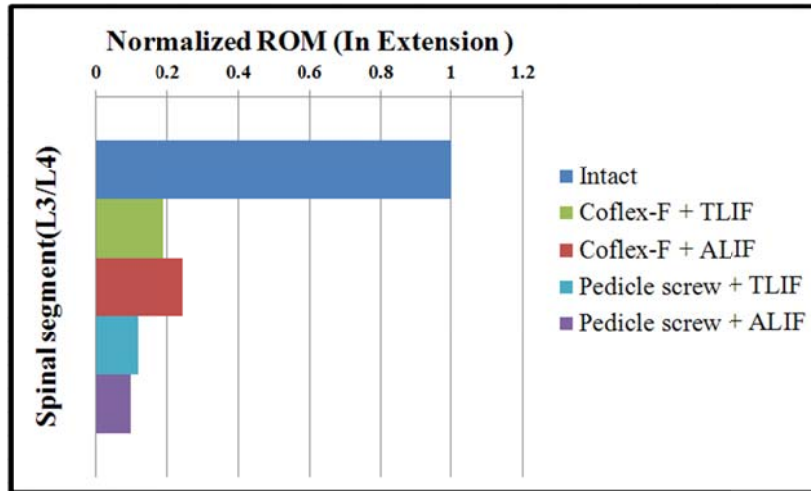


Figure 4.14: Range of motion normalized to intact model in extension.

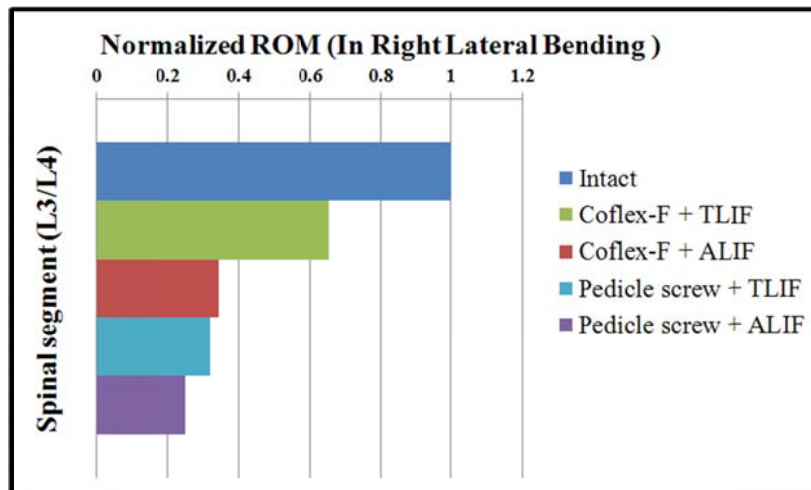


Figure 4.15: Range of motion normalized to intact model in right lateral bending.

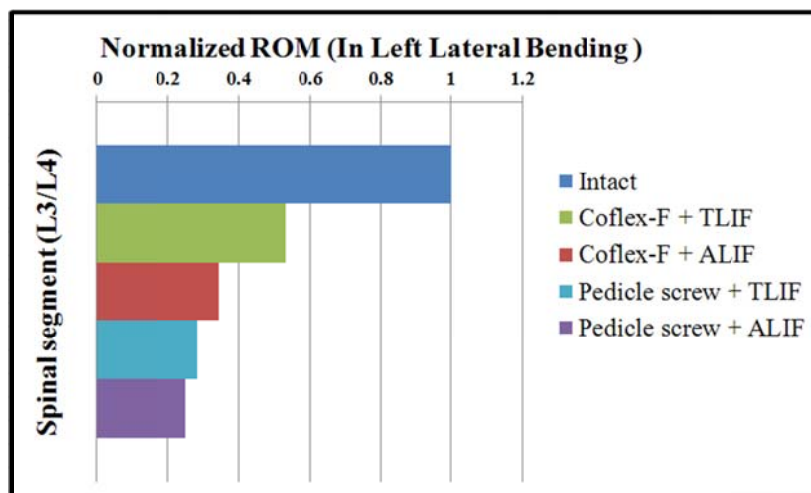


Figure 4.16: Range of motion normalized to intact model in left lateral bending.

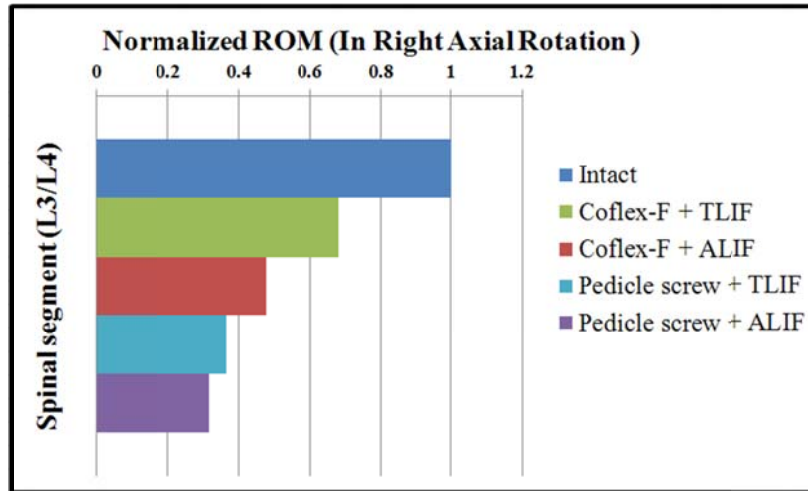


Figure 4.17: Range of motion normalized to intact model in right axial rotation.

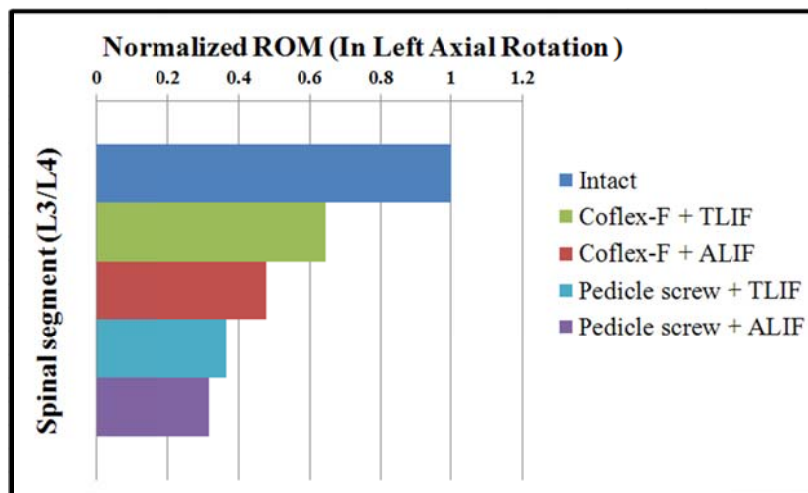


Figure 4.18: Range of motion normalized to intact model in left axial rotation.

4.2.2 Von-Mises stress distribution on the cage-bone interface

The concentration and distribution pattern of stress changed obviously on the cage-bone interface of the superior surface of the L4 vertebra at the surgical segment for four implant models. In lateral bending, the stresses were concentrated at the same side as lateral bending direction (Figure 4.19). The Coflex-F shows more significant stresses concentration than pedicle screw fixation, especially when combined with TLIF. In axial rotation, the stresses corresponding TLIFs were concentrated and correlated with axial rotation direction; on the contrary, the ALIFs show no directional effect (Figure 4.20). The Coflex-F models

result in more significant stresses concentration than pedicle screw fixation models. In flexion, the stresses on the cage-bone interface of the L4 vertebra were all concentrated at the anterior side of vertebra for all implant models, especially for the Coflex-F combined with ALIF model (Figure 4.21). In extension, none of the implant models stress shows significant stress concentration on the cage-bone interface.

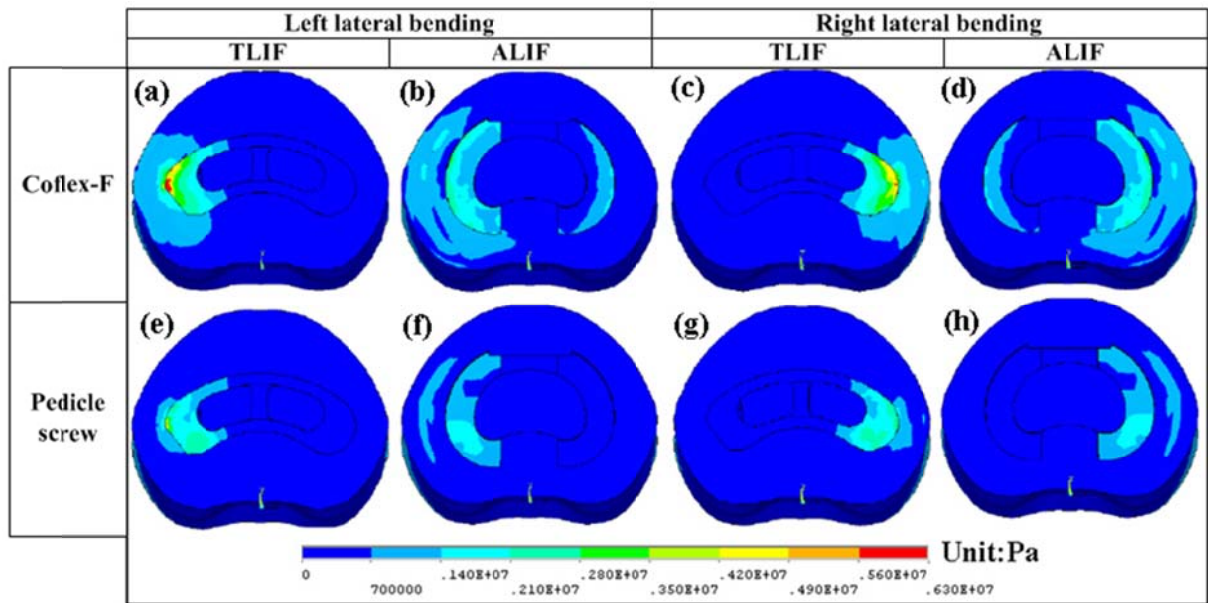


Figure 4.19: The von-Mises stress distribution on the cage-bone interfaces of the superior surface of the L4 vertebra under left lateral bending and right lateral bending.

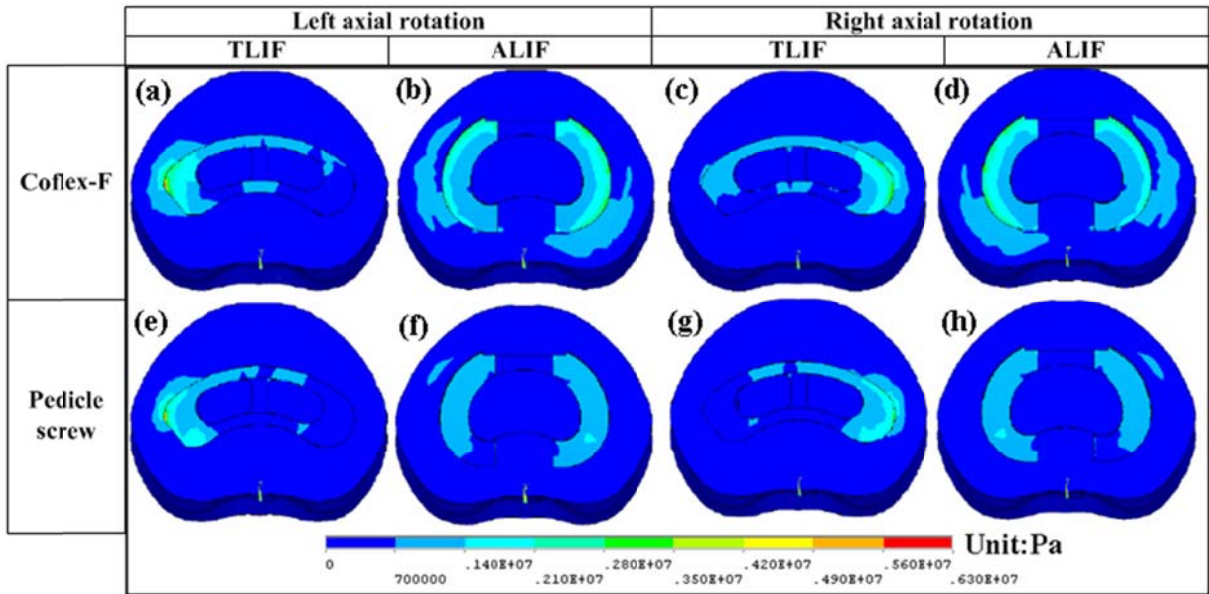


Figure 4.20: The von-Mises stress distribution on the cage-bone interfaces of the superior surface of the L4 vertebra under left axial rotation and right axial rotation.

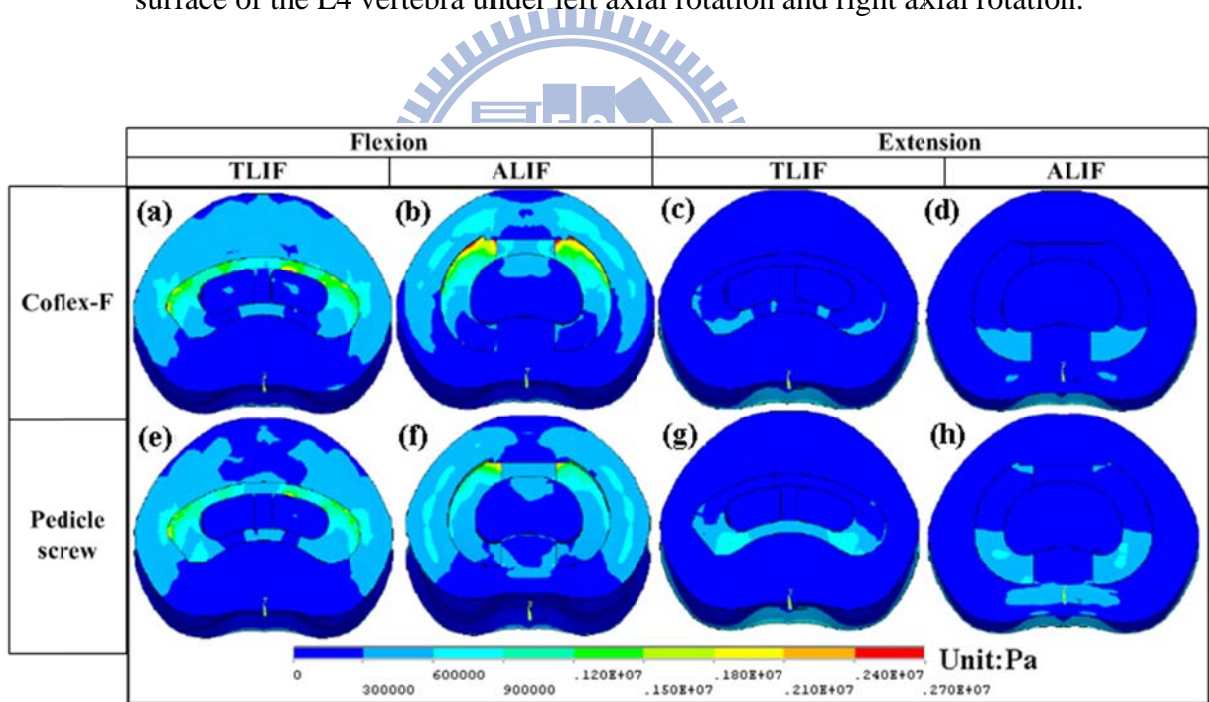


Figure 4.21: The von-Mises stress distribution on the cage-bone interfaces of the superior surface of the L4 vertebra under flexion and extension.

4.2.3 Von-Mises stress distribution for the Coflex-F and the pedicle screw

Figure 4.22 shows the contour plots of von-Mises stress values in the Coflex-F device and the pedicle screw for various loading cases. For all of these cases, the Coflex-F device has higher stresses than the pedicle screw when combined with TLIF or ALIF. Figure 4.23 shows the maximum von-Mises stress values in the Coflex-F and the pedicle screw for various loading cases. For all of these cases, the Coflex-F device has higher stress than the pedicle screw, when combined with either TLIF or ALIF.

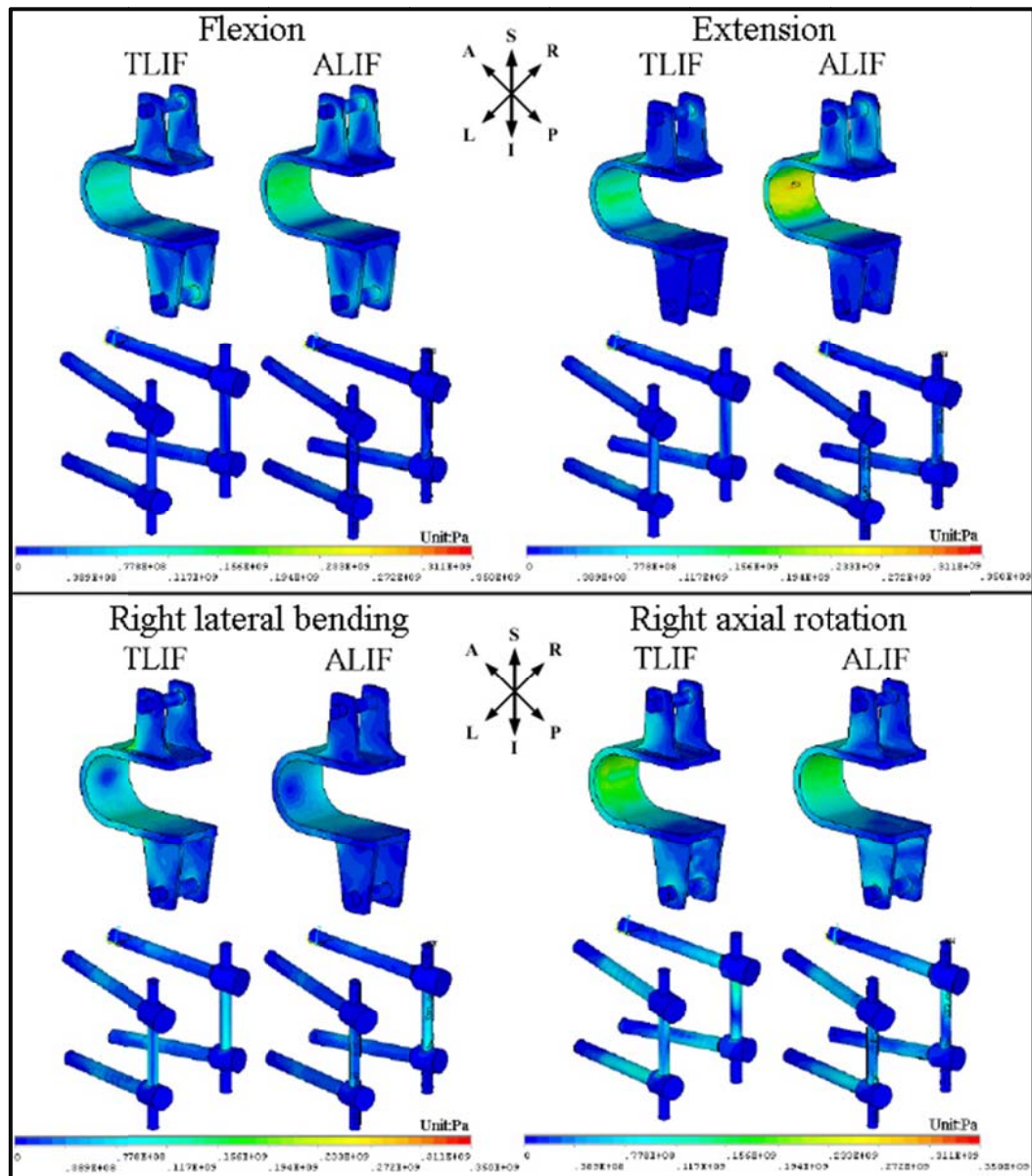


Figure 4.22: The von-Mises stress distribution in the Coflex-F device and the pedicle screw fixation under flexion, extension, right lateral bending, and right axial rotation.

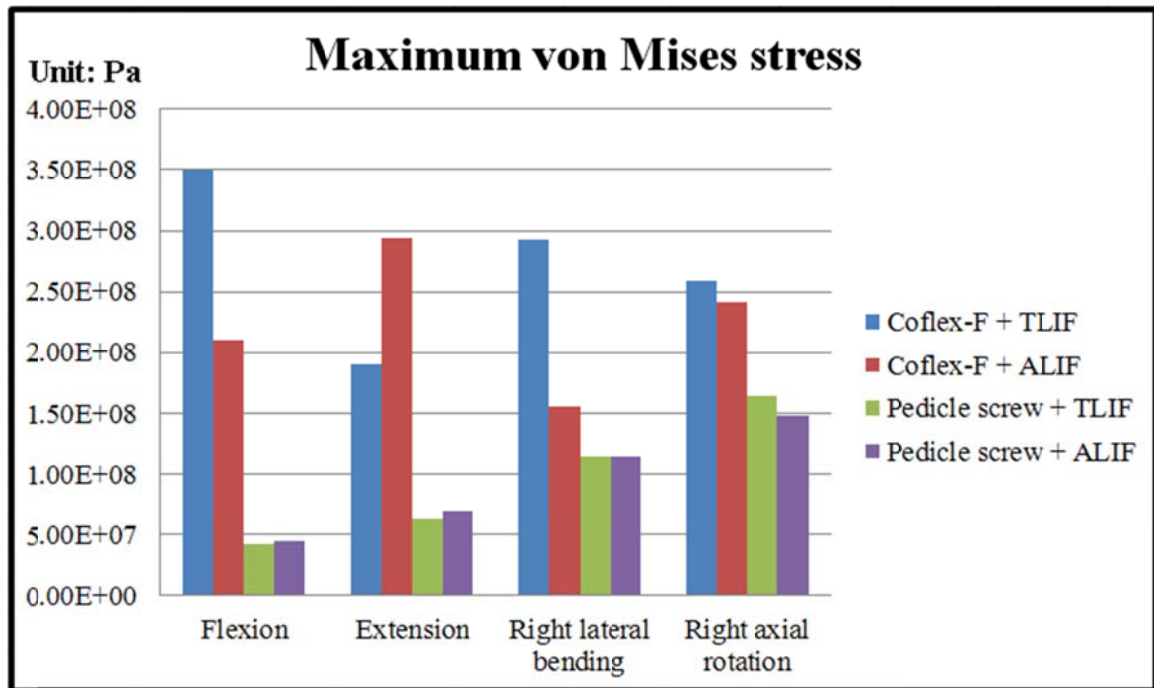


Figure 4.23: The maximum von-Mises stress of the Coflex-F device and pedicle screw under flexion, extension, right lateral bending, and right axial rotation.

4.3 Coflex-F in minimally invasive fusion surgery

Biomechanical behaviors of the lumbar spine with the TLIF combined with Coflex-F model, the TLIF combined with unilateral pedicle screw fixation and translaminar facet screw fixation model, and the TLIF combined with bilateral pedicle screw fixation model were compared with those of the intact model. Data were normalized with respect to the intact model as percentage values under each loading condition.

4.3.1 Range of motion

For the TLIF combined with Coflex-F, range of motion at the surgical segment (L3-L4) decreased by 75 %, 81 %, 35 %, 47 %, 32 %, and 36 % in flexion, extension, right lateral bending, left lateral bending, right axial rotation, and left axial rotation, respectively, in comparison with the intact model (Figure 4.24 ~ Figure 4.29). For the TLIF combined with unilateral pedicle screw fixation and translaminar facet screw fixation, ROM at the surgical

segment decreased by 84 %, 90 %, 73 %, 67 %, 66 %, and 66 % in the six physiological motions, respectively. For the TLIF combined with bilateral pedicle screw fixation, ROM at the surgical segment decreased by 84 %, 89 %, 68 %, 72 %, 64 %, and 64 % in six physiological motions, respectively.

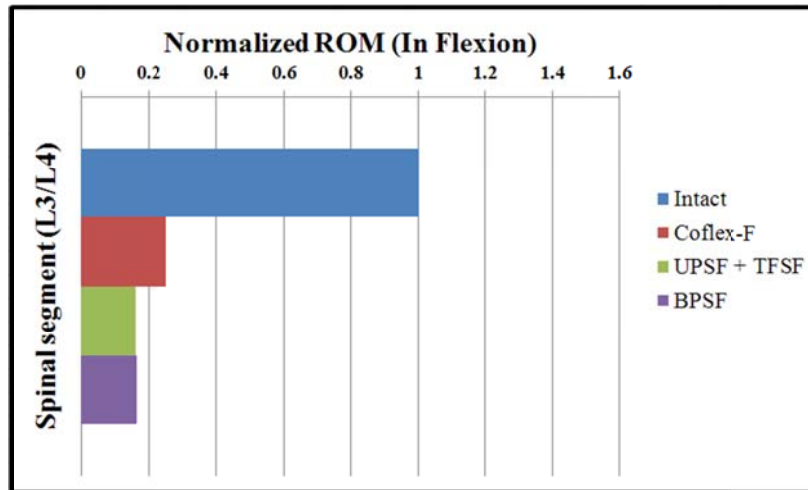


Figure 4.24: Range of motion normalized to intact model in flexion.

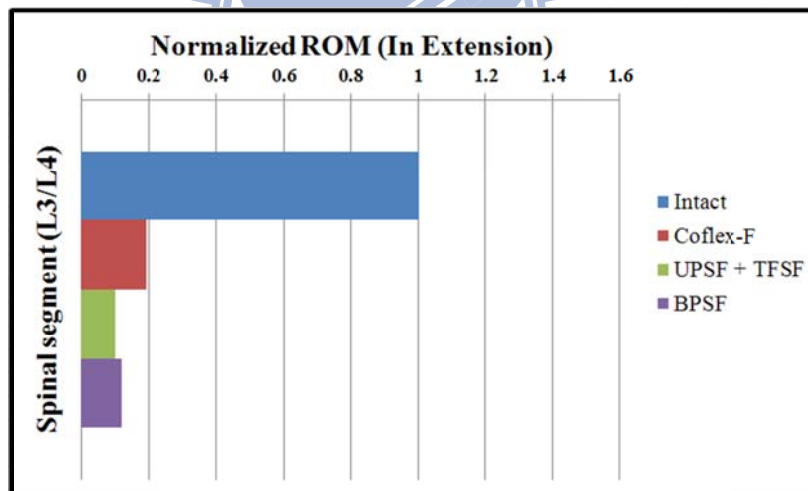


Figure 4.25: Range of motion normalized to intact model in extension.

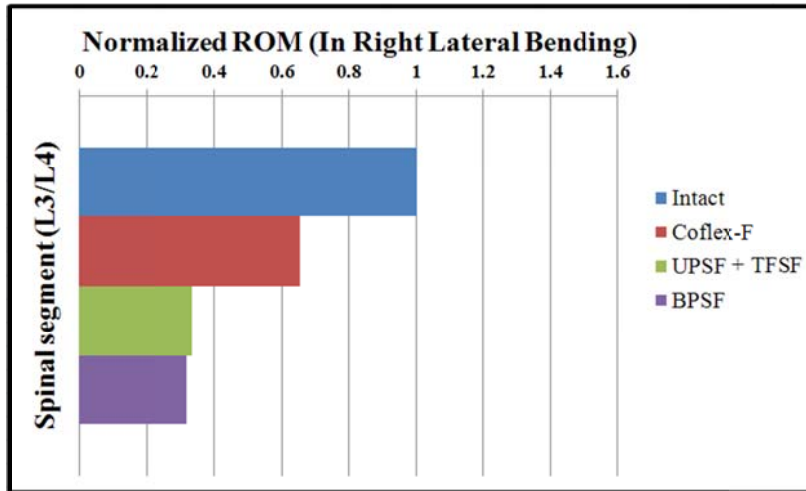


Figure 4.26: Range of motion normalized to intact model in right lateral bending.

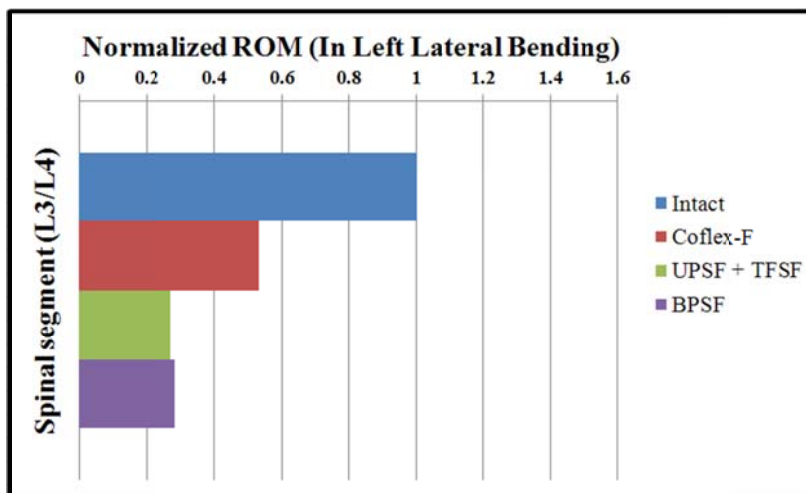


Figure 4.27: Range of motion normalized to intact model in left lateral bending.

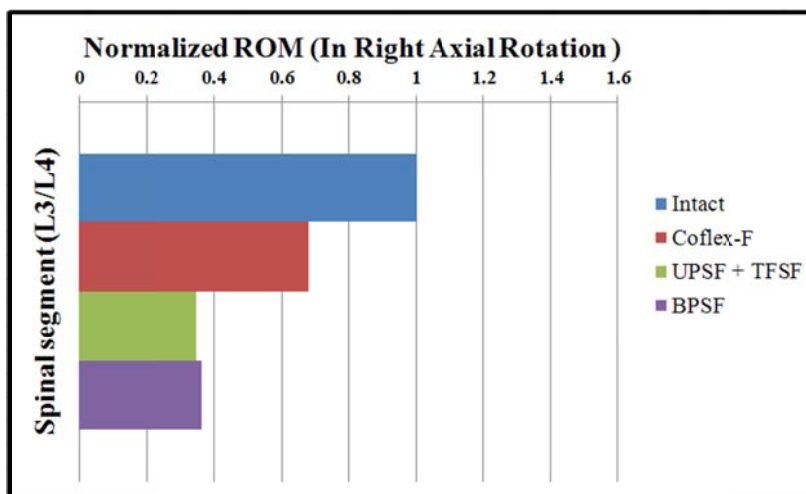


Figure 4.28: Range of motion normalized to intact model in right axial rotation.

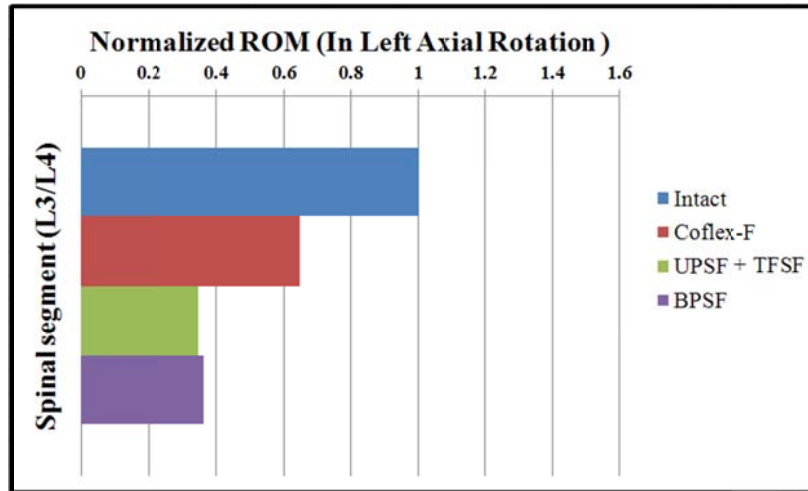
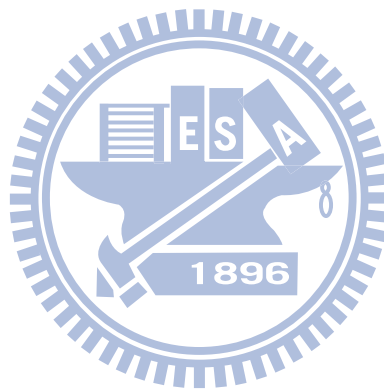


Figure 4.29: Range of motion normalized to intact model in left axial rotation.



Chapter 5 Discussion

5.1 Coflex and Coflex-F in non-fusion surgery

The subject study found that (1) the Coflex device can provide stability of the surgical segment in most motions, except in flexion; (2) the rivets of the Coflex-F link bone and implant and can provide stability in all motions, especially in flexion; (3) in flexion, the disc stress distribution of the surgical segment is improved by the use of rivets; (4) in flexion, the Coflex-F influenced the adjacent segments; and (5) in extension, all implants influenced the adjacent segments.

In the subject study, the Coflex device in the defect model was found to provide stability in most motions, except in flexion. The instability of the Coflex device in flexion causes stress concentration at the anterior regions of the disc annulus (close to the superior and inferior sides of the endplate). Wilke *et al.* [59] suggested that the key for the Coflex device to provide stability in flexion is based on whether the teeth on the wings of the Coflex can provide sufficient anchorage to the spinous process. Two factors can improve this stabilization effect. First, the surgeon must tighten the teeth on the wings against both edges of the spinous processes. Second, the bone density of the spinous processes should be strong enough to provide sufficient anchorage. However, both conditions are not always guaranteed.

For numerical analysis, the coefficient of friction in the interface between the implant and spinous processes was difficult to obtain. It is hypothesized that the teeth on the wings of the Coflex device will prevent implant slip motion in the spinous processes, and therefore a higher coefficient of friction (0.8) was used in the contact interface. In addition, this study also tested different coefficients of friction (0.4, 0.8, 1.2, and 1.6) to seek its influence on the effect of teeth on the wings of the Coflex device. The results show that the influence of the coefficient of friction is negligible.

The Coflex device was implanted between the interspinous processes located at the

posterior structure of the spine to resist instability in extension. By comparison with Tsai's results in cadaveric experiments [57], our data show discrepancies in lateral bending and axial rotation. It is inferred that these were caused by individual differences among cadaveric specimens and differing experimental conditions. In the subject study, a partial L3-L4 interspinous process was removed to provide sufficient space for the implant, and the spinous process interface was modeled as a perfect contact and was able to transmit both tensile and compression forces. This assumption is different from the results of cadaveric experiments.

Kettler *et al.* [55] reported implantation of the Coflex-F can provide stability for all motions in lumbar spine stability. In the subject study, we also showed that the rivet connecting the metal wings and bony spinous process provides more security than the conventional Coflex device. Therefore, the rivet can improve the load transmission on the posterior spinal structure to decrease the stress concentration on the disc annulus at the surgical segment in all motions.

There are limited reports about implanting the Coflex device in the long lumbar segment model. The potential side effects in the adjacent segments need to be addressed. In 1-year outcome evaluation, Kong *et al.* [58] reported that the Coflex device reduced the ROM at the surgical segment but did not affect the ROM at the adjacent segments. The subject study, using a long lumbar spine segment model of an implanted Coflex device, showed that the ROMs are increased at both adjacent segments in extension but are unchanged in other motions. Therefore, the Coflex device increased annulus stress at both adjacent segments in extension. However, the Coflex-F constrained the surgical segment in all motions and it increased ROM at adjacent segments, especially in flexion. Therefore, the Coflex-F increased annulus stress at both adjacent segments in flexion and extension. The Coflex-F and pedicle screw fixation have the same effect on the adjacent segments in both flexion and extension. In addition, the remote adjacent L1-L2 segment and adjacent L2-L3 segment demonstrate the same effect in all forms of implantations.

5.2 Coflex-F in fusion surgery

The subject study found that (1) The Coflex-F device combined with ALIF can provide stability similar to a pedicle screw fixation in combination with TLIF or ALIF. (2) larger stress at the cage-bone interface for the Coflex-F combined with TLIF, thus causing the exclusion of the pedicle screw fixation.

The present study used an FE lumbar model of the L1-L5 segments to compare the effects of the Coflex-F device and traditional bilateral pedicle screw fixation at the surgical segment after TLIF and ALIF implantation. According to the ROM results, the Coflex-F device combined with the TLIF model had lower stability than all the other models, especially in both directions of lateral bending and axial rotation. On the other hand, the pedicle screw fixation combined with the ALIF showed the highest stability among all model.

The primary factor in the Coflex-F results is the fixed position of its implantation. The motion segment, composed of two adjacent vertebrae and the associated soft tissues, is the functional unit of the spine. Each motion segment has three joints. It has a triangular stack of articulations, with symphysis joints between vertebral bodies on the anterior side and two sliding facet joints on the posterior side. The Coflex-F has rivets joining its wings to the spinous processes. The rivets can attach the implant more rigidly to the posterior spinous processes. However, the vertebral bodies of anterior side sustain the majority of the weight. Therefore, the rivets cannot provide sufficient stiffness in the motion segment for two adjacent vertebrae because the locations of attachment are within the posterior element, which is not as strong as vertebral bodies. However, pedicle screw fixation can fix vertebral bodies, and therefore provide sufficient stiffness in the motion segment for two adjacent vertebrae.

The geometry of the Coflex-F device supports a different function—its U-shaped structure retains the same design and flexibility of the Coflex, thus making it more flexible and deformable than pedicle screw fixation. Figure 4.22 shows the von-Mises stress of the

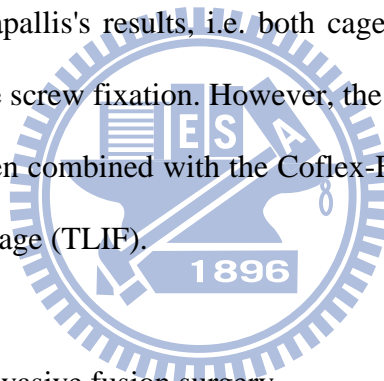
Coflex-F and the pedicle screw for various loading cases. In all of these cases, the Coflex-F has higher stress than the pedicle screw when combined with TLIF or ALIF. Figure 4.23 showed the von-Mises stress of the Coflex-F and the pedicle screw for various loading cases. The Coflex-F has higher von-Mises stress than the pedicle screw. Therefore, the fixed position and geometry of implantation have a great influence on stress distribution for Coflex-F

ALIF and TLIF are two common surgeries for achieving interbody arthrodesis. In the present study, a posterior instrumentation in combination with ALIF can provide higher stability than a posterior instrumentation in combination with TLIF. The ALIF procedure with anterior surgical approach allows expansion of disc space; it can use a larger cage to increase the contact area of cage-bone interface. The larger contact area distributes the load over the cage-bone interface area of the vertebra bone. Consequently, an ALIF cage does not create stress concentration on the cage-bone interface at the surgical segment. On the other hand, the TLIF procedure prohibited the use of a large cage, because a cage pathway would create limitations for the surgery. The TLIF procedure can only utilize cages with long and thin contact area on the cage-bone interface. Therefore, the TLIF cage suffers from stress concentration on the cage-bone interface at the surgical segment.

In extension, the stress concentration of all the models diminished between the cage-bone interfaces. In flexion, the stress concentration of all the models increased at the anterior side of the cage-bone interface. A posterior instrumentation combined with ALIF has higher stress concentration than a posterior instrumentation combined with TLIF. This is primarily due to flexion or extension motion. The posterior instrumentation and interbody cage share the same extension motion. Posterior instrumentation sustains most of the load transferred in extension, therefore reducing the stress concentration of all the models. In contrast, the anterior interbody cage sustains most of the load transferred in flexion, therefore resulting in the stress concentration in the ALIF model at the cage-bone interface, especially with Coflex-F implantation. The Coflex-F sustains larger moment than pedicle screw fixation

because the fixed position of the Coflex-F in the posterior interspinous processes causes a longer moment arm.

PEEK material has recently gained popularity for use in implants because of its mechanical properties. One of the PEEK material's biggest advantages is its modulus of elasticity ($E = 3.5$ GPa) which is closer to cortical bone ($E = 12$ GPa) and cancellous bone ($E = 0.14$ GPa) compared to that of titanium ($E = 113$ GPa). Vadapallis [106] performed a finite element investigation to study the effect of different spacer material property. The results from that study indicate that PEEK spacers provide initial stability similar to titanium spacers, and therefore might minimize the chances of subsidence. The present study uses two cage materials: titanium for the ALIF cage and PEEK for the TLIF cage for stability. This study's results are identical to Vadapallis's results, i.e. both cage materials provide similar stability when combined with pedicle screw fixation. However, the materials of these two cages do not provide similar stability when combined with the Coflex-F, the titanium cage (ALIF) provide higher stability than PEEK cage (TLIF).



5.3 Coflex-F in minimally invasive fusion surgery

The subject study found that (1) the TLIF combine with Coflex-F cannot provide sufficient stability of the surgical segment in lateral bending and axial rotation; (2) the TLIF combined with unilateral pedicle screw fixation and translaminar facet screw fixation can provide sufficient stability of the surgical segment all motion as TLIF combined with bilateral pedicle screw fixation.

Several lumbar interbody fusion methods have been used for degenerative disc diseases and instabilities via various approaches, such as ALIF, PLIF, and TLIF. The TLIF was involves removal of one facet joint and a lateral approach to the disc space, thus reducing the potential for nerve injury. The TLIF surgical construct requires less bone and soft tissue dissection, respects neural elements, laminar bone, facet and pars interarticularis on the

contralateral side for additional posterolateral fusion, and avoids the morbidity of ALIF and PLIF approaches.

Another minimally invasive fusion device, an interspinous process device Coflex-F may be used instead. This device requires only a minimal incision and disruption of the interspinous ligaments to insert one part of the device with a post which goes through the interspinous space.

Results showed that TLIF combined with Coflex-F provide lower stability than TLIF combined with unilateral pedicle screw and translaminar facet screw fixation. The primary factor is fixed position of Coflex-F implantation and Coflex-F structure as described previously 5.2 sections. Therefore, the TLIF combine with Coflex-F cannot provide sufficient stability of the surgical segment in lateral bending and axial rotation.

In this subject study, ROM results showed the fixation following TLIF of unilateral pedicle screws with a supplemental translaminar facet screw fixation showed no difference in stiffness to that of the standard bilateral pedicle screw fixation. The advantages of surgical procedure for unilateral pedicle screw and supplemental translaminar facet screw fixation were significantly reduced iatrogenic trauma and reduced surgical risks than bilateral pedicle screws fixation.

5.4 limitations

Several limitations in these studies are related to the simplified and idealized material properties during simulation, such as the linearized behavior of the spinal ligaments and pure elastic intact discs without degeneration [93][94]. A degenerative disc is common in many patients before surgery. The various grades of degeneration in the disc, such as delamination, dehydration or reduced disc height, do not allow for exact replication of the unique material properties of a degenerated disc. Therefore, normal material properties were used in this simulation.

In a real spine, the size of vertebrae and the orientation of the facet joint are different depending on each segment. The influence of geometry was not considered here, which might affect the absolute values of the vertebral stresses and facet joint loads.

The degree of gripping force applied between the wings of the Coflex-F device and the spinous process is determined by the clamping force that is applied by the surgeon, which is difficult to measure, and there have been different results presented in previous studies [55][57][59]. In addition, determination of gripping force must also consider bone strength and geometry of the spinous process. In this study, the degree of the gripping force was simplified and only considered the friction conditions between the teeth on the wings of the Coflex-F device and the spinous process. The coefficient of friction used here was based on the results of a previous study into friction parameters between the cage and the bone [93]. In addition, our simplified simulation of gripping force ignored the pre-force between the teeth of the wings and the spinous processes, as well as the inward and outward deformation of both side flanks of the Coflex-F device. Also, the constrained behavior used in the bone-screw interface, the thread of the pedicle screw, and the bone ingrowth into the cage were simplified.

Pretension should occur after inserting the device, which might distract the remaining annulus, reducing the ROM and facet loading at the implant level. This mechanism was not modeled here.

The loading conditions in the present FE simulations were similar to those of the traditional *in vitro* tests. Thus, muscle contraction and pelvic movement were not included in the present study. Furthermore, FE models should be interpreted only as a trend because of the variability among different human tissues.

Chapter 6 Conclusion and Future Work

6.1 Conclusion

In the non-fusion surgery, the Coflex implantation can provide stability in extension (ROM decreased 70%), lateral bending (ROM decreased 8%), and axial rotation (ROM decreased 4.3 %) at the surgical segment, and retain flexible in flexion (ROM increased 8%). It had no influence at adjacent segments except during extension (ROM increased 20~24%). Because Coflex device restrains extension motion, there can provide more space of foramen and spinal canal. Therefore, The Coflex device may improve or relieves the stenosis.

The rivets of the Coflex-F link bone and implant and can provide stability in all motions, especially in flexion (ROM decreased 52%). Also, the Coflex-F can reconstruct the posterior spinal structure for load sharing to reduce disc annulus stress at the surgical segment. Therefore, the Coflex-F device may be used to treat stenosis combined with mild degenerative disc disease.

In the fusion surgery, the Coflex-F device combined with ALIF can provide stability similar to a pedicle screw fixation in combination with TLIF or ALIF. The Coflex-F device combined with ALIF is preferable for providing more stability in spine fusions.

In the minimally invasive fusion surgery, the TLIF combine with Coflex-F cannot provide sufficient stability of the surgical segment in lateral bending and axial rotation. In however, The TLIF combined with unilateral pedicle screw fixation and translaminar facet screw fixation can provide sufficient stability as TLIF combined with bilateral pedicle screw fixation.

6.2 Future work

There are several topics can be extended for the non-fusion surgery combined with Coflex device.

The above studies are focused in single segment disease only. However, the disc

degeneration disease occurs sometime in the multi-segment or adjacent segment after fusion surgery. Adjacent segment degeneration is the tendency for clinical symptomatic changes to occur following fusion surgery. It is widely believed that spinal fusion significantly alters the biomechanical environment of the adjacent spinal motion segments leading to an acceleration of the normal degenerative process. Little *et al.* [108] reported the effect of anterior interbody fixation on facet capsule strains. Seven cadaveric lumbar spine specimens were evaluated during physiological motion in the intact state and following anterior interbody fusion. The reduction of motion induced by interbody fusion resulted in increased facet joint capsule strain at the adjacent segments. Weinhoffer *et al.* [109] investigated the intradiscal pressure changes occurring following instrumented lumbar fusion in a biomechanical study. Pressure transducers measured intradiscal pressures at L3-L4 and L4-L5 in intact specimens and following L5-S1 fusion. Pressure measurements were significantly increased following fusion. Additionally, as the number of fusion segments was increased, there was a corresponding increase in intradiscal pressure at the adjacent segment.

Therefore, for non-fusion surgery, one of the proposed study is going to compare the biomechanical characteristic of two-segment Coflex or Coflex-F implant and a hybrid implant (one-segment Coflex or Coflex-F and one-segment pedicle screw fixation) in the further.

There are also topics can be extended for the fusion surgery combined with Coflex-F device. Our existing studies used specific cage (semilunar cage) for minimally invasive transforaminal lumbar interbody fusion. Currently, many kinds of cage designs are available on the market, which can be classified by the various geometry, size and material. Cho *et al.* [110] compare three TLIF implant designs (Stryker AVS PL, AVS TL and the Medtronic Capstone) with different lengths and shapes (flat or biconvex, straight or banana shape) in terms of biomechanical stability on human cadaveric models. The results showed that the geometry of cages, including shape (banana or straight), length, surface profile (biconvex or flat), did not affect construct stability when the cages were used in conjunction with pedicle

screw fixation.

However, the relationship between the geometry of cage, the positions of cage insertion and the use of Coflex-F device are unknown. Therefore, the study concerning the fusion surgery combined with Coflex-F device can be focused on different kind cage together with different insert positions for TLIF in the further.



References

- [1] Lively MW. “Sports medicine approach to low back pain”, South Med J, 95(6), pp. 642-646, Jun 2002.
- [2] Hart LG, Deyo RA, Cherkin DC. “Physician office visits for low back pain. Frequency, clinical evaluation, and treatment patterns from a U.S. national survey”, Spine, 20(1), pp. 11-19, Jan 1995.
- [3] Frymoyer JW, Ducker TB, Hadler NM, Kostuik JP, Weinstein JN, Whitecloud TS. “The Adult Spine: Principles and Practice”, The economics of spinal disorders, Philadelphia, PA: Lippincott-Raven, pp. 143–150, 1997.
- [4] Christie SD, Song JK, Fessler RG. “Dynamic interspinous process technology”, Spine, 30(16 Suppl), pp. S73-S78, Aug 2005.
- [5] Kong DS, Kim ES, Eoh W. “One-year outcome evaluation after interspinous implantation for degenerative spinal stenosis with segmental instability”, J Korean Med Sci, 22(2), pp. 330-335, Apr 2007.
- [6] http://www.backpain-guide.com/Chapter_Fig_folders/Ch05_Anatomy_Folder/4OverallSpine.html
- [7] Hall SJ. Basic Biomechanics, 4th edition, McGraw-Hill, New York, 2004.
- [8] McBroom RJ, Hayes WC, Edwards WT, Goldberg RP, White AA 3rd. “Prediction of vertebral body compressive fracture using quantitative computed tomography”, J Bone Joint Surg Am, 67(8), pp.1206-1214, Oct 1985.
- [9] http://www.karger.com/gazette/65/anderson2/art_2_p.htm
- [10] Gower WE, Pedrini V. “Age-related variations in proteinpolysaccharides from human nucleus pulposus, annulus fibrosus, and costal cartilage”, J Bone Joint Surg Am, 51, pp.1154-1162, 1969.
- [11] Panagiotacopoulos ND, Pope MH, Krag MH, Block R. “Water content in human intervertebral discs. Part I. Measurements by magnetic resonance imaging”, Spine, 12, pp. 912-917, 1987.
- [12] Marchand F, Ahmed AM. “Investigation of the laminate structure of lumbar disc annulus fibrosus”, Spine, 15, pp. 402-410, 1990.
- [13] Adams M, Bogduk N, Burton K, Dolan P. The biomechanics of back pain, 2nd edition, Churchill Livingstone, Edinburgh, 2006.
- [14] Skaggs DL, Weidenbaum M, Iatridis JC, Ratcliffe A, Mow VC. “Regional variation in tensile properties and biochemical composition of the human lumbar anulus fibrosus”,

- Spine, 19(12), pp. 1310-1319. Jun 1994.
- [15] Setton LA, Zhu W, Weidenbaum M, Ratcliffe A, Mow VC. “Compressive properties of the cartilaginous end-plate of the baboon lumbar spine”, J Orthop Res, 11, pp. 228-239, Mar 1993.
- [16] Farfan H. Mechanical disorders of the low back, Philadelphia, 1937, Lea & Febiger.
- [17] Hutton WC, Stott JRR, Cyron BM. “Is spondylolysis a fatigue fracture?”, Spine, 2, pp. 202-209, 1977.
- [18] <http://www.spineuniverse.com/anatomy/ligaments>
- [19] <http://www.health.com/health/library/mdp/0,,zm2325,00.html>
- [20] Zucherman J, Hsu K, Picetti G 3rd, White A, Wynne G, Taylor L. “Clinical efficacy of spinal instrumentation in lumbar degenerative disc disease”, Spine, 17(7), pp. 834-837, Jul 1992.
- [21] Brantigan JW, Neidre A, Toohey JS. “The Lumbar I/F Cage for posterior lumbar interbody fusion with the variable screw placement system: 10-year results of a Food and Drug Administration clinical trial”, Spine J, 4(6), pp. 681-688, Nov-Dec 2004.
- [22] Verbiest H. “A radicular syndrome from developmental narrowing of the lumbar vertebral canal”, J Bone Joint Surg Br, 36-B (2), pp. 230-237, May 1954.
- [23] Arbit E, Pannullo S. “Lumbar stenosis: a clinical review”, Clin Orthop Relat Res, 384, pp. 137-143, Mar 2001.
- [24] Kirkaldy-Willis WH, Wedge JH, Yong-Hing K, Reilly J. “Pathology and pathogenesis of lumbar spondylosis and stenosis”, Spine, 3(4), pp. 319-328, Dec 1978.
- [25] Siebert E, Prüss H, Klingebiel R, Failli V, Einhäupl KM, Schwab JM. “Lumbar spinal stenosis: syndrome, diagnostics and treatment”. Nat Rev Neurol. 5(7), pp.392-403, Jul 2009.
- [26] Schulte TL, Bullmann V, Lerner T, Schneider M, Marquardt B, Liljenqvist U, Pietilä TA, Hackenberg L. “Lumbar spinal stenosis”, Orthopade, 35(6), pp.675-692, Jun 2006.
- [27] Singh K, Samartzis D, Vaccaro AR, Nassr A, Andersson GB, Yoon ST, Phillips FM, Goldberg EJ, An HS. “Congenital lumbar spinal stenosis: a prospective, control-matched, cohort radiographic analysis”, Spine J, 5(6), pp. 615-622, Nov-Dec 2005.
- [28] Tubbs RS, Oakes WJ. “An unusual presentation of achondroplasia. Case report”, J Neurosurg, 103(2 Suppl), pp. 170-170, Aug 2005.
- [29] DiMaio S, Marmor E, Albrecht S, Mohr G. “Ligamentum flavum cysts causing incapacitating lumbar spinal stenosis”, Can J Neurol Sci, 32(2), pp. 237-242, May 2005.

- [30] Park JB, Lee JK, Park SJ, Riew KD. "Hypertrophy of ligamentum flavum in lumbar spinal stenosis associated with increased proteinase inhibitor concentration", J Bone Joint Surg Am, 87(12), pp. 2750-2757, Dec 2005.
- [31] Sairyo K, Biyani A, Goel V, Leaman D, Booth R Jr, Thomas J, Gehling D, Vishnubhotla L, Long R, Ebraheim N. "Pathomechanism of ligamentum flavum hypertrophy: a multidisciplinary investigation based on clinical, biomechanical, histologic, and biologic assessments", Spine, 30(23), pp. 2649-2656, Dec 2005.
- [32] Yayama T, Baba H, Furusawa N, Kobayashi S, Uchida K, Kokubo Y, Noriki S, Imamura Y, Fukuda M. "Pathogenesis of calcium crystal deposition in the ligamentum flavum correlates with lumbar spinal canal stenosis", Clin Exp Rheumatol, 23(5), pp. 637-643, Sep-Oct 2005.
- [33] Kawaguchi Y, Oya T, Abe Y, Kanamori M, Ishihara H, Yasuda T, Nogami S, Hori T, Kimura T. "Spinal stenosis due to ossified lumbar lesions", J Neurosurg Spine, 3(4), pp. 262-270, Oct 2005.
- [34] Simotas AC. "Nonoperative treatment for lumbar spinal stenosis", Clin Orthop Relat Res, 384, pp. 153-161, Mar 2001.
- [35] Vo AN, Kamen LB, Shih VC, Bitar AA, Stitik TP, Kaplan RJ. "Rehabilitation of orthopedic and rheumatologic disorders. Lumbar spinal stenosis", Arch Phys Med Rehabil, 86(3 Suppl 1), pp. S69-S76, Mar 2005
- [36] Murphy DR, Hurwitz EL, Gregory AA, Clary R. "A non-surgical approach to the management of lumbar spinal stenosis: a prospective observational cohort study", BMC Musculoskelet Disord, 7, 16, Feb 2006.
- [37] van Tulder MW, Koes B, Malmivaara A. "Outcome of non-invasive treatment modalities on back pain: an evidence-based review", Eur Spine J, 15 Suppl 1, pp. S64-S81, Jan 2006.
- [38] van Tulder MW, Koes B, Seitsalo S, Malmivaara A. "Outcome of invasive treatment modalities on back pain and sciatica: an evidence-based review", Eur Spine J, 15 Suppl 1, pp. S82-S92, Jan 2006.
- [39] Wünschmann BW, Sigl T, Ewert T, Schwarzkopf SR, Stucki G. "Physical therapy to treat spinal stenosis", Orthopade, 32(10), pp. 865-868, Oct 2003.
- [40] Armin SS, Holly LT, Khoo LT. "Minimally invasive decompression for lumbar stenosis and disc herniation", Neurosurg Focus, 25(2), pp. E11, 2008.
- [41] Atlas SJ, Keller RB, Wu YA, Deyo RA, Singer DE. "Long-term outcomes of surgical and nonsurgical management of lumbar spinal stenosis: 8 to 10 year results from the

- maine lumbar spine study”, Spine, 30(8), pp. 936-943, Apr 2005.
- [42] Weinstein JN, Tosteson TD, Lurie JD, Tosteson AN, Blood E, Hanscom B, Herkowitz H, Cammisa F, Albert T, Boden SD, Hilibrand A, Goldberg H, Berven S, An H; SPORT Investigators. “Surgical versus nonsurgical therapy for lumbar spinal stenosis”, N Engl J Med, 358(8), pp. 794-810, Feb 2008.
- [43] Benz RJ, Ibrahim ZG, Afshar P, Garfin SR. “Predicting complications in elderly patients undergoing lumbar decompression”, Clin Orthop Relat Res, 384, pp. 116-21, Mar 2001.
- [44] Mayer HM, List J, Korge A, Wiechert K. “Microsurgery of acquired degenerative lumbar spinal stenosis. Bilateral over-the-top decompression through unilateral approach”, Orthopade, 32(10), pp. 889-895, Oct 2003.
- [45] Thomé C, Zevgaridis D, Leheta O, Bänzner H, Pöckler-Schöniger C, Wöhrle J, Schmiedek P. “Outcome after less-invasive decompression of lumbar spinal stenosis: a randomized comparison of unilateral laminotomy, bilateral laminotomy, and laminectomy”, J Neurosurg Spine, 3(2), pp. 129-141, Aug 2005.
- [46] Ng LC, Tafazal S, Sell P. “The effect of duration of symptoms on standard outcome measures in the surgical treatment of spinal stenosis”, Eur Spine J, 16(2), pp. 199-206, Feb 2007.
- [47] Postacchini F, Cinotti G. “Bone regrowth after surgical decompression for lumbar spinal stenosis”, J Bone Joint Surg Br, 74(6), pp. 862-869, Nov 1992.
- [48] Resnick DK, Choudhri TF, Dailey AT, Groff MW, Khoo L, Matz PG, Mummaneni P, Watters WC 3rd, Wang J, Walters BC, Hadley MN; American Association of Neurological Surgeons/Congress of Neurological Surgeons. “Guidelines for the performance of fusion procedures for degenerative disease of the lumbar spine. Part 9: fusion in patients with stenosis and spondylolisthesis”, J Neurosurg Spine, 2(6), pp. 679-685, Jun 2005.
- [49] Jutte PC, Castelein RM. “Complications of pedicle screws in lumbar and lumbosacral fusions in 105 consecutive primary operations”, Eur Spine J, 11(6), pp. 594-598. Dec 2002.
- [50] <http://www.orsoosti.com/procedure-information?id=228>
- [51] Mayer HM, Korge A. "Non-fusion technology in degenerative lumbar spinal disorders: facts, questions, challenges". Eur Spine J, 11, pp. S85-S91, 2002.
- [52] Eif M, Schenke H. “The Interspinous-U: Indications, experience, and results”, Spinal Arthroplasty Society, New York, May 2005.
- [53] Cho KS. “Clinical outcome of the Interspinous-U (posterior distraction device) in the

elderly lumbar spine”, Spinal Arthroplasty Society, New York, May 2005.

- [54] Kaech DL, Fernandez C, Lombardi Weber D. “The interspinous “U”: a new restabilization device for the lumbar spine”, Spinal Restabilization Procedures, Elsevier Science, pp. 355–362, 2002.
- [55] <http://www.spine-health.com/treatment/spinal-fusion/interspinous-process-spacers>
- [56] Kettler A, Drumm J, Heuer F, Haeussler K, Mack C, Claes L, Wilke HJ. “Can a modified interspinous spacer prevent instability in axial rotation and lateral bending? A biomechanical in vitro study resulting in a new idea”, Clin Biomech (Bristol, Avon), 23(2), pp. 242-247, Feb 2008.
- [57] Tsai KJ, Murakami H, Lowery GL, Hutton WC. “A biomechanical evaluation of an interspinous device (Coflex) used to stabilize the lumbar spine”, J Surg Orthop Adv, 15(3), pp. 167-172, 2006.
- [58] Kong DS, Kim ES, Eoh W. “One-year outcome evaluation after interspinous implantation for degenerative spinal stenosis with segmental instability”, J Korean Med Sci, 22(2), pp. 330-335, Apr 2007.
- [59] Wilke HJ, Drumm J, Häussler K, Mack C, Steudel WI, Kettler A. “Biomechanical effect of different lumbar interspinous implants on flexibility and intradiscal pressure”, Eur Spine J, 17(8), pp. 1049-1056, Aug 2008.
- [60] Ploumis A, Transfledt EE, Denis F. “Degenerative lumbar scoliosis associated with spinal stenosis”, Spine J, 7(4), pp. 428-436, Jul-Aug 2007.
- [61] Gelalis ID, Stafilas KS, Korompilias AV, Zacharis KC, Beris AE, Xenakis TA. “Decompressive surgery for degenerative lumbar spinal stenosis: long-term results”, Int Orthop, 30(1), pp. 59-63, Feb 2006.
- [62] Ikuta K, Arima J, Tanaka T, Oga M, Nakano S, Sasaki K, Goshi K, Yo M, Fukagawa S. “Short-term results of microendoscopic posterior decompression for lumbar spinal stenosis. Technical note”, J Neurosurg Spine, 2(5), pp. 624-33, May 2005.
- [63] Katz JN, Stucki G, Lipson SJ, Fossel AH, Grobler LJ, Weinstein JN. “Predictors of surgical outcome in degenerative lumbar spinal stenosis”, Spine, 24(21), pp. 2229-2233. Nov 1999.
- [64] Mackay DC, Wheelwright EF. “Unilateral fenestration in the treatment of lumbar spinal stenosis”, Br J Neurosurg, 12(6), pp. 556-558, Dec 1998.
- [65] Postacchini F. “Surgical management of lumbar spinal stenosis”, Spine, 24(10), pp. 1043-1047, May 1999.
- [66] Postacchini F, Cinotti G, Perugia D, Gumina S. “The surgical treatment of central

- lumbar stenosis. Multiple laminotomy compared with total laminectomy”, J Bone Joint Surg Br, 75(3), pp. 386-392, May 1993.
- [67] Spetzger U, Bertalanffy H, Reinges MH, Gilsbach JM. “Unilateral laminotomy for bilateral decompression of lumbar spinal stenosis. Part II: Clinical experiences”, Acta Neurochir (Wien), 139(5), pp. 397-403, 1997.
- [68] Herkowitz HN, Garfin SR, Eismont FJ, Bell GR. Balderston RA. Rothman-Simeone the spine, 4th edition, Harcourt Publishers International Company, Singapore, 1999.
- [69] Brantigan JW, Steffee AD, Lewis ML, Quinn LM, Persenaire JM. “Lumbar interbody fusion using the Brantigan I/F cage for posterior lumbar interbody fusion and the variable pedicle screw placement system: two-year results from a Food and Drug Administration investigational device exemption clinical trial”, Spine, 25(11), PP. 1437-1446, Jun 2000.
- [70] <http://www.spine-health.com/treatment/spinal-fusion/anterior-lumbar-interbody-fusion-alif-surgery>.
- [71] <http://www.spine-health.com/treatment/back-surgery/posterior-lumbar-interbody-fusion-plif-surgery>.
- [72] Ames CP, Acosta FL Jr, Chi J, Iyengar J, Muir W, Acaroglu E, Puttlitz CM. “Biomechanical comparison of posterior lumbar interbody fusion and transforaminal lumbar interbody fusion performed at 1 and 2 levels”, Spine, 30(19), pp.E562-E566, Oct 2005.
- [73] McAfee PC. “Interbody fusion cages in reconstructive operations on the spine”, J Bone Joint Surg Am, 81(6), pp.859-880, Jun 1999.
- [74] http://www.spineuniversity.com/anterior_lumbar_fusion_with_cages
- [75] <http://paradigm-spine.de/products/en/>
- [76] Slucky AV, Brodke DS, Bachus KN, Droge JA, Braun JT. “Less invasive posterior fixation method following transforaminal lumbar interbody fusion: a biomechanical analysis”, Spine J, 6(1), pp.78-85, Jan-Feb 2006.
- [77] Ferrara LA, Secor JL, Jin BH, Wakefield A, Inceoglu S, Benzel EC. “A biomechanical comparison of facet screw fixation and pedicle screw fixation: effects of short-term and long-term repetitive cycling”, Spine, 28(12), pp.1226-1234. Jun 2003.
- [78] Aepli M, Mannion AF, Grob D. “Translaminar screw fixation of the lumbar spine: long-term outcome”, Spine, 34(14), pp.1492-1498, Jun 2009.
- [79] Fan CY, Hsu CC, Chao CK, Lin SC, Chao KH. “Biomechanical comparisons of different posterior instrumentation constructs after two-level ALIF: a finite element

- study”, Med Eng Phys, 32(2), pp.203-211. Mar 2010.
- [80] Kumar MN, Baklanov A, Chopin D. “Correlation between sagittal plane changes and adjacent segment degeneration following lumbar spine fusion”, Eur Spine J, 10(4), pp. 314-319, Aug 2001.
- [81] Lu YM, Hutton WC, Gharpuray VM. “Do bending, twisting, and diurnal fluid changes in the disc affect the propensity to prolapse? A viscoelastic finite element model.” Spine, 21(22), pp.2570-2579, Nov 1996.
- [82] Goel VK, Monroe BT, Gilbertson LG, Brinckmann P. ”Interlaminar shear stresses and laminae separation in a disc. Finite element analysis of the L3-L4 motion segment subjected to axial compressive loads”, Spine, 20(6), pp. 689-698, Mar 1995.
- [83] Rohlmann A, Zander T, Bergmann G. “Effect of total disc replacement with ProDisc on intersegmental rotation of the lumbar spine”, Spine, 30(7), pp.738-743, Apr 2005.
- [84] Schmidt H, Heuer F, Simon U, Kettler A, Rohlmann A, Claes L, Wilke HJ. “Application of a new calibration method for a three-dimensional finite element model of a human lumbar annulus fibrosus”, Clin Biomech (Bristol, Avon), 21(4), pp. 337-344, May 2006.
- [85] Marchand F, Ahmed AM. “Investigation of the laminate structure of lumbar disc annulus fibrosus”, Spine, 15, pp. 402-410, 1990.
- [86] Polikeit A, Ferguson SJ, Nolte LP, Orr TE. “Factors influencing stresses in the lumbar spine after the insertion of intervertebral cages: finite element analysis”, Eur Spine J, 12(4), pp. 413-420, Aug 2003.
- [87] Shirazi-Adl A, Ahmed AM, Shrivastava SC. “Mechanical response of a lumbar motion segment in axial torque alone and combined with compression”, Spine, 11, pp. 914-927, 1986.
- [88] Panagiotacopoulos ND, Pope MH, Krag MH, Block R. “Water content in human intervertebral discs. Part I. Measurements by magnetic resonance imaging”, Spine, 12, pp. 912-917, 1987.
- [89] Agur AMR, Lee MJ. Grant’s atlas of anatomy, 10th edition, Lippincott Williams & Wilkins, Philadelphia, Pennsylvania, 1999.
- [90] White AA, Panjabi MM. Clinical biomechanics of the spine, 2nd edition, J.B. Lippincott Company, Philadelphia, Pennsylvania 1990.
- [91] Lee KK, Teo EC, Fuss FK, Vanneville V, Qiu TX, Ng HW, Yang K, Sabitzer RJ. “Finite-element analysis for lumbar interbody fusion under axial loading”, IEEE Trans. Biomed Eng, 51, pp. 393-400, 2004.

- [92] Polikeit A, Ferguson SJ, Nolte LP, Orr TE. "Factors influencing stresses in the lumbar spine after the insertion of intervertebral cages: finite element analysis", Eur Spine J, 12(4), pp.413-420, Aug 2003.
- [93] Chen SH, Zhong ZC, Chen CS, Chen WJ, Hung C. "Biomechanical comparison between lumbar disc arthroplasty and fusion", Med Eng Phys, 31(2), pp. 244-253, Mar 2009.
- [94] Zhong ZC, Chen SH, Hung CH. "Load- and displacement-controlled finite element analyses on fusion and non-fusion spinal implants", Proc Inst Mech Eng [H], 223(2), pp. 143-157, Feb 2009.
- [95] Patwardhan AG, Havey RM, Meade KP, Lee B, Dunlap B. "A follower load increases the load-carrying capacity of the lumbar spine in compression", Spine, 24(10), pp. 1003-1009, May 1999.
- [96] Zander T, Rohlmann A, Burra NK, Bergmann G. "Effect of a posterior dynamic implant adjacent to a rigid spinal fixator", Clin Biomech, 21(8), pp.767-774, Oct 2006.
- [97] Shirazi-Adl A, Parnianpour M. "Load-bearing and stress analysis of the human spine under a novel wrapping compression loading", Clin Biomech, 15(10), pp. 718-725, Dec 2000.
- [98] Renner SM, Natarajan RN, Patwardhan AG, Havey RM, Voronov LI, Guo BY, Andersson GB, An HS. "Novel model to analyze the effect of a large compressive follower pre-load on range of motions in a lumbar spine", J Biomech, 40(6), pp. 1326-1332, 2007.
- [99] Patwardhan AG, Havey RM, Carandang G, Simonds J, Voronov LI, Ghanayem AJ, Meade KP, Gavin TM, Paxinos O. "Effect of compressive follower preload on the flexion-extension response of the human lumbar spine", J Orthop Res, 21(3), pp. 540-546, 2003.
- [100] Panjabi MM, Henderson G, James Y, Timm JP. "StabilimaxNZ versus simulated fusion: evaluation of adjacent-level effects", Eur Spine J, 16(12), pp.2159-2165, Dec 2007.
- [101] Rohlmann A, Neller S, Claes L, Bergmann G, Wilke HJ. "Influence of a follower load on intradiscal pressure and intersegmental rotation of the lumbar spine", Spine, 26(24), pp. E557-E561, Dec 2001.
- [102] Panjabi MM. "Biomechanical testing to identify adjacent-level effects", Iv World Congress of Biomechanics, Calgary, Canada, August 4-9, 2002.
- [103] Panjabi MM. "Hybrid multidirectional test method to evaluate spinal adjacent-level effects", Clin Biomech, 22(3), pp.257-265, 2007.

- [104] Goel VK, Grauer JN, Patel TCh, Biyani A, Sairyo K, Vishnubhotla S, Matyas A, Cowgill I, Shaw M, Long R, Dick D, Panjabi MM, Serhan H. “Effects of charité artificial disc on the implanted and adjacent spinal segments mechanics using a hybrid testing protocol”, Spine, 30(24), pp. 2755-2764, Dec 2005.
- [105] Yamamoto I, Panjabi MM, Crisco T, Oxland T. “Three-dimensional movements of the whole lumbar spine and lumbosacral joint”, Spine, 14(11), pp. 1256-1260, Nov 1989.
- [106] Vadapalli S, Sairyo K, Goel VK, Robon M, Biyani A, Khandha A, Ebraheim NA. “Biomechanical rationale for using polyetheretherketone (PEEK) spacers for lumbar interbody fusion-A finite element study”, Spine, 31(26), pp. E992-E998, Dec 2006.
- [107] Goel VK, Lim TH, Gwon J, Chen JY, Winterbottom JM, Park JB, Weinstein JN, Ahn JY. “Effects of rigidity of an internal fixation device. A comprehensive biomechanical investigation”, Spine, 16(3 Suppl), pp.S155-S161, Mar 1991.
- [108] Little JS, Ianuzzi A, Chiu JB, Baitner A, Khalsa PS. “Human lumbar facet joint capsule strains: II. Alteration of strains subsequent to anterior interbody fixation”, Spine J, 4(2), pp. 153-162, Mar-Apr 2004.
- [109] Weinhoffer SL, Guyer RD, Herbert M, Griffith SL. “Intradiscal pressure measurements above an instrumented fusion. A cadaveric study”, Spine, 20(5), pp. 526-531, Mar 1995.
- [110] Cho W, Wu C, Mehbod AA, Transfeldt EE. “Comparison of cage designs for transforaminal lumbar interbody fusion: a biomechanical study” Clin Biomech, 23(8), pp. 979-985, Oct 2008.

Vita

個人簡介

中文姓名	羅正展	
英文姓名	Lo Cheng-Chan	
性別	男	
出生日期	民國 70 年 2 月 4 日	
E-mail	288061108@yahoo.com.tw	
電話	02-2968-0202	
地址	220 台北縣板橋市金華街 10 巷 48 弄 8 號 2 樓	

學歷

學校名稱	國別	主修學門系所	學位	起訖年月(西元年/月)
國立交通大學	中華民國	機械工程系	博士	2005 / 09 – 2011 / 01
逢甲大學	中華民國	機械工程系	碩士	2003 / 09 – 2005 / 06
國立虎尾科技大學	中華民國	機械設計工程系	學士	2001 / 09 – 2003 / 06
國立高雄應用科技大學	中華民國	模具工程系	專科	1999 / 09 – 2001 / 06
國立海山高工	中華民國	機械科	高中	1996 / 09 – 1999 / 06

Publication List

Journal Papers

1. **Cheng-Chan Lo**, Kai-Jow Tsai, Shih-Hao Chen, Zheng-Cheng Zhong, Chinghua Hung. “Biomechanical Effect after Coflex and Coflex rivet Implantation for Segmental Instability at Surgical and Adjacent Segments: A Finite Element Analysis”, Comput Methods Biomech Biomed Engin. (SCI, EI).
(In Press) (DOI: 10.1080/10255842.2010.502894)
2. **Cheng-Chan Lo**, Kai-Jow Tsai, Zheng-Cheng Zhong, Shih-Hao Chen, Chinghua Hung. “Biomechanical differences of Coflex-F and pedicle screw fixation combined with TLIF or ALIF - A Finite Element Study”, Comput Methods Biomech Biomed Engin. (SCI, EI).
(In Press) (DOI: 10.1080/10255842.2010.501762)

Conference Papers

International Conference Paper

1. **Cheng-Chan Lo**, Kai-Jow Tsai, Zheng-Cheng Zhong, Chinghua Hung. “Biomechanical behavior between Prodisc-L and Physio-L in total disc replacement”, ISTA2010, the 23rd Annual Congress of the International Society for Technology in Arthroplasty. Dubai, United Arab Emirates. October 6-9, 2010.
2. **Cheng-Chan Lo**, Kai-Jow Tsai, Zheng-Cheng Zhong, Chinghua Hung. “Biomechanical characteristic of Coflex-F and pedicle screw fixation with TLIF or ALIF surgery - A finite element study”, WCB2010, 6th World Congress on Biomechanics. Suntec Singapore International Convention & Exhibition Centre, Singapore. August 1 - 6, 2010.
3. Kai-Jow Tsai, **Cheng-Chan Lo**, Chinghua Hung. “Biomechanical effect of interspinous process decompression device (Coflex) for multilevel lumbar spinal stenosis”, World Forum for Spine Research 2010 - The Intervertebral Disc. Montreal, Canada. July 5 - 8, 2010.
4. **Cheng-Chan Lo**, Zheng-Cheng Zhong, Shih-Hao Chen, Ming-Chieh Chiang, Chinghua Hung. “Biomechanical effect of TLIF combined with Coflex-F or with unilateral pedicle screw fixation for minimally invasive surgery - A finite element study”, ESB2010, 17th Congress of the European Society of Biomechanics. University of Edinburgh, UK. July 5 - 8, 2010.
5. **Cheng-Chan Lo**, Zheng-Cheng Zhong, Shih-Hao Chen, Ming-Chieh Chiang, Chinghua Hung. “Biomechanical effect after interspinous process device (Coflex) implantation for multilevel decompression surgery - A finite element study”, ESB2010, 17th Congress of the European Society of Biomechanics. University of Edinburgh, UK. July 5 - 8, 2010.
6. **Cheng-Chan Lo**, Zheng-Cheng Zhong, Chinghua Hung. “Biomechanical differences between Coflex-F and traditional pedicle screw fixation on fusion surgery - A Finite Element Study”, ISTA 2009, the 22nd Annual Congress of the International Society for Technology in Arthroplasty. Big Island, Hawaii. October 22 - 24, 2009. (accepted abstracts will be published in JBJS British)

Domestic Conference Paper

1. **羅正展**、蔡凱宙、鍾政成、洪景華，「人工椎間盤 Physio-L 和 Prodisc-L 在不同 Follower Load 預負載下的生物力學行為分析」，2010 年台灣生物力學學會及台灣運動生物力學學會聯合年會暨學術研討會，國立成功大學，民國 99 年 10 月 29, 30 日。(October 29 - 30, 2010)
2. **羅正展**、蔡凱宙、鍾政成、陳世豪、洪景華，「Coflex-F™ 搭配 TLIF 或 ALIF 在融合手術下之有限元素生物力學研究」，第 58 屆中華民國骨科醫學會，中國醫藥大學附設醫院，民國 99 年 4 月 24 日。(April 24, 2010)
3. **羅正展**、蔡凱宙、鍾政成、陳世豪、洪景華，「TLIF 融合手術搭配 Coflex-F™ 或單側椎弓螺絲下之有限元素生物力學研究」，第 58 屆中華民國骨科醫學會，中國醫藥大學附設醫院，民國 99 年 4 月 24 日。(April 24, 2010)
4. 蔡凱宙、**羅正展**、鍾政成、洪景華，「脊突間減壓裝置(Coflex™)在多節手術的生物力學影響」，第 57 屆中華民國骨科醫學會，國立臺灣大學醫學院附設醫院，民國 98 年 10 月 24, 25 日。(October 24 - 25, 2009)
5. **羅正展**、蔡凱宙、鍾政成、洪景華，「Coflex-F™ 與 Pedicle Screw fixation 在融合手術下之有限元素生物力學研究」，第 57 屆中華民國骨科醫學會，國立臺灣大學醫學院附設醫院，民國 98 年 10 月 24, 25 日。(October 24 - 25, 2009)
6. 陳世豪、趙時恆、鍾政成、**羅正展**、洪景華，「減壓手術時 TLIF 搭配使用單側或雙側椎足螺釘系統之生物力學特徵比較-有限元素模擬分析」，台灣脊椎外科醫學會 98 年會員大會暨學術研討會，台北榮民總醫院，民國 98 年 3 月 13, 14, 15 日。(March 13 - 15, 2009)
7. 陳世豪、趙時恆、鍾政成、**羅正展**、洪景華，「兩種新型前位椎間融合器(SynFix and Stabilis)與傳統融合固定法之生物力學特徵比較 - 有限元素模擬分析」，第 55 屆中華民國骨科醫學會，林口長庚醫院，民國 97 年 10 月 25, 26 日。(October 25 - 26, 2008)
8. 陳世豪、**羅正展**、蔡凱宙、鍾政成、洪景華，「減壓手術後脊突間減壓裝置(Coflex™)的生物力學影響」，第 54 屆中華民國骨科醫學會，中國醫藥大學附設醫院，民國 97 年 4 月 19 日。(April 19, 2008)

9. 陳世豪、許培峰、鍾政成、羅正展、陳文哲、洪景華，「減壓手術時 TLIF 與 PLIF 置放物的生物力學比較」，第 53 屆中華民國骨科醫學會，林口長庚醫院，民國 96 年 10 月 27, 28 日。(October 27 - 28, 2007)

